GENETIC AND HORMONAL CONTROL OF MAIZE INFLORESCENCE ARCHITECTURE

by

QIUJIE LIU

A dissertation submitted to the

School of Graduate Studies

Rutgers, The State University of New Jersey

In partial fulfillment of the requirements

For the degree of

Doctor of Philosophy

Graduate Program in Plant Biology

Written under the direction of

Dr. ANDREA GALLAVOTTI

And approved by

_____

_____

_____

_____

New Brunswick, New Jersey

January 2019

ABSTRACT OF THE DISSERTATION

GENETIC AND HORMONAL CONTROL OF MAIZE INFLORESCENCE ARCHITECTURE

By

QIUJIE LIU

Dissertation Director:

Dr. Andrea Gallavotti

Maize (*Zea mays L.*) is one of the most important commercial crops in the world as well as an important model organism for basic research in plant biology. The shoot architecture of maize is primarily determined by apical and axillary meristems, specialized groups of stem cells that are responsible for producing branches, lateral organs, and stems. Thus the maintenance and initiation of meristems can directly affect maize reproductive potential and yield. A major goal of my research thesis was to understand the role of different genetic, hormonal and environmental factors in regulating maize shoot growth to shed light on the molecular mechanisms underlying maize architecture.

In the first chapter of my thesis, I contributed to the characterization of the role of auxin signaling in regulating maize architecture by studying two semi-dominant mutants defective in the early stages of reproductive organogenesis, *Barren inflorescence1* and *Barren inflorescence4* (*Bif1* and *Bif4*). *BIF1* and *BIF4* encode AUXIN/INDOLE-3-ACETIC ACID (Aux/IAA) proteins, important negative regulators of the auxin signaling pathway. By *in situ* hybridizations and yeast-2-hybrid screens, I showed that many maize activating AUXIN RESPONSE FACTORs (ARFs) interact with both BIF1 and BIF4 and could potentially play a role in regulating maize inflorescence development. As part of this study, we provided evidence that BARREN STALK1 (BA1), a basic helix-loop-helix (bHLH) transcriptional regulator essential for maize axillary meristem initiation (Gallavotti

et al., 2004), is a potential target of auxin signaling. This work has been published in PNAS in 2015 and I was a co-first author (Galli et al., 2015).

In the second chapter of my thesis, we provided new insights into the interplay between inflorescence development and mineral nutrition. Boron is a fundamental micronutrient for plant growth. Previous studies in our lab showed that ROTTEN EAR (RTE), a maize boron efflux transporter, is necessary for maize inflorescence development and fertility (Chatterjee et al., 2014). Here we characterized several *RTE-like* genes in maize, and showed that the close paralogous gene *RTE2*, which shares a similar expression pattern with *RTE,* strongly enhances the *rte* phenotype in boron deficient conditions, resulting in stunted plants with strong vegetative and reproductive defects. This work showed that in soils with poor boron content both transporter proteins, RTE and RTE2, are necessary to support growth and fertility of maize plants. My main contribution to this study, published in Genetics (Chatterjee et al., 2017), was to characterize the expression of different gene family members.

In the last chapter of my thesis, my research focused on a novel recessive mutant called *needle1 (ndl1). ndl1* is a temperature sensitive mutant with variable phenotypic expressivity, showing several defects in development, the most notable of which is the formation of tassels with reduced number of branches and spikelets. Interestingly, *ndl1* mutants showed strong genetic interactions with several auxin-related mutants, as well as a lower concentration of auxin in inflorescence meristems. By positional cloning and transgenic complementation, I demonstrated that *NDL1* encodes a mitochondrial metalloprotease belonging to the FTSH (FILAMENTOUS TEMPERATURE-SENSITIVE) protease family. In addition, *ndl1* mutants showed ROS (reactive oxygen species) hyperaccumulation and strong upregulation of many genes involved in stress responses and mitochondrial retrograde regulation (MRR). Thus the characterization and identification of *NDL1* provides new insights into the interaction between redox status and auxin function in meristems, and reveals how genetic and environmental factors contribute to the establishment of maize architecture. With the ongoing warming of our planet, it is more and more

important to better understand how crop plants can cope with extreme environments.

ACKNOWLEDGEMENTS

First, I would like to express my sincere thanks to my advisor Prof. Andrea Gallavotti. In the past five years, his support and advice allowed me to grow as a scientist and to become a better person. He always trusted me and gave me a lot of opportunities to prove and improve myself. I really enjoyed the days in the Gallavotti lab. I would like to thank every member and former members in our lab. Mary and Mithu helped me a lot to learn the basic molecular biology techniques. Xue, Weibin and Zongliang gave me a lot of precious suggestions for my projects. Thanks for being not just great advisor and colleagues, but families and friends.

My sincere thanks also go to Dr. Pal Maliga, Dr. Juan Dong and Dr. Andrew Singson for serving as my committee members. Their brilliant comments and suggestions incented me to widen my research from various perspectives. I got a lot of help from the Dong Lab for the Arabidopsis experiments.

A special thanks to my family: my parents, my sister and my husband, for their absolute supports. They mean everything to me. I'm so lucky and blessed to have them.

Last but not least, I would like to thank all the people who provided me help in the past five years, the Waksman Genomics Core Facility, the fellowship from China Scholarship Council and Charles and Johanna Bush Predoctoral Fellowship to support my study.

REFERENCES FOR THE INTRODUCTION

Chatterjee, M., Liu, Q., Menello, C., Galli, M., and Gallavotti, A. (2017). The Combined Action of Duplicated Boron Transporters Is Required for Maize Growth in Boron Deficient Conditions. Genetics *206*, 2041.

Chatterjee, M., Tabi, Z., Galli, M., Malcomber, S., Buck, A., Muszynski, M., and Gallavotti, A. (2014). The boron efflux transporter ROTTEN EAR is required for maize inflorescence development and fertility. Plant Cell *26*, 2962-2977.

Gallavotti, A., Zhao, Q., Kyozuka, J., Meeley, R.B., Ritter, M., Doebley, J.F., Pe, M.E., and Schmidt, R.J. (2004). The role of barren stalk1 in the architecture of maize. Nature *432*, 630-635.

Galli, M., Liu, Q.J., Moss, B.L., Malcomber, S., Li, W., Gaines, C., Federici, S., Roshkovan, J., Meeley, R., Nemhauser, J.L.*, et al.* (2015). Auxin signaling modules regulate maize inflorescence architecture. P Natl Acad Sci USA *112*, 13372-13377.

TABLE OF CONTENTS

LIST OF TABLES

LIST OF ILLUSTRATIONS

CHAPTER ONE

CHAPTER TWO

INTRODUCTION

The Poaceae, one of the largest families in Angiosperms, contains several agriculturally important crops. Among them, maize (*Zea mays*), rice (*Oryza sativa*) and wheat (*Triticum aestivum*) are the three major crops in the world and contribute to approximately one fifth of total plant calories that humans consume. Even though they all belong to the same family, maize displays a different shoot architecture when compared to those of rice and wheat, which produce plants with multiple tillers (vegetative shoots) and develop apical inflorescences with bisexual flowers. A modern maize plant instead develops a single stem devoid of tillers, allowing dense plantings in fields, as well as unisexual inflorescences borne on separate parts of the plant.

The shoot architecture of plants is determined to a large extent by branching patterns, which are produced by the shoot apical meristem (SAM) and axillary meristems (AMs) (Steeves and Sussex, 1989; Vollbrecht et al., 2005). Meristems are groups of pluripotent stem cells that are able to self-renew and differentiate into daughter cells. Plant developmental plasticity is predominantly based on the continuous activity of these stem cells (Gaillochet et al., 2015). Therefore, research on the molecular mechanisms regulating plant architecture primarily focuses on the maintenance of the SAM and the initiation and outgrowth of AMs. Extensive research has revealed that several environmental and developmental factors, such as transcription factors, plant hormones, redox status and different

stresses play key role in regulating plant architecture. Here we focused on the genetic and molecular mechanisms underlying maize shoot architecture, in particular during reproductive development and the establishment of its unisexual inflorescences, the male tassel and the female ear.

Shoot development in maize

Phytomers are the basic morphological units of plant architecture during shoot development, each of which consists of a node, an internode, a true or modified leaf, and one or more AMs (Galinat, 1959; Gray, 1879; McSteen and Leyser, 2005). During the vegetative phase of maize development, while the SAM produces leaves along the main axis of growth, AMs initiate at the leaf axils to produce leaf primordia and remain quiescent as axillary buds (Gallavotti, 2013). After the transition to reproductive development, the SAM converts to an inflorescence meristem (IM), producing the tassel at the shoot apex. In inflorescences, leaf primordia are still initiated but remain suppressed, producing modified primordia called suppressed bracts. Along the stem, the uppermost axillary buds become active and give rise to ears at the axils of one or more leaves (Kiesselbach, 1949). Eventually, a mature tassel consists of a central spike covered with spikelets and several asymmetric long branches. The spikelet is the basic unit of grass inflorescence architecture, consisting of two leaf-like structures called glumes and two florets, and in maize inflorescences spikelets are paired (Mcsteen et al., 2000). The presence of branches is the main morphological difference between tassels and ears. Except for that, tassel and ear early in development share an identical organogenesis process. At the peripheral zone,

IMs give rise to different types of reproductive AMs. The first AMs formed include the indeterminate branch meristems (BMs; formed only in tassels) and the determinate spikelet-pair meristems (SPMs; formed in both tassels and ears). Subsequently, each SPM gives rise to two secondary AMs called spikelet meristems (SMs), which finally produce two tertiary AMs called floral meristems (FMs) (Vollbrecht and Schmidt, 2009). Each maize floret consists of two bract-like structures called lemma and palea, equivalent to sepals, two petals homologous structures named lodicules, and the reproductive organs, stamens and carpels. During floret development, the stamens abort growth in the tassel and the carpels go through a similar fate in male florets (Bonnett, 1954; Irish, 1996). Thus maize is a monoecious plant species bearing two unisexual inflorescences.

The maintenance of the shoot apical meristem and the WUSCHEL-CLAVATA pathway

The organization of the SAM and the mechanisms regulating SAM activity have been extensively studied in recent decades. The dome-shaped SAM is organized into different functional domains (Somssich et al., 2016). The pluripotent stem cells are found in the central zone (CZ), under which lies the organizing center (OC), containing cells required to regulate and maintain stem cell fate. The rapidly dividing daughter cells produced by stem cells reside in the peripheral zone (PZ), where organ formation is initiated (Gaillochet et al., 2015; Mayer et al., 1998; Somssich et al., 2016). This functional organization and regulation of meristem activity has to be finely tuned to balance maintenance of the central zone and

lateral organ initiation at the peripheral zone. All shoot meristems, including IMs and AMs share a similar functional organization.

The WUSCHEL-CLAVATA (WUS-CLV) pathway has been identified as a key pathway that coordinates stem cell proliferation and organ initiation in the *Arabidopsis thaliana* SAM (Brand et al., 2000; Mayer et al., 1998; Schoof et al., 2000). WUSCHEL is a homeodomain transcription factor belonging to the WUS-homeobox (WOX) family, specifically expressed in the OC. Recent studies showed that the WUS protein is able to move from the OC to the CZ through plasmodesmata to maintain stem cell fate, and directly or indirectly activates the CZ specific expression of *CLAVATA3* (*CLV3)*, which produces a small peptide (Yadav et al., 2011). CLV3 peptides in turn restrict *WUS* expression in the OC through the action of several receptor membrane-bound proteins, such as CLAVATA1 (CLV1) and CLAVATA2 (CLV2) (Brand et al., 2000; Schoof et al., 2000). Arabidopsis mutants defective in the CLV pathway generally display enlarged meristems (Brand et al., 2000; Mayer et al., 1998; Schoof et al., 2000). Similarly, several maize mutants identified in the WUS-CLV pathway are characterized by thick tassels and fasciated ears, due to overproliferation of inflorescence meristems (Muller and Bleckmann, 2008; Pautler et al., 2015; Peter et al., 2005; Somssich et al., 2016; Taguchi-Shiobara et al., 2001). *THICK TASSEL DWARF1* (*TD1*) encodes a membrane localized receptor-like kinases homologous to *CLV1* (Peter et al., 2005). *FASCIATED EAR2* (*FEA2*) encodes a receptor-like protein orthologous to Arabidopsis CLV2, which lacks an internal kinase domain (Taguchi-Shiobara et al., 2001). In Arabidopsis, CLV2 has been

proposed to function by interacting with the cytoplasmic kinase CORYNE (CRN) (Muller and Bleckmann, 2008), but recently this model has been questioned as CRN likely lacks kinase activity (Nimchuk et al., 2011). In maize, the characterization of *compact plant2* (*ct2*) suggest that *CT2,* a α-subunit (Gα) of the heterotrimeric GTP-binding protein, may signal downstream of CLV2 (Bommert et al., 2013a). In addition, maize mutant analysis uncovered several new genes regulating IM size, such as *FASCIATED EAR3* (*FEA3*) (Je et al., 2016) and *FASCIATED EAR4* (*FEA4*) (Pautler et al., 2015), which encodes a novel CLV-type LRR receptor and a bZIP transcription factor, respectively, suggesting that the WUS-CLV pathway is not the only pathway contributing to the regulation of meristem size in maize.

Axillary meristems initiation and the role of auxin

Unlike the SAM, AMs are secondary meristems forming in the axils of primary organs during post-embryonic development (Bennett and Leyser, 2006). AMs are responsible for the production of secondary axes of growth by maintaining a core of stem cells, thus play an important role in shaping shoot architecture (Gallavotti, 2013). The identification of a group of mutants displaying abnormal shoot architecture highlighted the importance of the plant hormone auxin in regulating AM initiation (Bennett et al., 1995; Cheng et al., 2006; Gallavotti, 2013; Gallavotti et al., 2008a; Galli et al., 2015; Gälweiler et al., 1998; McSteen et al., 2007; Phillips et al., 2011; Przemeck et al., 1996). Auxins are a group of phytohormones that play many roles in plant growth and development. Thanks to an abundance of major breakthroughs, the basic molecular and cellular mechanisms regulating

auxin biology are now well understood. Nonetheless, major questions remain regarding the regulation of auxin functional specificity.

Auxin biosynthesis

In the past few years, it has been clearly shown that auxin biosynthesis is required for almost all major developmental processes (Zhao, 2018). In plants, indole-3-acetic acid (IAA) is the primary and most common natural auxin. IAA can be synthesized from tryptophan (Trp)-dependent and Trp-independent pathways (Ljung, 2013; Mashiguchi et al., 2011; Woodward and Bartel, 2005; Zhao, 2018). Among them, the only complete Trp-dependent auxin biosynthesis pathway identified so far is the TAA/YUC pathway. TRYPTOPHAN AMINOTRANSFERASE1 (TAA1) mediates the conversion of tryptophan to indole pyruvic acid (IPA) (Stepanova et al., 2008; Tao et al., 2008), which is subsequent transformed into IAA by a flavin monooxygenase enzyme belonging to the YUCCA (YUC) family (Zhao et al., 2001). The characterization of two maize mutants displaying a barren inflorescence phenotype, *vanishing tassel2* (*vt2*) and *sparse inflorescence1* (*spi1*), led to the identification of the maize orthologs of *TAA1* and *YUC4*, respectively (Gallavotti et al., 2008a; Phillips et al., 2011), suggesting that the TAA/YUC pathway is conserved between monocot and eudicot species, and that auxin biosynthesis greatly influences maize inflorescence architecture.

Auxin transport

The dynamic distribution of auxin and the establishment of auxin concentration gradients are known to have important roles in plant development (Heisler et al., 2005; Leyser, 2005). Two major pathways are used to transport auxin and regulate its distribution. One pathway is the long distance nonpolar translocation of auxin, while the other one is the short distance auxin polar transport, dependent on auxin influx and efflux transporters (Vanneste and Friml, 2009). One of the best-known polar auxin efflux transporters is PINFORMED1 (PIN1) of Arabidopsis, a plasma membrane localized protein, whose polar localization establishes auxin efflux directions (Gälweiler et al., 1998). PIN1 activity is positively regulated by PINOID (PID), a serine-threonine kinase (Friml et al., 2004), thus PID is involved in regulating polar auxin transport. In maize, 12 *PIN* family members have been identified, but no mutant has been reported so far, probably due to functional redundancy (Forestan et al., 2012; Gallavotti, 2013). However, the co-ortholog of the Arabidopsis *PID* gene*, BARREN INFLORESCENCE2* (*BIF2*), has been identified in maize. Similarly to other barren mutants, the initiation of reproductive AMs of *bif2* is severely impaired resulting in *pin-formed* inflorescences with few spikelet and branches, indicating that auxin transport plays a key role in inflorescence development in both monocot and eudicot species (McSteen et al., 2007).

Auxin conjugation and degradation

In addition to auxin biosynthesis and transport, auxin homeostasis is also regulated by auxin conjugation and degradation pathways (Ljung, 2013; Rosquete et al., 2012). Cellular IAA is generally stored as amide derivatives and ester-linked conjugates in Arabidopsis (Tam et al., 2000). Among the IAA conjugates, a fraction of them can be hydrolysed back to free IAA, such as IAA-Ala, IAA-Leu, IAA-Phe, whereas some of them, such as IAA-Asp and IAA-Glu, are irreversible and considered as precursors for degradation (Ludwig-Muller, 2011). Several genes are involved in auxin conjugation, including several members from the auxin-inducible *GRETCHEN HAGEN3* (*GH3*) family (Ljung, 2013; Ludwig-Muller, 2011).

Auxin oxidative degradation, the oxidation of IAA to 2-oxindole-3-acetic acid (oxIAA), a molecule with very low auxin activity, is believed to be another important but poorly understood pathway regulating auxin homeostasis (Pencik et al., 2013). Recently, the characterization and identification of a rice mutant displaying defective reproductive development suggested the involvement of *DIOXYGENASE FOR AUXIN OXIDATION* (*DAO*), which encodes a 2-oxoglutarate-dependent-Fe(II) dioxygenase, in regulating auxin oxidative degradation and plant development (Porco et al., 2016; Zhang et al., 2016; Zhao et al., 2013).

Auxin signaling

Auxin biosynthesis, transport, conjugation and degradation cooperate to ensure appropriate spatio-temporal auxin levels, downstream of which lies the auxin signaling pathway. AUXIN/INDOLE3 ACETIC ACIDs (Aux/IAAs) are a group of negative regulators of auxin signaling that recruit co-repressor proteins to repress auxin responsive gene transcription by AUXIN RESPONSE FACTORS (ARFs). Auxin functions as a molecular glue to stabilize the interaction of Aux/IAAs and F-box TRANSPORT INHIBITOR RESPONSE1/AUXIN SIGNALING F-BOX (TIR1/AFB) proteins, and by doing so it triggers the ubiquitination and degradation of Aux/IAAs. As a result, ARFs are released to promote the expression of downstream genes (Dharmasiri et al., 2005; Gray et al., 2001; Szemenyei et al., 2008; Weijers and Wagner, 2016). Aux/IAAs and ARFs interact with each other via the PB1 C-terminal domain, which is conserved between Aux/IAA family and most ARFs. The N-terminal of Aux/IAA contains a well-known repressor motif called EAR (Tiwari et al., 2004), and a degron domain which is critical for Aux/IAA stability (Gray et al., 2001). In Arabidopsis as in other species, mutations in the degron domains of different *Aux/IAAs* always result in dominant or semi-dominant mutants showing altered shoot morphology, such as abnormal leaf development and decreased apical dominance, indicating the importance of auxin signaling in regulating plant shoot architecture (Reed, 2001). Additional evidence came from the analysis of mutations in the Arabidopsis *MONOPTEROS* (*MP*) gene, which encodes ARF5, and show severe defects in shoot development, resulting in a pin-like inflorescence (Przemeck et al., 1996).

4. Other known regulators of plant architecture

In addition to the pathways mentioned above, plant architecture is also regulated by other endogenous and environmental cues. Moreover, besides auxin, several hormones are important regulators of plant architecture. One notable example is the role of cytokinin (CK) in regulating meristem size. In rice, mutants defective in CK biosynthesis produce smaller SAMs (Kurakawa et al., 2007), indicating a positive role of CK in meristem size regulation. Type-A *ARABIDOPSIS RESPONSE REGULATORS* (*ARRs*) are negative regulators of CK signaling (To and Kieber, 2008). In maize, mutations in the type-A ARRs regulator *ABNORMAL PHYLLOTAXY* (*ABPH1)* display enlarged SAMs (Giulini et al., 2004). In addition, many other studies in Arabidopsis have shown that WUS is able to repress type-A *ARR* (*ARR7* and *ARR15*), while *ARR7* and *ARR15* in turn are required for *CLV3* expression, which functions to limit *WUS* expression, providing a direct link between CK and WUS-CLV in meristem size regulation (Leibfried et al., 2005; Zhao et al., 2010).

While CK and WUS-CLV pathway display a positive action on the maintenance of the SAM by promoting the proliferation of undifferentiated cells, auxin functions in an antagonistic way to induce cellular differentiation and new primordia initiation among which are AMs in the PZ (Schaller et al., 2015; Shi et al., 2018; Su et al., 2011). At the flank of SAM, auxin maxima created by PIN-mediated polar auxin transport mark the incipient site of primordium initiation (Gallavotti et al., 2008b; Heisler et al., 2005)Moreover, recent studies suggested that localized auxin minima in the boundary zone between SAM and lateral

primordia are required for AM formation (Benková et al., 2003; Gallavotti et al., 2008b; Heisler et al., 2005; Hofmann, 2014; Qi et al., 2014; Wang et al., 2014). Thus the balance between auxin and CK is essential to control plant shoot development. High levels of CK generally induce *WUS* expression (Leibfried et al., 2005), whereas WUS functions to restrict auxin signaling and response in the SAM (Ma et al., 2018). In addition, auxin has been shown to suppress CK biosynthesis via the isopentenyladenosine-5'-monophosphate-independent pathway in the shoot (Nordstrom et al., 2004). Interestingly, recent studies suggested a synergy between auxin and CK by repressing the expression of *ARR7* and *ARR15* via a MP-mediated pathway in SAM development (Zhao et al., 2010).

Along with plant hormones, reactive oxygen species (ROS) are another group of molecules reported to play significant roles in interpreting environmental and developmental signals and regulating plant growth (Baxter et al., 2014; Gapper and Dolan, 2006; Sparks et al., 2013). In Arabidopsis, ROS have been identified as essential signaling molecules to regulate stem cell fate by affecting *WUS* expression (Zeng et al., 2017). One species of ROS, the superoxide anion ($O_2^{\bullet -}$), is able to activate *WUS* expression to maintain stem cell fate while hydrogen peroxide (H_2O_2), functions antagonistically to promote differentiation in the peripheral zone by negatively regulating superoxide anion biosynthesis (Zeng et al., 2017). To function as signaling molecules and mitigate their toxicity, ROS level are tightly regulated by ROS production and ROS-scavenging pathways (D'Autreaux and Toledano, 2007; Mittler et al., 2004). Defects in several

components involved in ROS scavenging pathways, such as Glutaredoxins (GRXs), and Thioredoxins (TRXs), result in abnormal inflorescence architecture (Bashandy et al., 2010; Yang et al., 2015). For example the Arabidopsis triple mutant *ntra;ntrab;cad2-1* affected in members of the TRX reductase family (*NTRA* and *NTRB*) and glutathione biosynthesis pathways (*CAD2*) shows a pin-formed phenotype similar to auxin mutants (Bashandy et al., 2010). These results suggest the importance of ROS signaling in regulating plant architecture and lateral organ initiation in meristems.

REFERENCES FOR THE INTRODUCTION

Bashandy, T., Guilleminot, J., Vernoux, T., Caparros-Ruiz, D., Ljung, K., Meyer, Y., and Reichheld, J.P. (2010). Interplay between the NADP-linked thioredoxin and glutathione systems in Arabidopsis auxin signaling. Plant Cell *22*, 376-391.

Baxter, A., Mittler, R., and Suzuki, N. (2014). ROS as key players in plant stress signalling. J Exp Bot *65*, 1229-1240.

Bennett, S.R., Alvarez, J., Bossinger, G., and Smyth, D.R. (1995). Morphogenesis in pinoid mutants of Arabidopsis thaliana. The Plant Journal *8*, 505-520.

Bennett, T., and Leyser, O. (2006). Something on the side: axillary meristems and plant development. Plant Mol Biol *60*, 843-854.

Bommert, P., Je, B.I., Goldshmidt, A., and Jackson, D. (2013). The maize Gα gene COMPACT PLANT2 functions in CLAVATA signalling to control shoot meristem size. Nature *502*, 555.

Bonnett, O.T. (1954). The Inflorescences of Maize. Science *120*, 77-87.

Brand, U., Fletcher, J.C., Hobe, M., Meyerowitz, E.M., and Simon, R. (2000). Dependence of stem cell fate in Arabidopsis on a feedback loop regulated by CLV3 activity. Science *289*, 617-619.

Cheng, Y., Dai, X., and Zhao, Y. (2006). Auxin biosynthesis by the YUCCA flavin monooxygenases controls the formation of floral organs and vascular tissues in Arabidopsis. Genes Dev *20*, 1790-1799.

D'Autreaux, B., and Toledano, M.B. (2007). ROS as signalling molecules: mechanisms that generate specificity in ROS homeostasis. Nat Rev Mol Cell Biol *8*, 813-824.

Dharmasiri, N., Dharmasiri, S., and Estelle, M. (2005). The F-box protein TIR1 is an auxin receptor. Nature *435*, 441-445.

Forestan, C., Farinati, S., and Varotto, S. (2012). The Maize PIN Gene Family of Auxin Transporters. Front Plant Sci *3*, 16.

Friml, J., Yang, X., Michniewicz, M., Weijers, D., Quint, A., Tietz, O., Benjamins, R., Ouwerkerk, P.B., Ljung, K., and Sandberg, G. (2004). A PINOID-dependent binary switch in apical-basal PIN polar targeting directs auxin efflux. Science *306*, 862-865.

Gaillochet, C., Daum, G., and Lohmann, J.U. (2015). O cell, where art thou? The mechanisms of shoot meristem patterning. Curr Opin Plant Biol *23*, 91-97.

Galinat, W.C. (1959). THE PHYTOMER IN RELATION TO FLORAL HOMOLOGIES IN THE AMERICAN MAYDEAE. Botanical Museum Leaflets Harvard University *19*, 1-xvi.

Gallavotti, A. (2013). The role of auxin in shaping shoot architecture. J Exp Bot *64*, 2593-2608.

Gallavotti, A., Barazesh, S., Malcomber, S., Hall, D., Jackson, D., Schmidt, R.J., and McSteen, P. (2008a). sparse inflorescence1 encodes a monocot-specific YUCCA-like gene required for vegetative and reproductive development in maize. P Natl Acad Sci USA *105*, 15196-15201.

Gallavotti, A., Yang, Y., Schmidt, R.J., and Jackson, D. (2008b). The relationship between auxin transport and maize branching. Plant Physiology *147*, 1913-1923.

Galli, M., Liu, Q.J., Moss, B.L., Malcomber, S., Li, W., Gaines, C., Federici, S., Roshkovan, J., Meeley, R., Nemhauser, J.L.*, et al.* (2015). Auxin signaling modules regulate maize inflorescence architecture. P Natl Acad Sci USA *112*, 13372-13377.

Gälweiler, L., Guan, C., Müller, A., Wisman, E., Mendgen, K., Yephremov, A., and Palme, K. (1998). Regulation of polar auxin transport by AtPIN1 in Arabidopsis vascular tissue. Science *282*, 2226-2230.

Gapper, C., and Dolan, L. (2006). Control of plant development by reactive oxygen species. Plant Physiol *141*, 341-345.

Giulini, A., Wang, J., and Jackson, D. (2004). Control of phyllotaxy by the cytokinin-inducible response regulator homologue ABPHYL1. Nature *430*, 1031.

Gray, A. (1879). Structural botany, Vol 1 (American Book Company).

Gray, W.M., Kepinski, S., Rouse, D., Leyser, O., and Estelle, M. (2001). Auxin regulates SCF(TIR1)-dependent degradation of AUX/IAA proteins. Nature *414*, 271-276.

Heisler, M.G., Ohno, C., Das, P., Sieber, P., Reddy, G.V., Long, J.A., and Meyerowitz, E.M. (2005). Patterns of auxin transport and gene expression during primordium development revealed by live imaging of the Arabidopsis inflorescence meristem. Curr Biol *15*, 1899-1911.

Hofmann, N.R. (2014). The Importance of Being Absent: Auxin Minima Are Required for Axillary Meristem Formation. Plant Cell *26*, 1836.

Irish, E.E. (1996). Regulation of sex determination in maize. Bioessays *18*, 363-369.

Je, B.I., Gruel, J., Lee, Y.K., Bommert, P., Arevalo, E.D., Eveland, A.L., Wu, Q.,

Goldshmidt, A., Meeley, R., Bartlett, M.*, et al.* (2016). Signaling from maize organ primordia via FASCIATED EAR3 regulates stem cell proliferation and yield traits. Nat Genet *48*, 785-791.

Kiesselbach, T. (1949). The structure and reproduction of corn. University of Nebraska, College ofAgriculture, Agricultural Experiment Station. Research Bulletin *161*.

Kurakawa, T., Ueda, N., Maekawa, M., Kobayashi, K., Kojima, M., Nagato, Y., Sakakibara, H., and Kyozuka, J. (2007). Direct control of shoot meristem activity by a cytokinin-activating enzyme. Nature *445*, 652-655.

Leibfried, A., To, J.P., Busch, W., Stehling, S., Kehle, A., Demar, M., Kieber, J.J., and Lohmann, J.U. (2005). WUSCHEL controls meristem function by direct regulation of cytokinin-inducible response regulators. Nature *438*, 1172-1175.

Leyser, O. (2005). Auxin distribution and plant pattern formation: how many angels can dance on the point of PIN? Cell *121*, 819-822.

Ljung, K. (2013). Auxin metabolism and homeostasis during plant development. Development *140*, 943-950.

Ludwig-Muller, J. (2011). Auxin conjugates: their role for plant development and in the evolution of land plants. J Exp Bot *62*, 1757-1773.

Ma, Y., Miotk, A., Sutikovic, Z., Medzihradszky, A., Wenzl, C., Ermakova, O., Gaillochet, C., Forner, J., Utan, G., and Brackmann, K. (2018). WUSCHEL acts as a rheostat on the auxin pathway to maintain apical stem cells in Arabidopsis. bioRxiv, 468421.

Mashiguchi, K., Tanaka, K., Sakai, T., Sugawara, S., Kawaide, H., Natsume, M., Hanada, A., Yaeno, T., Shirasu, K., and Yao, H. (2011). The main auxin biosynthesis pathway in Arabidopsis. Proceedings of the National Academy of Sciences *108*, 18512-18517.

Mayer, K.F., Schoof, H., Haecker, A., Lenhard, M., Jürgens, G., and Laux, T. (1998). Role of WUSCHEL in regulating stem cell fate in the Arabidopsis shoot meristem. Cell *95*, 805-815.

Mcsteen, P., Laudencia-Chingcuanco, D., and Colasanti, J. (2000). A floret by any other name: control of meristem identity in maize. Trends in Plant Science *5*, 61-66.

McSteen, P., and Leyser, O. (2005). Shoot branching. Annu Rev Plant Biol *56*, 353-374.

McSteen, P., Malcomber, S., Skirpan, A., Lunde, C., Wu, X., Kellogg, E., and Hake, S. (2007). barren inflorescence2 Encodes a co-ortholog of the PINOID

serine/threonine kinase and is required for organogenesis during inflorescence and vegetative development in maize. Plant Physiol *144*, 1000-1011.

Mittler, R., Vanderauwera, S., Gollery, M., and Breusegem, F.V. (2004). Reactive oxygen gene network of plants. Trends in Plant Science *9*, 490-498.

Muller, R., and Bleckmann, A., R (2008). The receptor kinase CORYNE of Arabidopsis transmits the stem cell-limiting signal CLAVATA3 independently of CLAVATA1. Plant Cell *20*, 934-946.

Nimchuk, Z.L., Tarr, P.T., and Meyerowitz, E.M. (2011). An evolutionarily conserved pseudokinase mediates stem cell production in plants. Plant Cell *23*, 851-854.

Nordstrom, A., Tarkowski, P., Tarkowska, D., Norbaek, R., Astot, C., Dolezal, K., and Sandberg, G. (2004). Auxin regulation of cytokinin biosynthesis in Arabidopsis thaliana: a factor of potential importance for auxin-cytokinin-regulated development. Proc Natl Acad Sci U S A *101*, 8039-8044.

Pautler, M., Eveland, A.L., LaRue, T., Yang, F., Weeks, R., Lunde, C., Je, B.I., Meeley, R., Komatsu, M., Vollbrecht, E.*, et al.* (2015). FASCIATED EAR4 encodes a bZIP transcription factor that regulates shoot meristem size in maize. Plant Cell *27*, 104-120.

Pencik, A., Simonovik, B., Petersson, S.V., Henykova, E., Simon, S., Greenham, K., Zhang, Y., Kowalczyk, M., Estelle, M., Zazimalova, E.*, et al.* (2013). Regulation of auxin homeostasis and gradients in Arabidopsis roots through the formation of the indole-3-acetic acid catabolite 2-oxindole-3-acetic acid. Plant Cell *25*, 3858-3870.

Peter, B., China, L., Judith, N., Erik, V., Mark, R., David, J., Sarah, H., and Wolfgang, W. (2005). thick tassel dwarf1 encodes a putative maize ortholog of the Arabidopsis CLAVATA1 leucine-rich repeat receptor-like kinase. Development *132*, 1235.

Phillips, K.A., Skirpan, A.L., Liu, X., Christensen, A., Slewinski, T.L., Hudson, C., Barazesh, S., Cohen, J.D., Malcomber, S., and McSteen, P. (2011). vanishing tassel2 encodes a grass-specific tryptophan aminotransferase required for vegetative and reproductive development in maize. Plant Cell *23*, 550-566.

Porco, S., Pencik, A., Rashed, A., Voss, U., Casanova-Saez, R., Bishopp, A., Golebiowska, A., Bhosale, R., Swarup, R., Swarup, K.*, et al.* (2016). Dioxygenase-encoding AtDAO1 gene controls IAA oxidation and homeostasis in Arabidopsis. Proc Natl Acad Sci U S A *113*, 11016-11021.

Przemeck, G.K., Mattsson, J., Hardtke, C.S., Sung, Z.R., and Berleth, T. (1996). Studies on the role of the Arabidopsis gene MONOPTEROS in vascular development and plant cell axialization. Planta *200*, 229-237.

Qi, J., Wang, Y., Yu, T., Cunha, A., Wu, B., Vernoux, T., Meyerowitz, E., and Jiao, Y. (2014). Auxin depletion from leaf primordia contributes to organ patterning. Proceedings of the National Academy of Sciences *111*, 18769-18774.

Reed, J.W. (2001). Roles and activities of Aux/IAA proteins in Arabidopsis. Trends in plant science *6*, 420-425.

Rosquete, M.R., Barbez, E., and Kleine-Vehn, J. (2012). Cellular auxin homeostasis: gatekeeping is housekeeping. Mol Plant *5*, 772-786.

Schaller, G.E., Bishopp, A., and Kieber, J.J. (2015). The yin-yang of hormones: cytokinin and auxin interactions in plant development. Plant Cell *27*, 44-63.

Schoof, H., Lenhard, M., Haecker, A., Mayer, K.F., Jürgens, G., and Laux, T. (2000). The stem cell population of Arabidopsis shoot meristems is maintained by a regulatory loop between the CLAVATA and WUSCHEL genes. Cell *100*, 635-644.

Shi, B., Guo, X., Wang, Y., Xiong, Y., Wang, J., Hayashi, K.I., Lei, J., Zhang, L., and Jiao, Y. (2018). Feedback from Lateral Organs Controls Shoot Apical Meristem Growth by Modulating Auxin Transport. Dev Cell *44*, 204-216 e206.

Somssich, M., Je, B.I., Simon, R., and Jackson, D. (2016). CLAVATA-WUSCHEL signaling in the shoot meristem. Development *143*, 3238-3248.

Sparks, E., Wachsman, G., and Benfey, P.N. (2013). Spatiotemporal signalling in plant development. Nat Rev Genet *14*, 631-644.

Steeves, T.A., and Sussex, I.M. (1989). Patterns in plant development (Cambridge University Press).

Stepanova, A.N., Robertson-Hoyt, J., Yun, J., Benavente, L.M., Xie, D.Y., Dolezal, K., Schlereth, A., Jurgens, G., and Alonso, J.M. (2008). TAA1-mediated auxin biosynthesis is essential for hormone crosstalk and plant development. Cell *133*, 177-191.

Su, Y.H., Liu, Y.B., and Zhang, X.S. (2011). Auxin-cytokinin interaction regulates meristem development. Mol Plant *4*, 616-625.

Szemenyei, H., Hannon, M., and Long, J.A. (2008). TOPLESS mediates auxin-dependent transcriptional repression during Arabidopsis embryogenesis. Science *319*, 1384-1386.

Taguchi-Shiobara, F., ., Yuan, Z., ., Hake, S., ., and Jackson, D., . (2001). The fasciated ear2 gene encodes a leucine-rich repeat receptor-like protein that regulates shoot meristem proliferation in maize. Genes & Development *15*, 2755-2766.

Tam, Y.Y., Epstein, E., and Normanly, J. (2000). Characterization of auxin conjugates in Arabidopsis. Low steady-state levels of indole-3-acetyl-aspartate, indole-3-acetyl-glutamate, and indole-3-acetyl-glucose. Plant Physiology *123*, 589-596.

Tao, Y., Ferrer, J.L., Ljung, K., Pojer, F., Hong, F., Long, J.A., Li, L., Moreno, J.E., Bowman, M.E., Ivans, L.J.*, et al.* (2008). Rapid synthesis of auxin via a new tryptophan-dependent pathway is required for shade avoidance in plants. Cell *133*, 164-176.

Tiwari, S.B., Hagen, G., and Guilfoyle, T.J. (2004). Aux/IAA proteins contain a potent transcriptional repression domain. Plant Cell *16*, 533-543.

To, J.P., and Kieber, J.J. (2008). Cytokinin signaling: two-components and more. Trends in plant science *13*, 85-92.

Vanneste, S., and Friml, J. (2009). Auxin: a trigger for change in plant development. Cell *136*, 1005-1016.

Vollbrecht, E., and Schmidt, R.J. (2009). Development of the Inflorescences. In Handbook of maize: Its biology (Springer), pp. 13-40.

Vollbrecht, E., Springer, P.S., Goh, L., Buckler, E.S.t., and Martienssen, R. (2005). Architecture of floral branch systems in maize and related grasses. Nature *436*, 1119-1126.

Wang, Y., Wang, J., Shi, B., Yu, T., Qi, J., Meyerowitz, E.M., and Jiao, Y. (2014). The Stem Cell Niche in Leaf Axils Is Established by Auxin and Cytokinin in Arabidopsis. Plant Cell *26*, 2055-2067.

Weijers, D., and Wagner, D. (2016). Transcriptional Responses to the Auxin Hormone. Annu Rev Plant Biol *67*, 539-574.

Woodward, A.W., and Bartel, B. (2005). Auxin: regulation, action, and interaction. Ann Bot *95*, 707-735.

Yadav, R.K., Perales, M., Gruel, J., Girke, T., Jonsson, H., and Reddy, G.V. (2011). WUSCHEL protein movement mediates stem cell homeostasis in the Arabidopsis shoot apex. Genes Dev *25*, 2025-2030.

Yang, F., Bui, H.T., Pautler, M., Llaca, V., Johnston, R., Lee, B.H., Kolbe, A., Sakai, H., and Jackson, D. (2015). A maize glutaredoxin gene, abphyl2, regulates shoot meristem size and phyllotaxy. Plant Cell *27*, 121-131.

Zeng, J., Dong, Z., Wu, H., Tian, Z., and Zhao, Z. (2017). Redox regulation of plant stem cell fate. EMBO J *36*, 2844-2855.

Zhang, J., Lin, J.E., Harris, C., Campos Mastrotti Pereira, F., Wu, F., Blakeslee,

J.J., and Peer, W.A. (2016). DAO1 catalyzes temporal and tissue-specific oxidative inactivation of auxin in Arabidopsis thaliana. Proc Natl Acad Sci U S A *113*, 11010-11015.

Zhao, Y. (2018). Essential roles of local auxin biosynthesis in plant development and in adaptation to environmental changes. Annual review of plant biology *69*, 417-435.

Zhao, Y., Christensen, S.K., Fankhauser, C., Cashman, J.R., Cohen, J.D., Weigel, D., and Chory, J. (2001). A role for flavin monooxygenase-like enzymes in auxin biosynthesis. Science *291*, 306-309.

Zhao, Z., Andersen, S.U., Ljung, K., Dolezal, K., Miotk, A., Schultheiss, S.J., and Lohmann, J.U. (2010). Hormonal control of the shoot stem-cell niche. Nature *465*, 1089-1092.

Zhao, Z., Zhang, Y., Liu, X., Zhang, X., Liu, S., Yu, X., Ren, Y., Zheng, X., Zhou, K., Jiang, L.*, et al.* (2013). A role for a dioxygenase in auxin metabolism and reproductive development in rice. Dev Cell *27*, 113-122.

CHAPTER ONE

Auxin signaling modules regulate maize inflorescence architecture

Mary Galli[a,1], Qiujie Liu[a,1], Britney L. Moss[b], Simon Malcomber[c,d], Wei Li[a], Craig Gaines[e], Silvia Federici[a], Jessica Roshkovan[a], Robert Meeley[f], Jennifer L. Nemhauser[b], and Andrea Gallavotti[a,g,2]

[a]Waksman Institute, Rutgers University, Piscataway, NJ 08854-8020; [b]Department of Biology, University of Washington, Seattle, WA 98195; [c]Department of Biological Sciences, California State University, Long Beach, CA 90840; [d]Division of Environmental Biology, National Science Foundation, Arlington, VA 22230; [e]Section of Cell and Developmental Biology, University of California, San Diego, La Jolla, CA 92093-0116; [f]Pioneer Hi-Bred International, Johnston, IA 50131; and [g]Department of Plant Biology and Pathology, Rutgers University, New Brunswick, NJ 08901

Edited by Mark Estelle, University of California, San Diego, La Jolla, CA, and approved September 18, 2015 (received for review August 19, 2015)

In plants, small groups of pluripotent stem cells called axillary meristems are required for the formation of the branches and flowers that eventually establish shoot architecture and drive reproductive success. To ensure the proper formation of new axillary meristems, the specification of boundary regions is required for coordinating their development. We have identified two maize genes, *BARREN INFLORESCENCE1* and *BARREN INFLORESCENCE4* (*BIF1* and *BIF4*), that regulate the early steps required for inflorescence formation. *BIF1* and *BIF4* encode AUXIN/INDOLE-3-ACETIC ACID (Aux/IAA) proteins, which are key components of the auxin hormone signaling pathway that is essential for organogenesis. Here we show that BIF1 and BIF4 are integral to auxin signaling modules that dynamically regulate the expression of BARREN STALK1 (BA1), a basic helix-loop-helix (bHLH) transcriptional regulator necessary for axillary meristem formation that shows a striking boundary expression pattern. These findings suggest that auxin signaling directly controls boundary domains during axillary meristem formation and define a fundamental mechanism that regulates inflorescence architecture in one of the most widely grown crop species.

auxin signaling | inflorescence development | axillary meristems | maize | boundary domains

Plant shoot architecture is primarily determined by small groups of pluripotent stem cells called meristems. Throughout their life cycle, plants generate different types of meristems whose main function is to drive postembryonic organ initiation. In particular, reproductive axillary meristems (AMs) form branches and flowers that contribute to naturally occurring variations in inflorescence architecture. Genes regulating AM function have been frequent targets during crop domestication (1), and several recent examples have demonstrated how modulation of meristem activity can directly affect yields (2, 3).

Mutations that affect the initial steps in reproductive AM formation often result in the formation of characteristic pin-like inflorescences. Several such mutants, first described in *Arabidopsis*, are predominantly affected in genes related to the hormone auxin, including *PIN-FORMED1* (*PIN1*) and *MONOPTEROS* (*MP*) (4–6). Analysis of these and other mutants has established that auxin is central to the generation of all primordia. Auxin is polarly transported to the site of primordia initiation, where it is perceived by the nuclear auxin receptor TRANSPORT INHIBITOR RESPONSE1/AUXIN SIGNALING F-BOX PROTEIN (TIR1/AFB), part of an E3 ligase that rapidly degrades AUXIN/INDOLE-3-ACETIC ACID (Aux/IAA) coreceptor proteins and disrupts their recruitment of TOPLESS (TPL) corepressors. The auxin-dependent degradation of Aux/IAAs frees interacting activating AUXIN RESPONSE FACTOR (ARF) transcription factors from TPL repression, allowing them to activate downstream genes (7). Although it is known that ARFs bind to auxin-responsive cis-regulatory elements (AuxREs) composed of the core TGTC sequence, few downstream developmental pathways have been characterized (8–13). All components of the auxin signaling machinery are encoded by multimember gene families, and the combinatorial complexity afforded by the various members may contribute to auxin's capacity to regulate multiple aspects of plant development (14–19). How auxin regulatory components work together to trigger specific developmental responses in reproductive tissues, including grain-bearing inflorescences, remains an unaddressed aspect with important implications for crop productivity and improvement.

Grasses such as maize and rice contain inflorescences with multiple types of specialized reproductive AMs. In maize, these AMs give rise to two types of inflorescences: kernel-laden ears and tassels optimized for pollen dispersal. Maize inflorescence mutants with a pin-like phenotype are classically called *barren* mutants, with the founding member, *barren stalk1* (*ba1*), originally described more than 85 years ago. *BA1* encodes a basic helix-loop-helix (bHLH) transcription factor (20), and loss-of-function *ba1* mutants produce earless plants with tassels devoid of reproductive AMs. Additional *barren* mutants led to the discovery of proteins involved in auxin transport and biosynthesis (21–23), indicating that auxin-related defects often underlie this family of mutants.

Here we provide insight into the molecular mechanisms of auxin signaling during reproductive AM initiation by characterizing two *barren* mutants of maize. We identify the Aux/IAA proteins BARREN INFLORESCENCE1 and BARREN INFLORESCENCE4 (BIF1 and BIF4) and show that they are essential for organogenesis in maize inflorescences. We demonstrate that BIF1 and BIF4 are integral parts of functionally redundant signaling modules that directly control the transcription of *BA1*, thereby establishing critical boundary domains that ensure the formation of new AMs.

Significance

Axillary meristems are groups of plant pluripotent stem cells responsible for the formation of secondary axes of growth, such as branches and flowers. A crucial step in the initiation of new axillary meristems is the establishment of boundary domains that allow organ separation and prevent fusion defects during development. This work provides clues on the molecular mechanism by which the plant hormone auxin is involved in the formation of axillary meristems in maize inflorescences. Auxin signaling modules containing the AUXIN/INDOLE-3-ACETIC ACID proteins BARREN INFLORESCENCE1 and BARREN INFLORESCENCE4 and AUXIN RESPONSE FACTOR (ARF) transcriptional regulators are involved in the regulation of the boundary basic helix-loop-helix transcription factor BARREN STALK1, suggesting auxin is directly responsible for establishing boundary regions.

Author contributions: M.G., B.L.M., S.M., J.L.N., and A.G. designed research; M.G., Q.L., B.L.M., S.M., W.L., C.G., S.F., J.R., and A.G. performed research; R.M. contributed new reagents analytic tools; M.G., Q.L., B.L.M., S.M., J.L.N., and A.G. analyzed data; and M.G., B.L.M., S.M., and A.G. wrote the paper.

The authors declare no conflict of interest.

This article is a PNAS Direct Submission.

[1]M.G. and Q.L. contributed equally to this work.

[2]To whom correspondence should be addressed. Email: agallavotti@waksman.rutgers.edu.

This article contains supporting information online at www.pnas.org/lookup/suppl/doi:10.1073/pnas.1516473112/-/DCSupplemental.

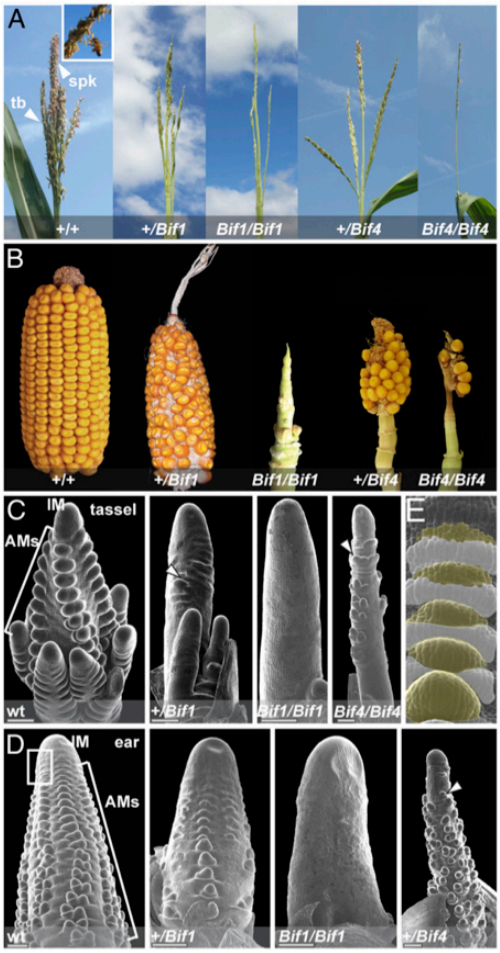

Fig. 1. *Bif1* and *Bif4* mutant phenotype. (*A*) Mature tassel phenotype. Normal tassels produce spikelets and flowers that are reduced in both mutants. (*Inset*) Spikelets with protruding anthers. tb, tassel branch. spk, spikelet. (*B*) Mature ear phenotype. (*C–E*) Scanning electron microscope image of early tassel and ear development in normal and mutant plants. Arrowheads point to a few axillary meristems forming in mutant plants. Primordia are absent in homozygous *Bif1* mutants. Boxed region in *D* marks the peripheral zone of the IM. (*E*) Close-up of the peripheral zone of the IM. White and yellow colors mark suppressed bract primordia and AMs, respectively. Note the acropetal development of primordia (from top, younger, to bottom, older).

Results

***Bif1* and *Bif4* Are Semidominant Mutants Affected in Reproductive Organogenesis.** The semidominant *barren* mutants *Bif1* (24, 25) and *Bif4* were originally isolated from ethyl methanesulfonate (EMS) mutagenesis screens and displayed similar inflorescence defects. After undergoing a normal vegetative-to-reproductive transition, *Bif1* and *Bif4* plants developed tassels with reduced numbers of branches and spikelets, the floral unit of grass inflorescences (Fig. 1*A* and Fig. S1). Ears appeared shortened and displayed disorganized rows of kernels, as well as areas completely devoid of kernels (Fig. 1*B*). These defects were more pronounced in homozygous *Bif1* and *Bif4* plants (Fig. 1 *A* and *B* and Fig. S1).

SEM analysis of young inflorescences revealed that the *Bif1* and *Bif4* phenotypes resulted from defects in primordium initiation at the peripheral zone of the apical inflorescence meristem (IM), where organogenesis occurs (Fig. 1 *C* and *D*). Normally in maize inflorescences, the first primordia to appear are suppressed bracts (SBs; Fig. 1*E*). These structures are followed shortly after by the formation of a series of reproductive AMs (branch, spikelet-pair, spikelet and floral meristems) that initiate at the bract axils and eventually give rise to spikelets and flowers (Fig. 1 *C* and *D*). In *Bif1* tassels and ears, a severe reduction in the initiation of AMs was observed (Fig. 1 *C* and *D*). Homozygous mutants produced smooth structures (albeit with a normal IM), indicating that both bract primordia and AM initiation were defective. Similar defects were also observed in *Bif4* mutant tassels and ears (Fig. 1 *C* and *D*). Double-mutant analysis of *Bif1* and *Bif4* showed a strong synergistic effect (Fig. 2*A*). In +/*Bif1*;+/*Bif4* tassels and ears, all primordia were missing, resulting in pin-like inflorescences in which organogenesis was often completely impaired (Fig. 2 *A* and *B*). Because of the missing floral organs, we were only able to generate +/*Bif1*;*Bif4*/*Bif4* plants that resembled +/*Bif1*;+/*Bif4* double heterozygotes. No significant vegetative defects were observed in either single or double mutants (Fig. S1). On the basis of this analysis, we conclude that *BIF1* and *BIF4* are essential for organogenesis during inflorescence development and function together in the initiation of lateral primordia (SBs and AMs).

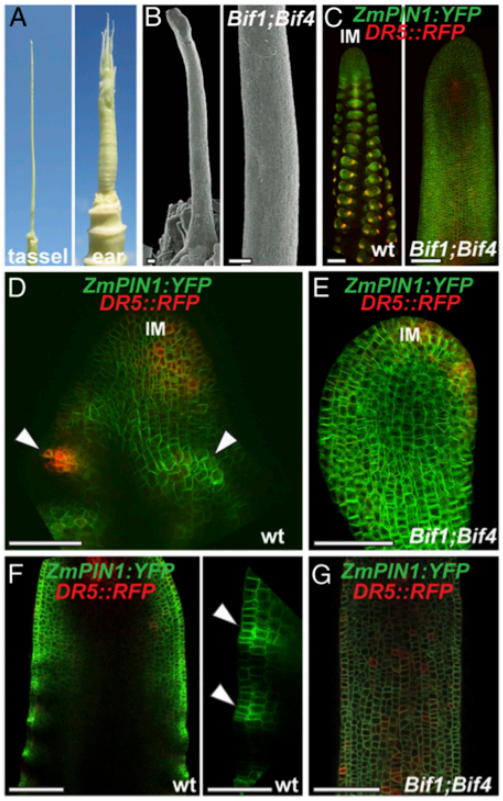

Fig. 2. *BIF1* and *BIF4* are required for patterning of primordium initiation. (*A*) Mature inflorescence phenotype of the double heterozygous *Bif1* and *Bif4* mutant. (*B*) Scanning electron microscope image of a young *Bif1*;*Bif4* tassel showing lack of primordium initiation. (Scale bars, 100 μm.) (*C*) Confocal images of normal and *Bif1*;*Bif4* tassels expressing ZmPIN1a-YFP fusion proteins and DR5::RFP. (*D* and *E*) Maximum projections of confocal images of wild-type and *Bif1*;*Bif4* mutant IMs. (*F* and *G*) Confocal images of the peripheral zone of immature tassels showing up-regulation of ZmPIN1a-YFP signals in normal tassels (*F*, arrowheads in close-up right panel) that is missing in double *Bif1*;*Bif4* mutants (*G*).

Because of the striking similarity between the inflorescences of the double *+/Bif1;+/Bif4* mutant and *Arabidopsis* auxin transport mutants, we used confocal microscopy to investigate how the expression of the membrane-localized auxin efflux transporter ZmPIN1a:YFP was affected in *+/Bif1;+/Bif4* inflorescences. We simultaneously monitored auxin signaling using the *DR5rev::RFP* reporter (26) (Fig. 2 and Fig. S2). Whereas in wild-type immature tassels the patterning of primordia at the periphery of the IM was marked by increased ZmPIN1a-YFP and RFP signals, in *+/Bif1;+/Bif4* plants, this patterning was completely absent ($n = 5$; Fig. 2 *C*–*G* and Fig. S2). This indicates that although ZmPIN1a is still expressed in *+/Bif1;+/Bif4* IMs, the normal auxin-driven patterning of primordia is completely disrupted and suggests that BIF1 and BIF4 are required for the upregulation of PIN-mediated auxin transport. In double-mutant tassels, RFP signal was observed in the IM, confirming that the IM is unaffected (Fig. 2*E*), and in occasional cells and inner tissue along the main axis (Fig. 2*G* and Fig. S2), suggesting that auxin signaling is not completely disrupted in these plants.

***Bif1* and *Bif4* Harbor Mutations in *Aux/IAAs* Expressed in the Early Stages of Inflorescence Development.** The underlying molecular cause of the *Bif1* mutant has remained unknown since its discovery in 1977 (24). On the basis of its auxin-related phenotype and semidominance, we reasoned that *BIF1* might encode one of the 38 maize *Aux/IAA* genes (27, 28), known negative regulators of auxin signaling that give rise to dominant mutants (7). We searched the maize genome for *Aux/IAAs* that were located in the region of chromosome 8, where the *BIF1* locus was previously mapped (25). Single-amino acid substitutions in the degron domain of GRMZM2G130953/IAA27 were observed in all *Bif1* alleles (Fig. 3 *C* and *D*). The degron domain is a highly conserved amino acid sequence found in Aux/IAA proteins that confers auxin-induced degradation and is consistently mutated in all known dominant *aux/iaa* mutants. Because *Bif4* showed an identical phenotype to *Bif1*, we used a similar approach, which revealed an amino acid substitution in the degron domain of GRMZM5G864847/IAA20 (Fig. 3*B*). These results show that *BIF1* encodes an Aux/IAA protein, and equally suggest it for *BIF4*.

Phylogenetic analysis of *BIF1/IAA27* and *BIF4/IAA20* revealed that the two genes belong to separate clades and share only 39% amino acid identity (Fig. S3*A*). To examine their expression pattern, we carried out RNA in situ hybridizations in developing inflorescences (Fig. 3 *C*–*J*). Both genes were broadly expressed in the IM, and in its peripheral zone in both tassels and ears (Fig. 3 *C*, *E*, *G*, and *I*). As the newly formed AMs developed, *BIF1* and *BIF4* showed strong expression in the central zone of all AMs (Fig. 3 *D*, *F*, *H*, and *J*). Similarly, maize transgenic lines expressing a VENUS-BIF4 fusion protein driven by the endogenous *BIF4* promoter showed VENUS-BIF4 protein in AMs (Fig. 3*K*). These expression patterns are consistent with the mutant phenotypes and support a role for *BIF1* and *BIF4* in initiating reproductive primordia.

BIF1 and BIF4 Show Distinct Auxin-Response Dynamics. Despite having similar phenotypes and localization patterns, *BIF1* and *BIF4* displayed different degrees of auxin inducibility when subjected to exogenous auxin treatments (Fig. 3*L*), as previously reported for other *Aux/IAA* genes. Because auxin signaling relies on the rapid degradation of Aux/IAA proteins, we monitored the stability of the two proteins in the presence of auxin, using a yeast synthetic assay (29, 30). We engineered yeast expressing BIF1 or BIF4 and monitored their degradation dynamics in combination with the *Arabidopsis* auxin receptor TIR1 (Fig. 3*M*). This analysis revealed that BIF1 displayed a slower rate of degradation than BIF4. We also tested the degradation rates of mutant alleles of BIF1 and BIF4, and all showed strong auxin insensitivity (Fig. 3*M*). These data, together with the observation that the same mutation in IAA20 and BIF1-N1440 stabilizes both proteins, provided additional confirmation that the *Bif4* phenotype is caused by a mutation in *IAA20*. The degradation rate of BIF1 was slower compared with the closest putative co-ortholog AtIAA15 and with other closely related Aux/IAAs (Fig. 3*N* and Fig. S4). In contrast, we observed similar degradation rates of BIF4 compared with its respective co-orthologs in *Arabidopsis*, suggesting there may be an evolutionarily conserved sequence-based bias for the stability of certain Aux/IAAs. Overall, this analysis indicates that *BIF1* and *BIF4* have unique auxin-response dynamics, suggesting the two genes may have subtle functional differences.

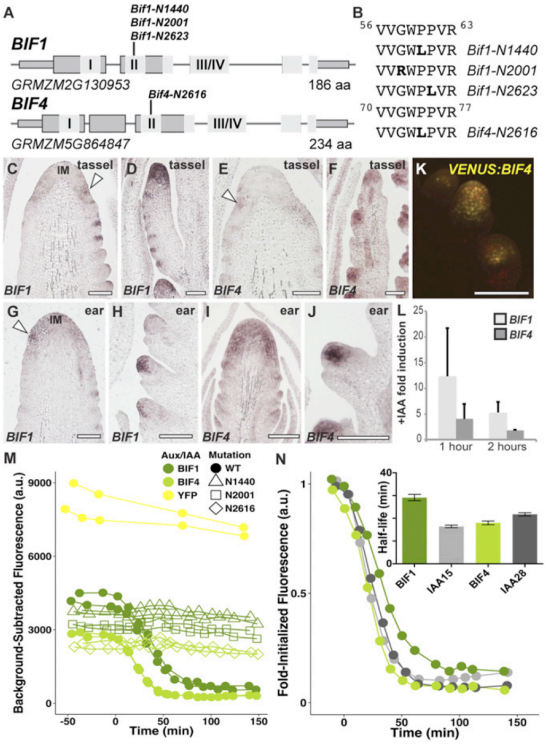

Fig. 3. *BIF1* and *BIF4* encode Aux/IAA proteins. (*A*) Schematic representation of *BIF1* and *BIF4* genes. Exons are depicted as gray rectangles. I and II represent the EAR repressor motif and the degron domain; III/IV corresponds to the dimerization domain. (*B*) The amino acid sequence of the degron domains of BIF1 and BIF4 and the mutations identified. (*C*–*J*) mRNA in situ hybridizations of immature inflorescences with *BIF1* and *BIF4* antisense probes. Arrowheads, localized signals at the peripheral zone of the IM. (*D* and *F*) Branch meristems are shown; (*H* and *J*) spikelet meristems. (Scale bars, 100 μm.) (*K*) Confocal image of VENUS-BIF4 in spikelet meristems. (*L*) Auxin inducibility of *BIF1* and *BIF4*. Error bars show SD. (*M* and *N*) Auxin-induced degradation profiles of normal and mutant BIF1 and BIF4 proteins.

Maize-Activating ARFs Are Expressed in Defined Domains of the Inflorescence Meristem. Aux/IAA proteins interact with and regulate the activity of ARF transcription factors. To determine which ARFs function with BIF1 and BIF4, we first took a reverse genetic approach. When grown to the adult stage, the *Arabidopsis mp* mutant shows pin-like inflorescences (5). Therefore, we hypothesized that the closest maize homologs of *MP*, *ZmARF4*, and *ZmARF29* (duplicated genes with 96% aa similarity; Fig. S3*B*) would be likely candidates to work with BIF1 and BIF4 in reproductive organogenesis. We identified exonic transposon insertions in both genes (Fig. S5*A*); however, double *arf4;arf29* mutants showed no phenotype in either shoot or reproductive development.

Suspecting *ARFs* may work redundantly, we mined public transcriptome databases and found 13 maize-activating *ARFs* expressed in inflorescences. To obtain an expression map of these *ARFs* and assess whether they were coexpressed with *BIF1* and *BIF4*, we performed in situ hybridizations on immature inflorescences (Fig. S5 *B*–*D*). All *ZmARFs* except *ARF16* were expressed in specific

domains of the IM: *ARF1* and *35* showed broad expression; *ARF4*, *ARF18*, *ARF20*, *ARF22*, *ARF29*, and *ARF34* showed strong expression at the peripheral zone of the IM; and *ARF3*, *ARF27*, and *ARF30* showed narrow expression in developing primordia. Expression patterns of the different *ARFs* also varied in developing AMs; the majority were predominantly restricted to the meristematic core of the different types of AMs (*ARF1*, *ARF4*, *ARF9*, *ARF16*, *ARF20*, *ARF22*, *ARF29*, *ARF34*, *ARF35*), and others such as *ARF3* and *ARF30* appeared localized in more restricted domains at the base of AMs and at their boundary, whereas *ARF18* and *ARF22* localized to the suppressed bracts and glume primordia (Fig. S5). Strong vasculature expression was also observed for *ARF4*, *ARF9*, *ARF20*, and *ARF29*. Overall, these domains largely overlapped with those of *BIF1* and *BIF4*.

To determine whether all activating ARFs were capable of physically interacting with BIF1 and BIF4 proteins, we performed yeast 2-hybrid (Y2H) assays and detected interaction of BIF1 and BIF4 with all activating ARFs (Fig. S6). We verified by Y2H, BiFC, and in vitro pull-down that BIF1 and BIF4 interacted with REL2, a functional homolog of the *Arabidopsis* TPL corepressor (31). Furthermore, we showed that BIF1 and BIF4 homo and heterodimerize (Fig. S6 *A–C*). Overall, our expression and protein interaction data suggest functional redundancy among BIF1/BIF4-ARFs transcriptional repression modules and that multiple ARFs work together with BIF1 and BIF4 during the initial stages of reproductive organogenesis.

***BARREN STALK1* Is an Early Target of the Auxin Signaling Pathway.** One of the earliest genes expressed at the peripheral zone of the IM is *BA1*, whose mRNA expression marks a boundary domain in newly forming AMs that is necessary for meristem formation (20). Severe *ba1* mutants lack all AMs but form enlarged suppressed bracts (Fig. S7*A*). Because of the phenotypic resemblance between *ba1* and *Bif1;Bif4* mutants, we hypothesized that *BA1* may be directly regulated by transcriptional repressor complexes containing BIF1 and BIF4. To investigate this possibility, we first checked the genetic interaction between *Bif1, Bif4*, and *ba1*, using a weak, fertile allele of *ba1* (*ba1-mum1*) (20). Analysis of double *+/Bif1; ba1-mum1/ba1-mum1* and *+/Bif4;ba1-mum1/ba1-mum1* mutants showed that *ba1* strongly enhanced the phenotype of heterozygous *Bif1* and *Bif4* mutants in both tassels and ears, impairing both branch and spikelet formation (Fig. 4*A* and Fig. S7 *B* and *C*). These data suggest that *BIF1*, *BIF4*, and *BA1* function either in the same or in parallel pathways contributing to AM formation.

If BIF1 and BIF4 formed repressor complexes targeting *BA1* transcription, *BA1* expression should be down-regulated in auxin-insensitive tassels. Quantitative RT-PCR on immature *+/Bif1;+/Bif4* tassels supported this prediction, as no significant expression of *BA1* was detected (Fig. 4*B* and Fig. S7 *D* and *F*). Conversely, in situ hybridizations showed that both *BIF1* and *BIF4* expression were unchanged in strong *ba1* mutant tassels, as were *SPI1*, an auxin biosynthetic gene, *ARF4*, and *ZYB15*, a marker for SBs (Fig. 4*C*) (22, 32), suggesting that auxin biosynthesis, signaling, and SB patterning are unaffected in *ba1* mutants. Furthermore, expression of *SPI1* was observed in the peripheral zone of the IM before the appearance of *BA1*, whereas *ARFs* showed expression patterns that preceded but subsequently partially overlapped with *BA1*, indicating that *BA1* functions downstream of auxin biosynthesis and signaling (Fig. S7 *G–I*). Finally, in situ hybridizations of *BA1* and *BIF1* on consecutive sections showed that *BIF1* was broadly expressed in the peripheral zone of the IM, whereas *BA1* was present only in a small number of cells (Fig. 4*D*). However, as the AM developed, the two genes showed a striking complementary expression, with *BIF1* being expressed in the center of the meristem and *BA1* in its characteristic boundary domain (Fig. 4*E*). This analysis shows that *BA1* and *BIF1* expression patterns, although initially overlapping, are subsequently partitioned in two distinct domains of the AM: the boundary domain and the meristem center. Overall, these results are consistent with the hypothesis that BIF1 and BIF4 directly repress *BA1* transcription.

To assess whether coexpressed BIF-ARF repression modules directly bind the *BA1* promoter, we expressed a subset of

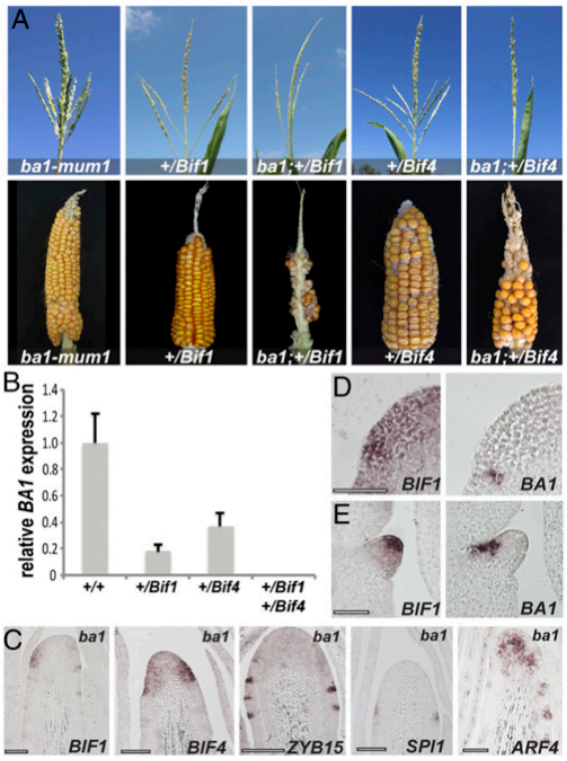

Fig. 4. Genetic and expression analysis of *ba1* mutants. (*A*) Double-mutant analysis of *Bif1* and *Bif4* with *ba1-mum1* in A619 background. (*B*) qRT-PCR of *BA1* in double *Bif1;Bif4* mutants. Error bars, SD. (*C*) In situ hybridization of immature *ba1-ref* tassels with specific markers. (Scale bars, 100 μm.) (*D* and *E*) mRNA in situ hybridizations on consecutive sections of immature inflorescences with *BIF1* and *BA1* antisense probes. (Scale bars, 50 μm.)

nonparalogous maize-activating ARFs and carried out electrophoretic mobility shift assays (EMSAs) with four regions of the ~7-kb *BA1* promoter enriched for the core TGTC AuxRE element (Fig. 5*A*). ARF4, ARF16, ARF27, ARF29, and ARF34 strongly bound to all four probes, whereas ARF22 and ARF35 bound only a subset of these regions (Fig. 5*B* and Fig. S8). Competition with unlabeled probe or mutation of the core TGTC elements inhibited binding (Fig. 5*C* and Fig. S8). No detectable binding was observed for ARF1, ARF3, ARF9, or ARF30; however, all ARFs bound to the *DR5* promoter, albeit with varying intensities (Fig. S8*B*). No ARFs bound to regions containing only a single AuxRE (Fig. 5*D*, probes E and F). These results demonstrate that various activating ARFs directly bind to the *BA1* promoter and suggest that multiple BIF1,4-ARF modules regulate the expression of *BA1* (Fig. 5*E*).

Discussion

A major outstanding question in auxin signaling is the degree of specificity existing among the various components, and whether combinatorial complexity plays a role in the multitude of processes controlled by auxin. The *Bif1* and *Bif4* mutants represent a striking case of stabilized Aux/IAAs that specifically confer phenotypes resembling the pin-like inflorescences of *Arabidopsis pin1* and *mp* mutants, indicating a specific and predominant role for both genes in reproductive organogenesis. However, previous analysis suggested a synergistic interaction of *Bif1* with *bif2*, an auxin transport mutant, during vegetative development (25), raising the possibility that other Aux/IAAs may function redundantly with BIF1 and BIF4 during shoot development.

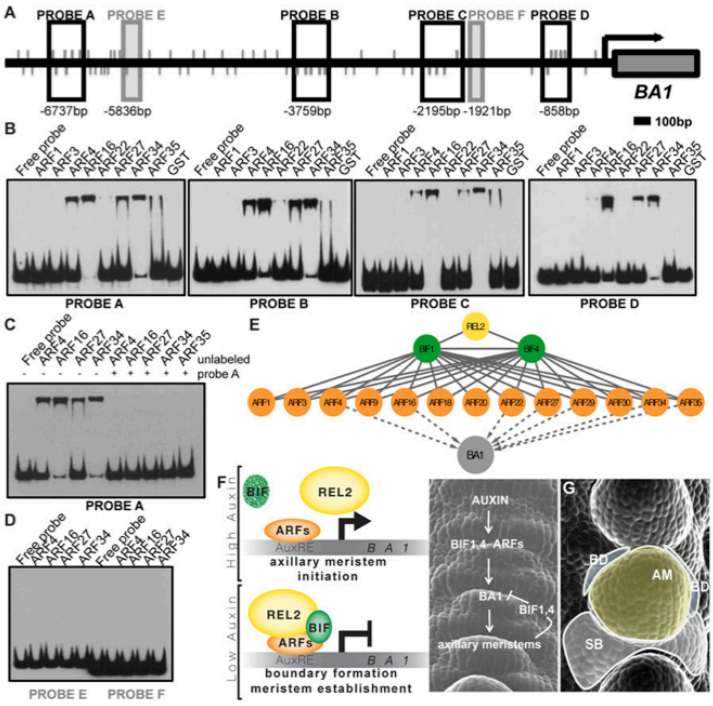

Fig. 5. *BA1* is a target of BIF/ARF transcriptional regulatory modules. (*A*) Schematic showing *BA1* genomic locus including 7 kb of putative promoter. Promoter fragments used as probes in EMSAs are shown as boxed regions. Values below boxes indicate position relative to BA1 start codon (+1). Gray lines indicate TGTC core AuxRE elements. (*B*) EMSAs show that various activating ARFs bind to BA1 promoter fragments; GST alone does not. (*C*) EMSA showing specificity of ARF binding to probe A. Addition of unlabeled probe A outcompetes binding to labeled probe A. (*D*) EMSA showing ARFs do not bind non-TGTC-enriched promoter fragments E and F. (*E*) Summary of protein–protein (solid lines) and protein–DNA (dashed lines) interactions identified in this study. (*F*) Molecular model of organogenesis in the peripheral zone of maize IMs. (*G*) Diagram of the resulting functional domains (false-colored). SB, suppressed bract; BD, boundary domain; AM, axillary meristem.

Stabilizing degron mutations in *Arabidopsis Aux/IAA* genes that are closely related to *BIF1* (*AXR2/IAA7*, *AXR3/IAA17*, *SLR/IAA14*, and *IAA16*) and *BIF4* (*IAA28*) (Fig. S3) were reported to show decreased shoot branching, dwarfism, and partial infertility (33–38). Some of these phenotypes may point to functional homology, as mutations in both species affect reproductive branching. Alternatively, the lack of severe pin-like inflorescence phenotypes in *Arabidopsis* may indicate that BIF1 and BIF4 were specifically co-opted for patterning maize reproductive AMs. Although *Arabidopsis mp* mutants display strong pleiotropic defects, no phenotype was observed in the orthologous maize *arf4;arf29* double mutants. Overall, our findings from maize suggest specificity among Aux/IAA function, as well as redundancy among activating ARFs. However, *ARF* expression patterns suggest that although several *ARFs* are expressed in the peripheral zone of the IM early in inflorescence development, they subsequently acquire more specific domains of expression (AMs vs. suppressed bracts and glumes).

The reproductive defects observed in both mutants suggest that the function of BIF1 and BIF4 is to negatively regulate organogenesis in the peripheral zone of the IM, and that their auxin-induced degradation is necessary for new primordia to initiate. Analysis of the *ZmPIN1a-YFP* reporter line in *+/Bif1;+/Bif4* tassels also indicates that BIF1 and BIF4 are part of a core signaling mechanism that regulates the patterning of maize inflorescences and is required for the local up-regulation of the polar auxin transport components necessary for organogenesis. Previous reports suggested that auxin negatively regulates boundary domain genes during embryo and leaf development (39, 40). Together with a general role in organogenesis, our data support a model in which multiple auxin signaling modules involving BIF1 and BIF4 directly regulate the formation of boundary regions during AM initiation (Fig. 5*F*). In this model, auxin, first synthesized and transported in the peripheral zone of the IM (22, 26), triggers the transcription of the early-response genes *BIF1* and *BIF4* (Fig. 3*L*). Both BIF1 and BIF4 proteins are, in turn, rapidly degraded in the presence of auxin (Fig. 3*M*), and activating *ARFs* expressed in this region can promote transcription of their targets to initiate organogenesis. Among these targets, *BA1* is specifically required for initiating AMs (20). As meristems develop, auxin is transported to the inner tissue for vasculature formation and to nearby areas to promote new primordia initiation (41, 42). Therefore, in the central zone of developing AMs, BIF1 and BIF4 are no longer efficiently degraded and can form stable repressor complexes on the *BA1* promoter. This repression restricts *BA1* expression and establishes boundary domains essential for AM formation (Fig. 5 *F* and *G*).

Recent reports in tomato and *Arabidopsis* have established that low auxin at the adaxial boundary of leaf primordia is necessary for vegetative AM formation (43–45). Whether a similar mechanism is established during reproductive development is not known. In maize inflorescences, SB (modified leaves) and AM primordia, although initially overlapping, subsequently resolve and acquire distinct identities (46), making it inherently difficult to test whether auxin minima exist at the axils of SBs. Nonetheless, the auxin-dependent regulation of *BA1* transcription, a key regulator of maize inflorescence architecture, ensures that axillary meristems are established throughout reproductive development. Our results pave the way for future biotechnological strategies aimed at modifying reproductive structures. For example, by modulating the auxin-dependent stability of BIF1 and BIF4 proteins, using engineered variants of their degron motifs (47), it may be possible to alter the position and number of primordia initiated by the IM. Similar strategies could be used in other species as well, allowing optimization of inflorescence architecture in crops.

Methods

All *Bif1* and *Bif4* alleles were generated by EMS mutagenesis by Gerry Neuffer. The Mutator transposon insertion lines were obtained from the UniformMu collection (mu1021266; *ARF4*) (48), and the Pioneer TUSC population (BT94 27C-05 and BT94 27E-08; *ARF29*) (49). Experimentally verified full-length cDNAs of *BIF1* and *BIF4* genes correspond to *GRMZM2G130953_T02* and *GRMZM5G864847_T01*, respectively (GenBank KT819172 and KT819173).

Full-length *ZmARFs* ORFs were cloned from B73 mixed-stage inflorescence cDNA. EMSAs were performed using recombinant ARFs and the Lightshift Chemiluminescent kit. Auxin-induced degradation assays were carried out as in Havens et al. (29). In situ hybridizations, qRT-PCRs, analysis of transgenic lines, and detailed description of all methods are provided in *SI Experimental Procedures*.

ACKNOWLEDGMENTS. We thank Gerry Neuffer and the Maize Inflorescence Project for generating mutants; the Maize Genetics Cooperation Stock Center for providing seeds; UniformMu for insertion lines; Marc Probasco for field and greenhouse care; David Jackson for SEM use; Sharon Stanfield for preliminary experiments; and Robert Schmidt, Brian Crawford, Rhiannon Macrae, and Mithu Chatterjee for critical reading of the manuscript. We acknowledge funding from National Science Foundation (IOS-08207291/ 1114484 to A.G. and S.M.; MCB-1411949 to J.L.N.), NIH (R01-GM107084 to J.L.N.; F32CA180514 to B.L.M.), the China Scholarship Council (Q.L.), and the Waksman Institute (A.G.). Any opinion, findings, and conclusions or recommendations expressed in this material are those of the authors and do not necessarily reflect the views of the National Science Foundation.

1. Doebley JF, Gaut BS, Smith BD (2006) The molecular genetics of crop domestication. *Cell* 127(7):1309–1321.
2. Bommert P, Nagasawa NS, Jackson D (2013) Quantitative variation in maize kernel row number is controlled by the FASCIATED EAR2 locus. *Nat Genet* 45(3):334–337.
3. Park SJ, et al. (2014) Optimization of crop productivity in tomato using induced mutations in the florigen pathway. *Nat Genet* 46(12):1337–1342.
4. Gälweiler L, et al. (1998) Regulation of polar auxin transport by AtPIN1 in Arabidopsis vascular tissue. *Science* 282(5397):2226–2230.
5. Przemeck GK, Mattsson J, Hardtke CS, Sung ZR, Berleth T (1996) Studies on the role of the Arabidopsis gene MONOPTEROS in vascular development and plant cell axialization. *Planta* 200(2):229–237.
6. Hardtke CS, Berleth T (1998) The Arabidopsis gene MONOPTEROS encodes a transcription factor mediating embryo axis formation and vascular development. *EMBO J* 17(5):1405–1411.
7. Salehin M, Bagchi R, Estelle M (2015) SCFTIR1/AFB-based auxin perception: Mechanism and role in plant growth and development. *Plant Cell* 27(1):9–19.
8. Okushima Y, Fukaki H, Onoda M, Theologis A, Tasaka M (2007) ARF7 and ARF19 regulate lateral root formation via direct activation of LBD/ASL genes in Arabidopsis. *Plant Cell* 19(1):118–130.
9. Schlereth A, et al. (2010) MONOPTEROS controls embryonic root initiation by regulating a mobile transcription factor. *Nature* 464(7290):913–916.
10. Yamaguchi N, et al. (2013) A molecular framework for auxin-mediated initiation of flower primordia. *Dev Cell* 24(3):271–282.
11. Oh E, et al. (2014) Cell elongation is regulated through a central circuit of interacting transcription factors in the Arabidopsis hypocotyl. *eLife* 3:3.
12. Crawford BC, et al. (2015) Plant development. Genetic control of distal stem cell fate within root and embryonic meristems. *Science* 347(6222):655–659.
13. Ripoll JJ, et al. (March 30, 2015) microRNA regulation of fruit growth. *Nature Plants*, 10.1038/nplants.2015.36.
14. Weijers D, et al. (2005) Developmental specificity of auxin response by pairs of ARF and Aux/IAA transcriptional regulators. *EMBO J* 24(10):1874–1885.
15. Vernoux T, et al. (2011) The auxin signalling network translates dynamic input into robust patterning at the shoot apex. *Mol Syst Biol* 7:508.
16. Guilfoyle TJ, Hagen G (2012) Getting a grasp on domain III/IV responsible for Auxin Response Factor-IAA protein interactions. *Plant Sci* 190:82–88.
17. Boer DR, et al. (2014) Structural basis for DNA binding specificity by the auxin-dependent ARF transcription factors. *Cell* 156(3):577–589.
18. Nanao MH, et al. (2014) Structural basis for oligomerization of auxin transcriptional regulators. *Nat Commun* 5:3617.
19. Korasick DA, et al. (2014) Molecular basis for AUXIN RESPONSE FACTOR protein interaction and the control of auxin response repression. *Proc Natl Acad Sci USA* 111(14):5427–5432.
20. Gallavotti A, et al. (2004) The role of barren stalk1 in the architecture of maize. *Nature* 432(7017):630–635.
21. McSteen P, et al. (2007) barren inflorescence2 Encodes a co-ortholog of the PINOID serine/threonine kinase and is required for organogenesis during inflorescence and vegetative development in maize. *Plant Physiol* 144(2):1000–1011.
22. Gallavotti A, et al. (2008) sparse inflorescence1 encodes a monocot-specific YUCCA-like gene required for vegetative and reproductive development in maize. *Proc Natl Acad Sci USA* 105(39):15196–15201.
23. Phillips KA, et al. (2011) vanishing tassel2 encodes a grass-specific tryptophan aminotransferase required for vegetative and reproductive development in maize. *Plant Cell* 23(2):550–566.
24. Neuffer M, Coe E, Wessler S (1997) *Mutants of Maize. 1997* (Cold Spring Harbor Laboratory Press, Cold Spring Harbor, New York).
25. Barazesh S, McSteen P (2008) Barren inflorescence1 functions in organogenesis during vegetative and inflorescence development in maize. *Genetics* 179(1):389–401.
26. Gallavotti A, Yang Y, Schmidt RJ, Jackson D (2008) The Relationship between auxin transport and maize branching. *Plant Physiol* 147(4):1913–1923.
27. Ludwig Y, Zhang Y, Hochholdinger F (2013) The maize (Zea mays L.) AUXIN/INDOLE-3-ACETIC ACID gene family: Phylogeny, synteny, and unique root-type and tissue-specific expression patterns during development. *PLoS One* 8(11):e78859.
28. Burdo B, et al. (2014) The Maize TFome–development of a transcription factor open reading frame collection for functional genomics. *Plant J* 80(2):356–366.
29. Havens KA, et al. (2012) A synthetic approach reveals extensive tunability of auxin signaling. *Plant Physiol* 160(1):135–142.
30. Pierre-Jerome E, Jang SS, Havens KA, Nemhauser JL, Klavins E (2014) Recapitulation of the forward nuclear auxin response pathway in yeast. *Proc Natl Acad Sci USA* 111(26):9407–9412.
31. Gallavotti A, et al. (2010) The control of axillary meristem fate in the maize ramosa pathway. *Development* 137(17):2849–2856.
32. Whipple CJ, et al. (2010) A conserved mechanism of bract suppression in the grass family. *Plant Cell* 22(3):565–578.
33. Rogg LE, Lasswell J, Bartel B (2001) A gain-of-function mutation in IAA28 suppresses lateral root development. *Plant Cell* 13(3):465–480.
34. Nagpal P, et al. (2000) AXR2 encodes a member of the Aux/IAA protein family. *Plant Physiol* 123(2):563–574.
35. Leyser HM, Pickett FB, Dharmasiri S, Estelle M (1996) Mutations in the AXR3 gene of Arabidopsis result in altered auxin response including ectopic expression from the SAUR-AC1 promoter. *Plant J* 10(3):403–413.
36. Fukaki H, Tameda S, Masuda H, Tasaka M (2002) Lateral root formation is blocked by a gain-of-function mutation in the SOLITARY-ROOT/IAA14 gene of Arabidopsis. *Plant J* 29(2):153–168.
37. Muto H, Watahiki MK, Nakamoto D, Kinjo M, Yamamoto KT (2007) Specificity and similarity of functions of the Aux/IAA genes in auxin signaling of Arabidopsis revealed by promoter-exchange experiments among MSG2/IAA19, AXR2/IAA7, and SLR/IAA14. *Plant Physiol* 144(1):187–196.
38. Rinaldi MA, Liu J, Enders TA, Bartel B, Strader LC (2012) A gain-of-function mutation in IAA16 confers reduced responses to auxin and abscisic acid and impedes plant growth and fertility. *Plant Mol Biol* 79(4-5):359–373.
39. Furutani M, et al. (2004) PIN-FORMED1 and PINOID regulate boundary formation and cotyledon development in Arabidopsis embryogenesis. *Development* 131(20): 5021–5030.
40. Bilsborough GD, et al. (2011) Model for the regulation of Arabidopsis thaliana leaf margin development. *Proc Natl Acad Sci USA* 108(8):3424–3429.
41. Benková E, et al. (2003) Local, efflux-dependent auxin gradients as a common module for plant organ formation. *Cell* 115(5):591–602.
42. Heisler MG, et al. (2005) Patterns of auxin transport and gene expression during primordium development revealed by live imaging of the Arabidopsis inflorescence meristem. *Curr Biol* 15(21):1899–1911.
43. Wang Q, Kohlen W, Rossmann S, Vernoux T, Theres K (2014) Auxin Depletion from the Leaf Axil Conditions Competence for Axillary Meristem Formation in Arabidopsis and Tomato. *Plant Cell* 26(5):2068–2079.
44. Qi J, et al. (2014) Auxin depletion from leaf primordia contributes to organ patterning. *Proc Natl Acad Sci USA* 111(52):18769–18774.
45. Wang Y, et al. (2014) The Stem Cell Niche in Leaf Axils Is Established by Auxin and Cytokinin in Arabidopsis. *Plant Cell* 26(5):2055–2067.
46. Chuck G, Whipple C, Jackson D, Hake S (2010) The maize SBP-box transcription factor encoded by tasselsheath4 regulates bract development and the establishment of meristem boundaries. *Development* 137(8):1243–1250.
47. Guseman JM, et al. (2015) Auxin-induced degradation dynamics set the pace for lateral root development. *Development* 142(5):905–909.
48. Settles AM, et al. (2007) Sequence-indexed mutations in maize using the UniformMu transposon-tagging population. *BMC Genomics* 8:116.
49. Bensen RJ, et al. (1995) Cloning and characterization of the maize An1 gene. *Plant Cell* 7(1):75–84.
50. Gallavotti A, et al. (2011) BARREN STALK FASTIGIATE1 is an AT-hook protein required for the formation of maize ears. *Plant Cell* 23(5):1756–1771.
51. Bolduc N, et al. (2012) Unraveling the KNOTTED1 regulatory network in maize meristems. *Genes Dev* 26(15):1685–1690.
52. Eveland AL, et al. (2014) Regulatory modules controlling maize inflorescence architecture. *Genome Res* 24(3):431–443.
53. Xing H, et al. (2011) Genome-wide identification and expression profiling of auxin response factor (ARF) gene family in maize. *BMC Genomics* 12:178.
54. Edgar RC (2004) MUSCLE: A multiple sequence alignment method with reduced time and space complexity. *BMC Bioinformatics* 5:113.
55. Darriba D, Taboada GL, Doallo R, Posada D (2011) ProtTest 3: Fast selection of best-fit models of protein evolution. *Bioinformatics* 27(8):1164–1165.
56. Jones DT, Taylor WR, Thornton JM (1992) The rapid generation of mutation data matrices from protein sequences. *Comput Appl Biosci* 8(3):275–282.
57. Ronquist F, et al. (2012) MrBayes 3.2: Efficient Bayesian phylogenetic inference and model choice across a large model space. *Syst Biol* 61(3):539–542.
58. Gibson DG, et al. (2009) Enzymatic assembly of DNA molecules up to several hundred kilobases. *Nat Methods* 6(5):343–345.
59. Frame BR, et al. (2002) Agrobacterium tumefaciens-mediated transformation of maize embryos using a standard binary vector system. *Plant Physiol* 129(1):13–22.
60. Arabidopsis Interactome Mapping C; Arabidopsis Interactome Mapping Consortium (2011) Evidence for network evolution in an Arabidopsis interactome map. *Science* 333(6042):601–607.
61. Remington DL, Vision TJ, Guilfoyle TJ, Reed JW (2004) Contrasting modes of diversification in the Aux/IAA and ARF gene families. *Plant Physiol* 135(3):1738–1752.

Supporting Information

Galli et al. 10.1073/pnas.1516473112

SI Experimental Procedures

Plant Material and Phenotyping. All *Bif1* and *Bif4* alleles were obtained from the Maize Genetics Cooperation Stock Center. *Bif1-N2623* and *Bif4-N2616* were previously designated as *Bif*-N2623* and *Bif*-N2616*. The mutants used for all phenotypic analysis were introgressed in B73 or A619 with a minimum of two backcrosses. The *ba1-mum1* allele (20) was introgressed in (backcross) A619, where it shows a weak phenotype. Analysis of double *Bif1;ba1-mum1* and *Bif4;ba1-mum1* were carried out in BC2 and BC4 (backcross) A619 populations, respectively. For quantification of phenotypic defects, we followed previous protocols (50). The quantifications of the single- and double-mutant phenotypes in Fig. S1 were conducted in B73 and A619 backgrounds, respectively. Student *t*-test was used for statistical analysis.

Cloning of *BIF1* and *BIF4* and Phylogenetic Analysis of ZmAux/IAAs and ZmARFs. *Bif1* was previously mapped to chromosome 8 (24, 25). Two Aux/IAAs (*GRMZM2G126422* and *GRMZM2G130953*) were found to reside in the mapping window. Sequencing of both genes in homozygous *Bif1* mutants revealed single-amino acid substitution in all three alleles of *GRMZM2G130953*. The *Bif4* mutant was rough mapped by bulk segregant analysis in a BC1 mapping population, using 39 simple sequence repeat (SSR) markers across the genome, selected on MaizeGDB. The *BIF4* locus mapped between markers umc1014 and umc2170 on chromosome 6, with perfect linkage to bnlg1136 (0 recombinants out of 20 chromosomes).

Thirty-eight *ZmAux/IAA* gene sequences were compiled from Ludwig et al. and Burdo et al. (27, 28), following the nomenclature adopted in these publications. Gene models were verified or manually corrected using publicly available (51, 52) RNA-seq data visualized in the IGV browser (Broad Institute). *ZmIAA35*, *ZmIAA36*, *ZmIAA38*, *ZmIAA39*, *ZmIAA40*, and *ZmIAA41* were excluded from our analysis because of the lack of expression evidence. Thirty-two *ZmARF* gene sequences were compiled from Burdo et al. and Xing et al. (28, 53), using the nomenclature of Burdo et al. Gene models were verified or manually corrected as described earlier for *ZmAux/IAAs*. *ZmARF6*, *ZmARF31*, *ZmARF32*, *ZmARF33*, *ZmARF37*, and *ZmARF38* were excluded from our analysis due to a lack of expression evidence in which to confirm the gene model. *GRMZM2G017187*, which corresponds to *ARF6* in Xing et al. (53), was not annotated in Burdo et al. (28). To avoid confusion, we therefore refer to this ARF as *ZmARF39*.

Sequences were imported into Mesquite 3.02 (mesquiteproject.org) and aligned using MUSCLE (54), before being adjusted manually. Regions that were too divergent to align reliably were removed and not included in subsequent analyses. The resulting ARF matrix comprised 55 taxa and 614 characters, whereas the Aux/IAA matrix comprised 67 taxa and 173 characters. ProtTest 3 (55) identified the Jones, Taylor, and Thornton (JTT) (56) substitution model, estimated portions of invariable states, an estimated gamma distribution parameter, and estimated amino acid frequencies (JTT + I + G + F) as the best-fit model of evolution for both the ARF and Aux/IAA matrices. Bayesian phylogenetic analyses were conducted using MrBayes 3.2.3 (57) on the iPlant parallel processing cluster at the University of Arizona, using a fixed JTT amino acid substitution model, four rate categories approximating a gamma distribution, four separate runs with four chains, and 4,000,000 generations. The first 25% of resulting trees were removed as burn-in. SD of split frequencies at the end of the analyses were 0.002193 (ARF) and 0.009407 (Aux/IAA), respectively.

Expression Analysis, Confocal Microscopy, and Transgenic Line Construction. For in situ hybridizations, 0.2–0.5 cm inflorescences were fixed in paraformaldehyde acetic acid (PFA). Hybridizations were carried out at 55 °C. The *BA1*, *SPI1*, and *ZYB15* probes have been described before (20, 22, 50). The antisense in situ probes for both *BIF1* and *BIF4* were synthesized by in vitro transcription (T7 RNA polymerase, Promega) of both genes cloned in pAD-GAL4 and digested with EcoRI, and encompassed the entire coding sequences. For the maize *ARF* genes, the vectors and enzymes used for probe design are listed in Table S1.

For qRT-PCR, dissected immature inflorescences were pooled (at least three per pool) from different genotypes. Two biological replicates were performed for each assay. The qScript cDNA synthesis kit was used for cDNA synthesis, and the PerfeCTa SYBR Green FastMix for amplification (Quanta Biosciences). All reactions were carried out on an Illumina Eco Real-Time PCR System and quantified using the Eco Real-Time PCR System Software v4 (Illumina). The analysis was carried out in two different genetic backgrounds, B73 and A619, with analogous results (Fig. S7). For auxin induction experiments, dissected B73 ears (0.2–0.4 cm) were incubated with 100 μM IAA in 1% DMSO, with gentle shaking at room temperature. The control samples were incubated in 1% DMSO only. After incubation, all samples were treated as described earlier. Expression levels were calculated relative to ubiquitin for IAA inductions and actin in Fig. 4. Primers used in qRT-PCR experiments are listed in Table S2.

The *ZmPIN1a-YFP* and *DR5::RFP* transgenic maize lines (26) were crossed to *Bif1* and *Bif4* mutants in A619, and subsequently the two heterozygous mutant lines were crossed together and imaged. The *VENUS-BIF4* line was imaged in the T0 generation. Reporter genes were visualized in developing tassels (0.3–0.6 cm), using a Leica SP5 confocal microscope. YFP and VENUS signals were imaged using 514 excitation and 520–575 emission. RFP signals were imaged using 594 excitation and 625–655 emission. Images were analyzed using FIJI.

A Leica DM5500B microscope equipped with a DFC450 C digital camera was used to image all in situ hybridizations. Scanning electron microscope analysis was performed as previously described (31).

The *pBIF4::VENUS:BIF4* construct was assembled using the Gibson assembly cloning method (58) and cloned into the maize transformation vector pTF101.1 digested with HindIII/EcoRI. The construct includes an 8,018-bp region upstream of the start codon and a 2,467-bp fragment downstream of the stop codon. Transformation of maize embryos by Agrobacterium infection was performed according to published protocols (59). Seven independent lines were obtained, and expression was detected in three lines.

Cloning of *ZmARFs*, Protein–Protein Interaction Assays, Protein Expression, and Electrophoretic Mobility Shift Assays. Full-length activating *ZmARFs* ORFs were cloned into the SfiI sites of pENTR223-Sfi (60), using standard restriction enzyme-based cloning. pENTR-ARF clones were recombined into pDEST-AD using LR clonase II (Life Technologies). BIF1 and BIF4 ORFs were cloned into pENTR223-Sfi and recombined into pDEST-DB, using LR clonase II. pDEST-AD and pDEST-DB clones were transformed into mating compatible yeast strains Y8800 and Y8930, respectively, using the LiAc transformation method. Mating was carried out according to standard procedures. Reporter gene activation was determined by assessing growth on −Leu/−Trp/−His +1 mM 3AT (3-amino-1,2,4-triazole) media after 3 d at 30 °C.

For pull-down experiments, *BIF1* was cloned in pGEX-4T-3, using EcoRI/XhoI sites; *pENTR223-Sfi-BIF4* was recombined in the pIX-GST vector (60). The EAR motif of BIF1 (LALTLRLP) was changed in FAFTFRFP in the *BIF1mEAR* clones. The *REL2ΔWD40* clone was previously described (31). For BiFC, *BIF1* and *REL2* were cloned in SPYCE and SPYNE vectors, whereas *BIF4* was recombined in a Gateway-compatible pCYFP vector. BiFC and in vitro pull-down experiments were performed as previously described (31).

pENTR-ARF clones were recombined into pDEST15 (Life Technologies), using LR clonase II. GST-ARF clones were subsequently transformed in BL21DE3 codon plus cells (Stratagene). Protein expression was induced with 0.4 mM IPTG (isopropyl β-D-1-thiogalactopyranoside) and carried out at 23°C for 4 h. Cells from 0.5 L media were harvested and resuspended in 10 mL HDB buffer at pH 7.3 [25 mM Hepes, 0.7 mM Na_2HPO_4, 137 mM NaCl, 5 mM KCl, 1 mM AEBSF, protease inhibitor mixture (Roche), and 2 mM lysozyme] and sonicated. Cleared lysate was applied to GST Gravitrap Glutathione Sepharose 4B (GE Healthcare) columns and washed thoroughly. GST-ARF fusions were eluted with 10 mM reduced glutathione and concentrated using Amicon Ultra 30K concentrators (Millipore).

For EMSAs, selected regions of ~200–250 bp within the *BA1* promoter that were enriched for core TGTC elements were PCR amplified, gel purified, and biotinylated using the Biotin 3′ End DNA Labeling Kit (ThermoScientific) according to the manufacturer's recommendations. Primers used to amplify the seven probes are listed in Table S1. DNA binding assays were performed using the Lightshift Chemiluminescent EMSA kit (ThermoScientific) as follows: binding reactions containing 1× Binding Buffer, 50 ng/μL polydI/dC, 2.5% glycerol, 2 μL biotinylated probe, and 1 μL purified GST-ARF protein or GST alone were incubated at room temperature for 20 min and loaded on a 6% DNA retardation gel (Life Technologies) before transfer to a nylon membrane. Subsequent detection was carried out according to the manufacturer's recommendations. Competition with unlabeled probe was carried out using 50-fold excess of unlabeled probe. Mutated probe A* was generated by annealing two complementary oligos in which the core TGTC elements were changed to AAAA. ARF18 and ARF20 were not analyzed by EMSA because of high homology with ARF22 and ARF35.

Aux/IAA Degradation Assays in Yeast. Diploid yeast strains coexpressing stably integrated *Arabidopsis thaliana* TIR1 and YFP-tagged Aux/IAA proteins were prepared by transferring a freshly grown colony from YPD plates into Synthetic Complete media. Flow cytometry was used to estimate the cell density and dilute cells to 0.5 events·μL^{-1}, such that cultures were in log phase 16 h later and for the duration of the experiment. All cultures were grown at 30 °C with shaking. Preauxin measurements were taken to ascertain baseline expression, followed by addition of auxin (10 μM indole-3-acetic acid) or mock treatment (95% [vol/vol] ethanol). Measurements were acquired over the course of 150 min after auxin treatment, with intervals ranging from 10 min early in the YFP-Aux/IAA degradation phase to 30 min later in the degradation phase. Controls were measured every hour for the duration of the experiment. Data normalization was carried out by subtracting background autofluorescence and normalizing to preauxin fluorescence levels for each yeast strain. Nonlinear regression analysis (plateau followed by one-phase decay) was performed in Prism6 (GraphPad), using raw data to calculate degradation half-lives with 95% confidence intervals.

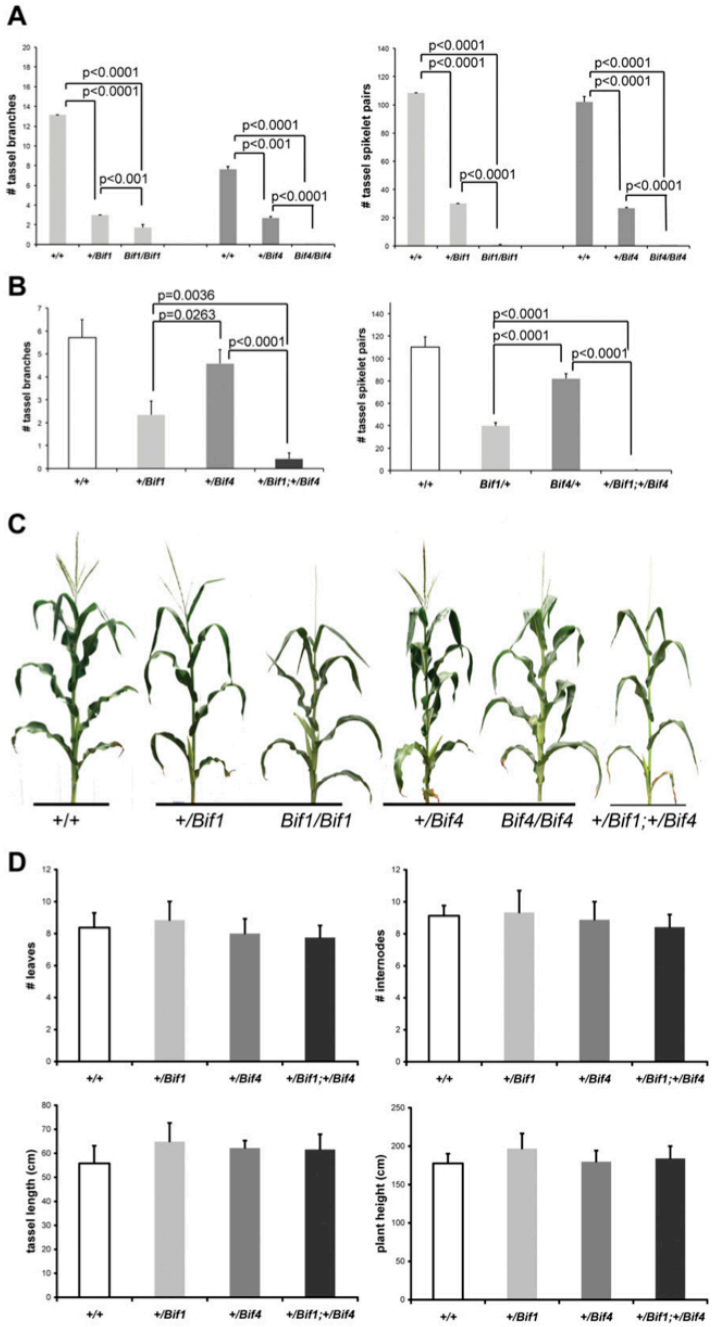

Fig. S1. Quantification of the phenotypic defects of *Bif1* and *Bif4* mutants. (*A*) Reproductive defects in tassels of single mutants in B73 background ($n \geq 7$). (*B*) Analysis of double mutants in A619 background ($n \geq 7$). (*C*) Whole-plant images. (*D*) Analysis of vegetative and reproductive phenotypes with no detectable difference ($n \geq 6$). Error bars show SD.

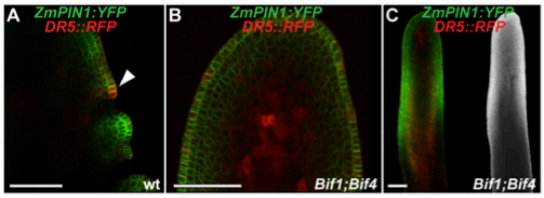

Fig. S2. Confocal analysis of *ZmPIN1a:YFP* and *DR5rev::RFP* transgenes. (*A*) Wild-type tassel, showing the peripheral zone of the IM with an emerging primordium (arrowhead). (*B* and *C*) *+/Bif1;+/Bif4* tassels. In *B* is a close-up view of the IM. (*C*, *Right*) Brightfield image of the confocal sample. (Scale bars, 100 μm.)

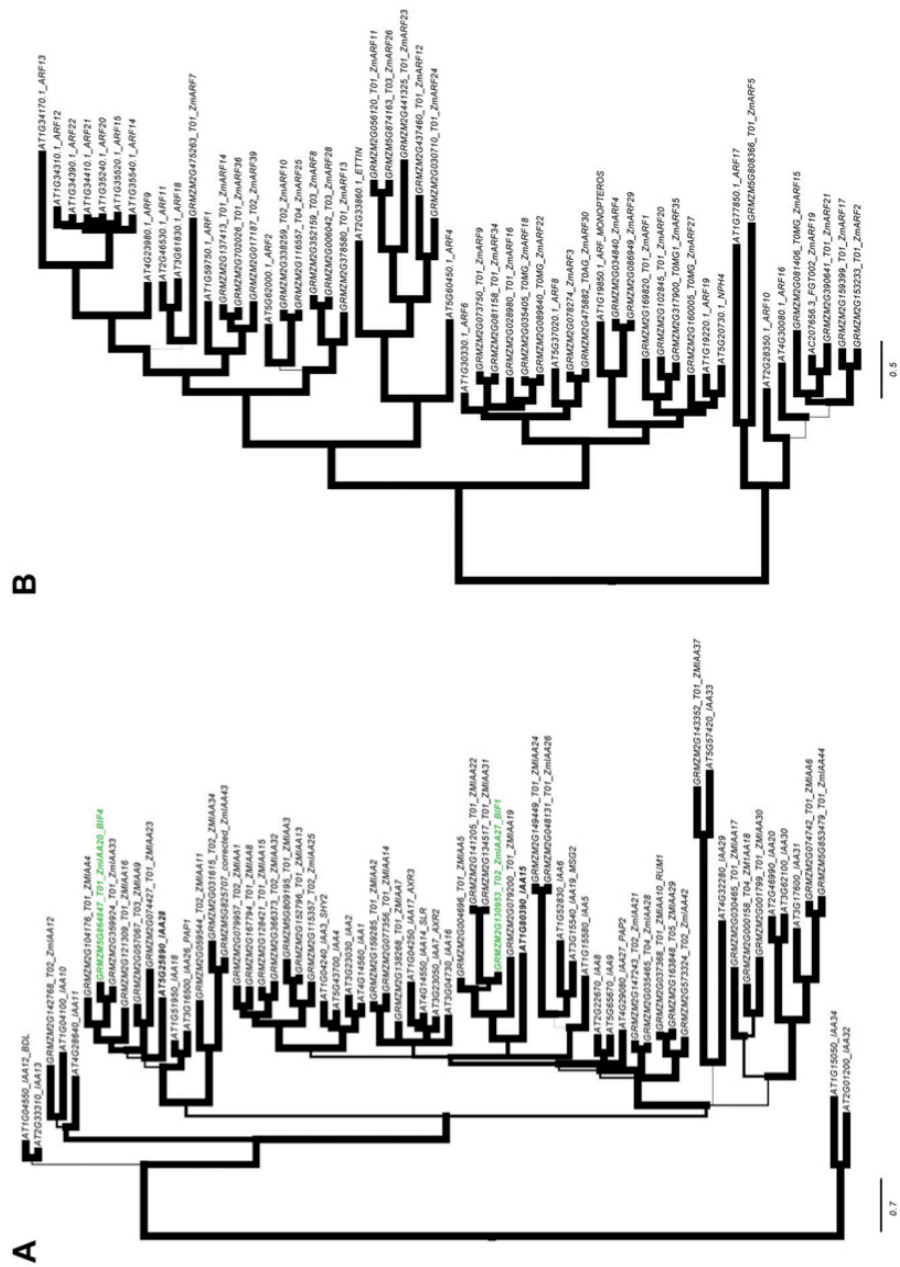

Fig. 53. Phylogenetic analysis. (*A*) Bayesian consensus phylogram of 67 *Arabidopsis* (At) and maize (GRMZM) Aux/IAA protein sequences. The maize BIF1 and BIF4 sequences and their closest *Arabidopsis* relatives, ATIAA15, and ATIAA28, respectively, are bolded. Phylogram is rooted using *Arabidopsis* IAA32 and IAA34 based on Remington (61). Branch widths are proportional to support with bold branches equivalent to greater than or equal to 0.95 clade credibility. (*B*) Bayesian consensus phylogram of 55 *Arabidopsis* (At) and maize (GRMZM) ARF protein sequences. Phylogram is rooted using the *Arabidopsis* ARF10, ARF16, and ARF17 clade, based on Remington (61). Branch widths are proportional to support with bold branches equivalent to greater than or equal to 0.95 clade credibility. (Scale bars, substitution per site.)

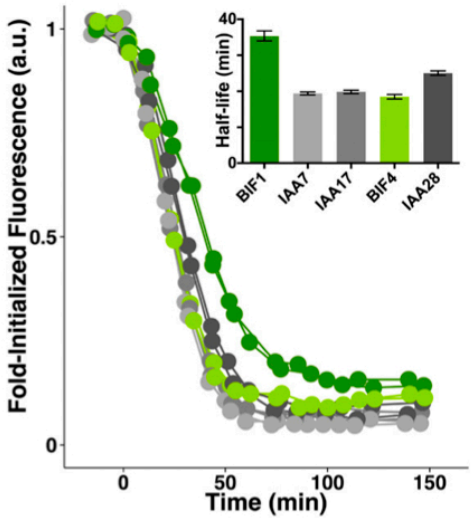

Fig. S4. Auxin-induced degradation of wild-type BIF1 and BIF4 proteins in a yeast synthetic system compared with similar *Arabidopsis* proteins.

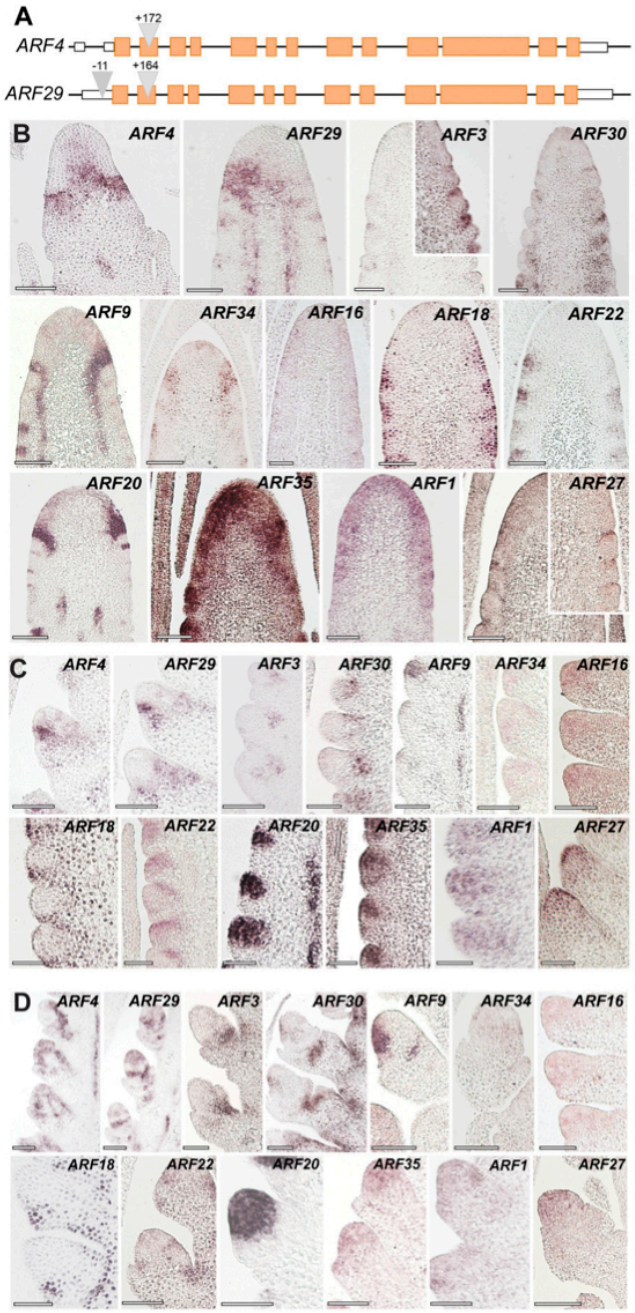

Fig. S5. The maize *ARF* gene family. (*A*) Gene structure of *ZmARF4* and *ZmARF29*, the maize co-orthologs of *Arabidopsis MONOPTEROS*. Triangles represent transposon insertions. Orange boxes, exons; white boxes, UTR regions. (*B–D*) Inflorescence-specific expression of maize-activating *ARF* genes by mRNA in situ hybridizations in immature tassels. Expression pattern in inflorescence meristems (*B*), spikelet-pair (*C*), and spikelet meristems (*D*). (Scale bars, 100 μm.)

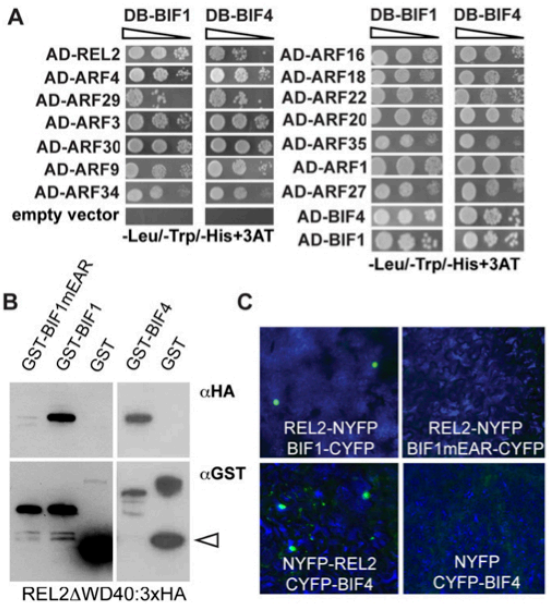

Fig. S6. Protein–protein interaction assays. (*A*) Y2H analysis of BIF1 and BIF4 with the 13 activating ARFs and REL2. (*B*) The interaction of BIF1 and BIF4 with REL2 in in vitro pull-down assays. Arrowhead points to GST. (*C*) BiFC assay by transient expression in tobacco leaves.

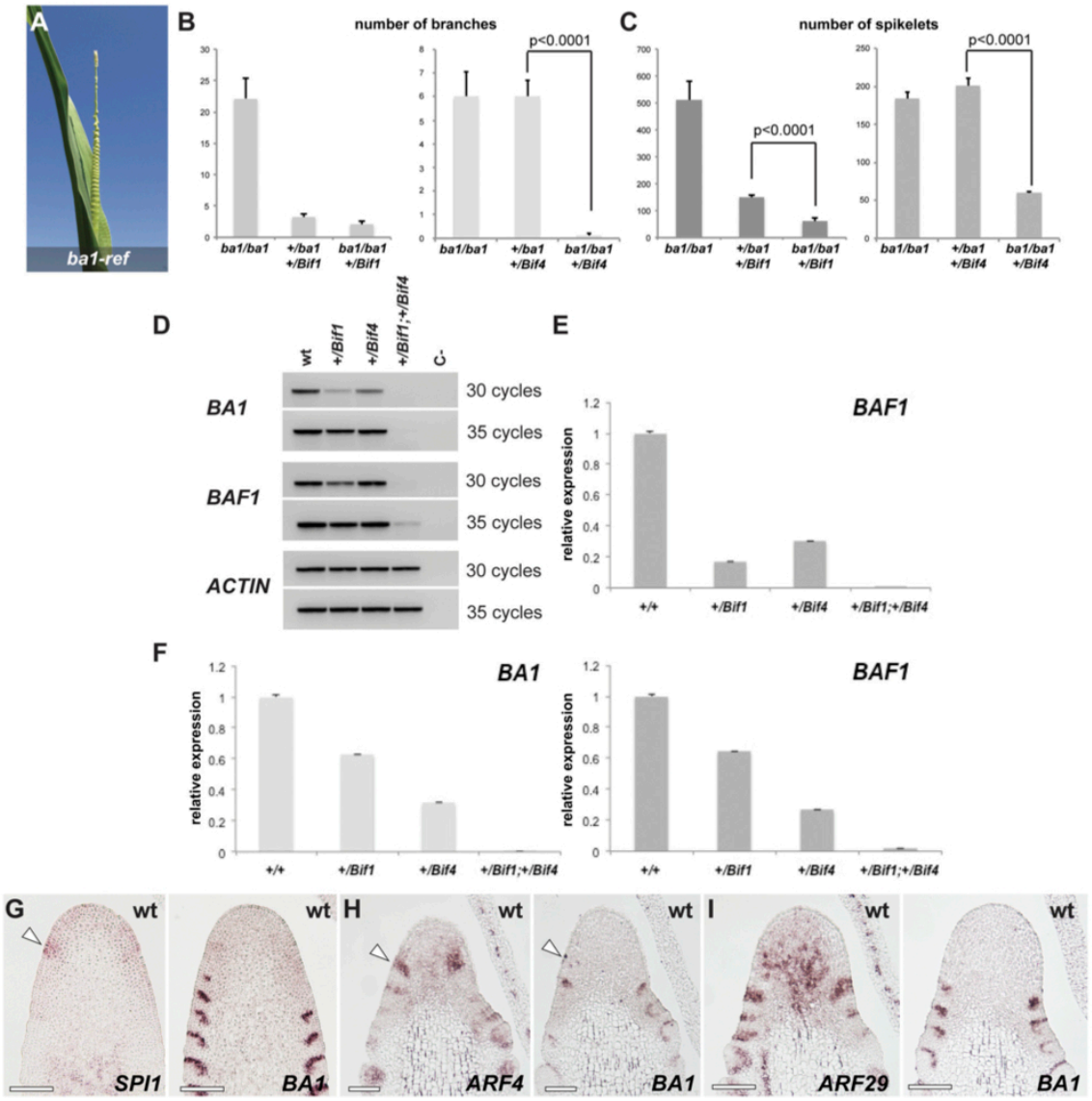

Fig. S7. Genetic and expression analysis. (*A*) *ba1-ref* tassel. Note the enlarged suppressed bracts. (*B* and *C*) Quantification of tassel phenotypes (branch and spikelet-pair number) in *Bif1;ba1-mum1* and *Bif4;ba1-mum1* double mutants ($n \geq 6$). Error bars, SEM. (*D*) Semiquantitative RT-PCRs of *BA1*, and *BAF1* and *ACTIN* controls in single- and double-mutant tassels. *BAF1* is a boundary-expressed gene that functions upstream of *BA1* (50). (*E*) Quantitative RT-PCR of BAF1 (same samples as in Fig. 4; background A619). (*F*) Quantitative RT-PCR of *BA1* and *BAF1* in a B73 background. (*G–I*) Consecutive sections of young IMs hybridized with different in situ probes. (*G*) Note that *SPI1* expression (arrowhead) appears before *BA1*. (*H* and *I*) *ARF* expression precedes *BA1* expression (arrowheads), but later overlaps with it in slightly broader domains.

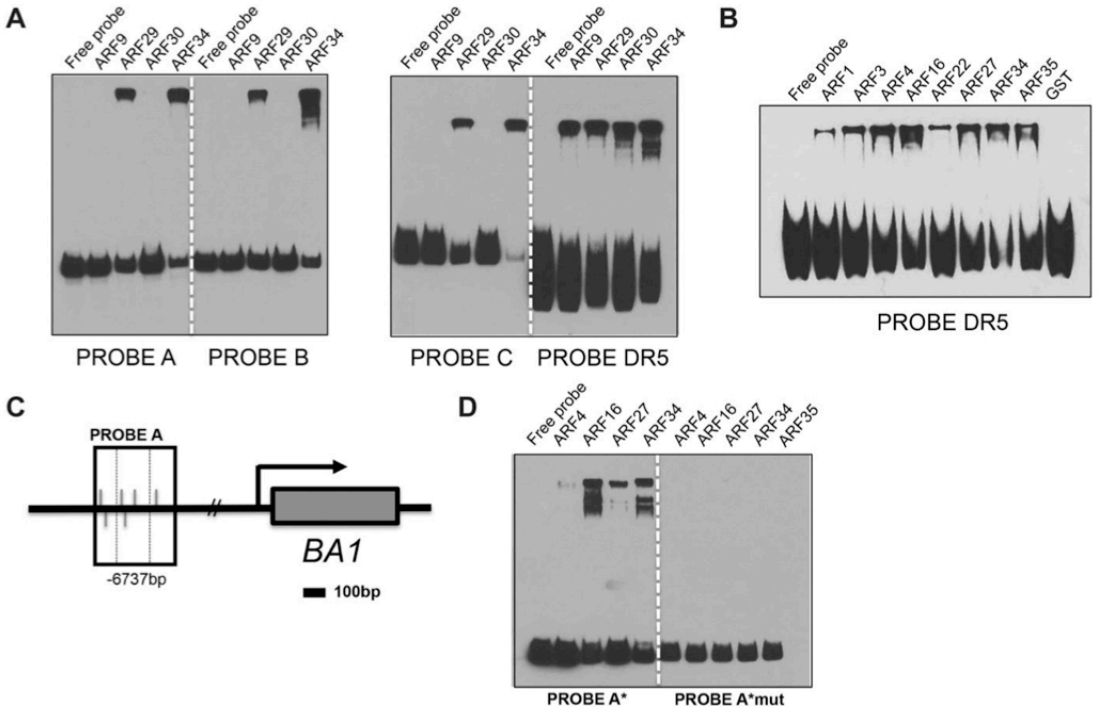

Fig. S8. Multiple-activating ARFs directly bind to the *BA1* promoter. (*A*) EMSAs showing that ARF29 and ARF34 bind to probes A, B, C, and DR5. (*B*) EMSA showing that all ARFs tested bind to a 9xAuxRE DR5 probe. (*C*) Schematic showing simplified *BA1* genomic locus. Promoter fragment used for probe A in EMSAs is shown as boxed region; dashed box in probe A corresponds to 100-bp probe A*. Values below boxes indicate position relative to BA1 start codon (+1). Gray lines indicate TGTC core AuxRE elements. (*D*) EMSA showing that mutation of core TGTCs in probe A* eliminates binding of ARF4, ARF16, ARF27, and ARF34.

Table S1. Vectors and primers used for *ARF* cloning and expression analysis

Gene name	Vector	Use	Fwd primer 5′-3′	Rev primer 5′-3′	Enzyme
GRMZM2G073750/ARF9	pENTR223-Sfi	Y2H in situ	GAATTCGGCCGTCAAGGCCAATGAACCTCTCACCGCCCAGGATG	AGTCGACGGCCCATGAGGCCGTAGTCCAGAGGCACCACAGGTGCG	SpeI
GRMZM2G081158/ARF34	pENTR223-Sfi	Y2H	GAATTCGGCCGTCAAGGCCAATGAACCTCTCCCCGCCCAAG	AGTCGACGGCCCATGAGGCCGTAGTCCAGAGGCACCACAGG	
GRMZM2G081158/ARF34	pGEM T-Easy	In situ	TCCCGCAGCCCAGCCATTCT	TCAACAGGGCCTGAGACTGAGAG	PstI
GRMZM2G028980/ARF16	pENTR223-Sfi	Y2H in situ	GAATTCGGCCGTCAAGGCCAATGAAGCTCTCGCCGTCGG	AGTCGACGGCCCATGAGGCCGAACTCGACCGAACCCACCG	SmaI
GRMZM2G035405/ARF18	pENTR223-Sfi	Y2H in situ	GAATTCGGCCGTCAAGGCCAATGAGGCTCTCGTCGTCGTCC	AGTCGACGGCCCATGAGGCCTCCCAACTCGACCGAACCGAC	BglII
GRMZM2G089640/ARF22	pENTR223-Sfi	Y2H in situ	GTACAAAAAAGCAGAAGGGCCGTCAAGGCCAATGTCACCAGTT-CATTCTCCCATG	ACTTTGTACAAGAAAGCTGGGCCCATGAGGCCAACTCGACCGAAC-CCACGGACGC	BglII
GRMZM2G160005/ARF27	pENTR223-sfi	Y2H in situ	GAATTCGGCCGTCAAGGCCAATGAAGGATCACGGATCGGGC	AGTCGACGGCCCATGAGGCCGGCCCTCCATGCATTTGCGT	HindIII
GRMZM2G169820/ARF1	pENTR223-sfi	Y2H in situ	GAATTCGGCCGTCAAGGCCAATGGAGGCGCCGGGGACGAGCT	AGTCGACGGCCCATGAGGCCTCGCCGGTGACCCTCCACGGACGA	MluI
GRMZM2G102845/ARF20	pENTR223-sfi	Y2H in situ	GAATTCGGCCGTCAAGGCCAATGAAGCAGTCCCCGGCCA	AGTCGACGGCCCATGAGGCCCTCAAATTGGTCGTAGAACCCGATGG	NotI
GRMZM2G317900/ARF35	pENTR223-sfi	Y2H in situ	GAATTCGGCCGTCAAGGCCAATGATCAAGCAGCAGCAGCAGC	AGTCGACGGCCCATGAGGCCCTGGTCATATGAACCAGTAGATGGG	HindIII
GRMZM2G034840/ARF4	pAD-GAL4	Y2H in situ	AATTCTCTAATGCTTCTCGAGATGATGACGTCCTCGTACGA	GACTCACTATAGGGCTCTAGATCAAGCCATTTGCATGCAGT	XhoI
GRMZM2G086949/ARF29	pAD-GAL4	Y2H in situ	AATTCTCTAATGCTTCTCGAGATGATGGCCTCCTCGCAGGAG	GACTCACTATAGGGCTCTAGACTAAGCTATTTGGATGCAGT	XhoI
GRMZM2G078274/ARF3	pENTR223-Sfi	Y2H in situ	GAATTCGGCCGTCAAGGCCAATGAGCTCCTCGTCCGCG	AGTCGACGGCCCATGAGGCCAGATAGGTAGCGTGGATC	NdeI
GRMZM2G475882/ARF30	pENTR223-Sfi	Y2H in situ	GAATTCGGCCGTCAAGGCCAATGAGCTCCTCGTCCGCG	AGTCGACGGCCCATGAGGCCAGATAGGTAGCGTGGATC	NdeI

Table S2. List of primers used in this study

Primer name	Sequence 5′-3′	Use
ProbeA-FWD	GGCAAACATATGACATTAGTGG	EMSA
ProbeA-REV	CTTAGATCAAGAATTCTCACCCC	EMSA
ProbeB-FWD	CCAATTCAATGACATGTCTCT	EMSA
ProbeB-REV	GGTCGTTGAGAACCGTCAGTAAA	EMSA
ProbeC-FWD	CGTGCACACTAGTTATAAGATATGG	EMSA
ProbeC-REV	CGACTTCCCTTCGAGGCCAA	EMSA
ProbeD-FWD	GCTTAGAGGTGGAAAGTACGAC	EMSA
ProbeD-REV	GACAAATACAAACATGTCTGTTAC	EMSA
ProbeE-FWD	CACTACACTAAACCAGGGCG	EMSA
ProbeE-REV	GGACATAAATTACTCCGACAACC	EMSA
ProbeF-FWD	CCGTCGTCGACGTAGCCTCA	EMSA
ProbeF-REV	CTCGACTGGCGCCGGAGCTC	EMSA
ProbeG-FWD	GATGCAATGTGTTATCGAGTG	EMSA
ProbeG-REV	CCATACATGCACCTTTGATCAG	EMSA
BA1-F19	GTGGTTGGTGACAACGAGGT	qRT-PCR
BA1-R5	CGAGGAAGATGCAAGAAGCAG	qRT-PCR
BAF1-F3	CAGCTGCTGCTAAGACTCAATCC	qRT-PCR
BAF1-R3	AGACTGACATGCAGTTCCAAGC	qRT-PCR
BIF1-RT-F1	CAGTACGCACTGGCTTTTAGTGG	qRT-PCR
BIF1-RT-R1	ACAAACTTTCCTCAGGCAAAAGC	qRT-PCR
BIF4-RT-F3	CGTACCCTGGAGTCTCAACTCTG	qRT-PCR
BIF4-RT-R3	ATCTCCTCTAGATTCCTGCTTCC	qRT-PCR
ACTIN-F3	CTCATGCTATTCTCCGTTTGG	qRT-PCR
ACTIN-R3	TCAGGCATCTCGTAGCTCTTC	qRT-PCR
UBIQUITIN-F1	GAGTGCCCCAACGCCGAGTG	qRT-PCR
UBIQUITIN-R1	CTACGCCTGCTGGTTGTAGACGTA	qRT-PCR

CHAPTER TWO

The Combined Action of Duplicated Boron Transporters Is Required for Maize Growth in Boron-Deficient Conditions

Mithu Chatterjee,* Qiujie Liu,* Caitlin Menello,* Mary Galli,* and Andrea Gallavotti*,†,1
*Waksman Institute of Microbiology, Rutgers University, Piscataway, New Jersey 08854-8020 and †Department of Plant Biology, Rutgers University, New Brunswick, New Jersey 08901

ABSTRACT The micronutrient boron is essential in maintaining the structure of plant cell walls and is critical for high yields in crop species. Boron can move into plants by diffusion or by active and facilitated transport mechanisms. We recently showed that mutations in the maize boron efflux transporter ROTTEN EAR (RTE) cause severe developmental defects and sterility. *RTE* is part of a small gene family containing five additional members (*RTE2–RTE6*) that show tissue-specific expression. The close paralogous gene *RTE2* encodes a protein with 95% amino acid identity with RTE and is similarly expressed in shoot and root cells surrounding the vasculature. Despite sharing a similar function with *RTE*, mutations in the *RTE2* gene do not cause growth defects in the shoot, even in boron-deficient conditions. However, *rte2* mutants strongly enhance the *rte* phenotype in soils with low boron content, producing shorter plants that fail to form all reproductive structures. The joint action of RTE and RTE2 is also required in root development. These defects can be fully complemented by supplying boric acid, suggesting that diffusion or additional transport mechanisms overcome active boron transport deficiencies in the presence of an excess of boron. Overall, these results suggest that *RTE2* and *RTE* function are essential for maize shoot and root growth in boron-deficient conditions.

KEYWORDS boron transport; RTE; BOR1; maize; gene duplication

BORON is an essential microelement for plant growth and development. The most well-known role of boron is the cross-linking of the pectic polysaccharide rhamnogalacturonan-II (RG-II), an essential structural component of the cell wall (Kobayashi *et al.* 1996; O'Neill *et al.* 2001). In general, monocot species have lower boron content than dicotyledonous species, a fact that correlates with an overall difference in pectin content in the cell wall (Hu *et al.* 1996). Nonetheless, actively growing tissues need a constant supply of exogenous boron given that the majority of endogenous boron in plants is trapped in the cell wall (Shelp *et al.* 1995; O'Neill *et al.* 1996). Boron has a narrow range of concentrations that span deficiency to toxicity levels, therefore its uptake needs to be carefully regulated.

doi: https://doi.org/10.1534/genetics.116.198275
Manuscript received November 14, 2016; accepted for publication June 5, 2017; published Early Online June 21, 2017.
Supplemental material is available online at www.genetics.org/lookup/suppl/doi:10.1534/genetics.116.198275/-/DC1.
[1]Corresponding author: Waksman Institute of Microbiology, Rutgers University, 190 Frelinghuysen Rd., Piscataway, NJ 08854-8020. E-mail: agallavotti@waksman.rutgers.edu

It was originally believed that passive diffusion was the primary mechanism of boron transport in plants (Raven 1980; Shelp *et al.* 1995). However, more recent experiments have shown that boron uptake involves an active, carrier-mediated process (Dordas and Brown 2001; Stangoulis *et al.* 2001; Brown *et al.* 2002). Several members of the major intrinsic protein family have since been identified as boric acid channels (Takano *et al.* 2006; Tanaka *et al.* 2008; Durbak *et al.* 2014). These channel proteins facilitate the transport of boron from the soil into the root cells (Takano *et al.* 2008; Miwa and Fujiwara 2010). The first identified efflux-type active boron transporter, AtBOR1, was shown to play a major role in loading boron into the xylem in *Arabidopsis thaliana* (Noguchi *et al.* 1997; Takano *et al.* 2002). Under low boron conditions, *bor1* mutants showed reduced rosette leaves, and loss of apical dominance and fertility. Overexpression of BOR1, on the other hand, improved seed production under boron-limiting conditions (Miwa *et al.* 2006). Six additional *BOR1*-like genes were identified in the *Arabidopsis* genome, and tissue- and cell-specific expression patterns indicated that these genes play distinct roles in boron transport (Miwa *et al.* 2006, 2007, 2013). *BOR2*, a close paralog of

BOR1, is strongly expressed in the lateral root cap and elongation zones of the root epidermis. *bor2* mutant roots showed reduced cell elongation and reduced levels of cross-linked RG-II under low boron conditions (Miwa *et al.* 2013). In contrast, *BOR4* was found to mediate tolerance to high boron levels and its overexpression improved boron tolerance by removing excess boron from roots (Miwa *et al.* 2007; Miwa and Fujiwara 2010). In addition, in eudicots, functional *BOR1*-like genes have been studied in several species, such as grapes (Perez-Castro *et al.* 2012), *Brassica napus* (Sun *et al.* 2012), and *Citrus macrophylla* (Canon *et al.* 2013).

In cereals, boron deficiency and toxicity affect yield and constrain productivity (Gupta *et al.* 1985; Mickelbart *et al.* 2015). To address this problem, various boron channel proteins and transporters were characterized in cereals (Nakagawa *et al.* 2007; Reid 2007; Sutton *et al.* 2007; Schnurbusch *et al.* 2010; Leaungthitikanchana *et al.* 2013; Chatterjee *et al.* 2014; Durbak *et al.* 2014; Liu *et al.* 2015) and landraces that can grow in soil with wide ranges of boron concentration were identified (Reid 2007; Sutton *et al.* 2007; Pallotta *et al.* 2014; Hayes *et al.* 2015). For example, rice has four *BOR1*-like genes (Nakagawa *et al.* 2007). Among them, *OsBOR1* is required for xylem loading and for efficient uptake of boron in roots under low boron conditions. OsBOR4 is instead a pollen-specific efflux transporter and is essential for normal pollen germination and pollen-tube elongation (Tanaka *et al.* 2013). In barley, *Bot1/HvBOR2* is responsible for the high boron tolerance of the Sahara landrace. Compared to intolerant genotypes, Sahara has four tandem copies of the *Bot1* gene and higher transcript levels, and a direct correlation exists between *Bot1* expression levels and the degree of tolerance in various landraces (Hayes and Reid 2004; Reid 2007; Sutton *et al.* 2007; Mickelbart *et al.* 2015). Similarly, a study of bread and durum wheat showed that variation in *Bot-B5/D5* alleles influenced the degree of boron tolerance in various cultivars and landraces (Pallotta *et al.* 2014). Determining the number and function of boron transporters in crop species and landraces therefore has practical implications for the development of varieties that can grow in soils with differing boron availability.

Among cereals, maize has a relatively small requirement for boron but it is nonetheless affected by boron deficiency around the world (Shorrocks 1997; Lordkaew *et al.* 2011). The most common boron-deficiency symptom in maize is the formation of small cobs with few kernels, resulting in lower yields. In general, reproductive tissues are more sensitive and plants with marginal boron deficiency show poor pollen germination (Agarwala *et al.* 1981; Lordkaew *et al.* 2011). Under severe boron-deficiency conditions, leaves develop white necrotic spots and streaking (Lordkaew *et al.* 2011; Chatterjee *et al.* 2014). Only recently have the first maize mutants affected in boron transport been reported. The maize *tassel-less1* (*tls1*) mutant exhibited symptoms of boron deficiency in vegetative and inflorescence development. *TLS1* encodes an aquaporin and is coorthologous to known *Arabidopsis* channel proteins (Durbak *et al.* 2014; Leonard *et al.* 2014). We recently characterized a maize mutant called *rotten ear* (*rte*) that displayed severe defects in inflorescence development, as well as necrotic lesions in leaves under boron-deficient conditions. RTE is a functional homolog of the boron efflux transporter BOR1 protein. Under low boron conditions, maize inflorescences exhibited widespread tissue death, likely due to loss of cell wall integrity (Chatterjee *et al.* 2014).

In this study, we identified five additional boron transporter-like genes in the maize genome (*RTE2–RTE6*). One of these genes, *RTE2*, is a close paralog of *RTE*. Functional characterization of *RTE2* showed that the dual action of both RTE and RTE2 is required for maize vegetative and reproductive development in boron-deficient conditions.

Materials and Methods

Plant materials and phenotypic analysis

RTE2 transposon insertion lines were obtained from the Maize Genetics Cooperation Stock Center (UFMu-02112, UFMu-02812, and UFMu-01459) (Settles *et al.* 2007). The transposon insertions are located at position +303 (UFMu-02112; target site duplication ACGGTGCTC; *rte2-1*), +321 (UFMu-02812; target site duplication TTCATGTTC; *rte2-2*), and +1670 (UFMu-01459; target site duplication GTTGGTCTG; *rte2-3*) of the *RTE2/GRMZM2G082203* coding sequence. These lines were backcrossed once in Mo17 and A619. For *rte;rte2* double mutants, *rte-1* and *rte-2* alleles (Chatterjee *et al.* 2014) in Mo17 and A619 backgrounds were crossed with all three *rte2* transposon insertion lines and self-fertilized. The resulting segregating F_2 populations all showed the same *rte;rte2* double mutant phenotype shown by representative plants in Figure 3.

The vegetative phenotype was analyzed using 6-week-old plants grown in Rutgers University fields. Plant height was measured as the distance from the ground to the upper leaf node. For root length measurements, F_2 seeds from a cross of *rte-1* (BC3 A619) and UFMu-02812 (BC1 A619) were germinated in greenhouses using low-boron-content field soil (from Rutgers fields). Wild-type and mutant plants were genotyped and used for primary root length measurements in two separate experiments. Student's *t*-test was used to determine statistical significance.

Boron measurements

Leaf samples (upper three leaves per each plant) were collected from ~45-day-old, field-grown plants, and at least six plants were bulked per sample (Supplemental Material, Table S1 in File S1). For greenhouse samples (Figure 4), all leaves above the top elongated internode were collected from 50-day-old plants grown in pots containing Rutgers field soil for both treated and control samples. Each data point represents the average of two bulked samples (total number of individuals is listed). All samples were air dried and analyzed by inductively coupled plasma optical emission spectroscopy by the Missouri University Plant and Soil Analysis Facility. Data are expressed in micrograms of boron per gram of dry weight.

For *Arabidopsis* measurements (Table S1 in File S1), rosette leaves from 4-week-old plants were bulked from at least three lines and subject to the same analysis highlighted above.

Boric acid rescue and soil analysis

Double *rte-1;rte2-2* mutant and normal plants were germinated in pots containing soil from Rutgers fields and grown in standard greenhouse conditions. A stock solution of 100 mM boric acid (Sigma Chemical, St. Louis, MO) in Milli-Q water was diluted in tap water to a final concentration of 200 μM and used to regularly water plants. For the control experiment, Milli-Q water without the addition of boric acid was diluted in the same tap water. Plants were watered as required for growth.

Soil samples from treated and control pots were collected according to standard practices and analyzed at the New Jersey Agricultural Experiment Station, Rutgers University (Table S2 in File S1).

Phylogenetic tree construction

The amino acid sequences of RTE-like proteins were identified through searches at National Center for Biotechnology Information (NCBI), Phytozome, and MaizeGDB, and aligned using MUSCLE (Edgar 2004). The evolutionary history was inferred by the maximum-likelihood method using MEGA6.0 (Tamura *et al.* 2013). The percentage of trees in which the associated taxa clustered together is shown next to the branches. The analysis included proteins encoded by the following 33 gene models: *RTE/GRMZM2G166159/KP751214*, *RTE2/GRMZM2G082203* (NCBI KY053531), *RTE3/GRMZM2G051753* (corrected gene model; NCBI KY129660), *RTE4/GRMZM2G374989*, *RTE5/GRMZM2G302559*, and *RTE6/GRMZM2G454327* (corrected gene model; NCBI KY129661) (maize); *OsBOR1/AK070617*, *OsBOR2/DQ421408*, *OsBOR3/AK072421*, and *OsBOR4/DQ421409* (rice); *Sb08g018440*, *Sb09g005350*, and *Sb03g004180* (sorghum); *TaBOR1.1/BAO98796*, *TaBOR1.2/BAO98797*, *TaBOR1.3/BAO98798*, *TaBOR2/ABX26206*, *TaBot-D5b/AHY28551*, and *TaBot-B5b/AHY28552.1* (wheat); *ABX26122* (*Hordeum vulgare*); *AtBOR1/AT2G47160*, *AtBOR2/AT3G62270*, *AtBOR3/AT3G06450*, *AtBOR4/AT1G15460*, *AtBOR5/AT1G74810*, *AtBOR6/*AT5G25430, and *AtBOR7/AT4G32510* (*A. thaliana*); *S1g057770*, *S6g071500*, *S3g120020*, and *S8g066960* (*Solanum lycopersicum*); and *ScBOR1*, *NP_014124* (*Saccharomyces cerevisiae*). *ScBOR1* was used as an outgroup.

The comparison of colinearity within genomic regions of different *RTE*-like genes was performed using CoGe SynMap (Lyons *et al.* 2008; https://genomevolution.org/coge).

Expression analysis

Total RNA was extracted from different tissues obtained from pools of three or more B73 plants using TRIzol reagents (ThermoFisher Scientific) as per manufacturer's instructions. Samples used for analysis included embryos and endosperm at 10 days after pollination, mature leaf blades, seedling shoots and roots, pollen, and 1-cm tassel and ear primordia. Complementary DNA (cDNA) was obtained using the qScript cDNA Synthesis Kit and amplified with PerfeCTa SYBR Green FastMix (Quanta Biosciences). For tissue-specific expression, quantitative real-time reverse-transcription PCR (qRT-PCR) was performed using gene-specific primers (Table S3 in File S1). *UBIQUITIN* was used as internal control. The cycle threshold (CT) values for all genes in different RNA samples were normalized to the CT value of the internal control gene. Relative messenger RNA (mRNA) levels of each gene in different tissue samples were calculated using the $2^{-\Delta\Delta Ct}$ method (Livak and Schmittgen 2001). Two biological replicates with at least three technical replicates per each pooled sample were used in the analysis.

Tissue-specific RNA-sequencing (RNA-seq) data were taken from Walley *et al.* (2016). Normalized average values of fragments per kilobase of transcript per million mapped reads from three replicates were converted to $\log_{10} + 1$ and plotted using the aheatmap function in the R package NMF (Gaujoux and Seoighe 2010).

For expression analysis of *RTE2* in *Arabidopsis*, RNA was extracted from rosette leaves of T1 plants and treated as described above. For analysis of *RTE2* expression in insertion lines, RNA from homozygous plants and wild-type siblings for all three alleles was extracted from seedling shoots in two separate biological replicates. RT-PCR products were gel purified and sequenced to verify the identity of the amplified fragment. Primers used for qRT-PCR and RT-PCR are listed in Table S3 in File S1.

For *in situ* hybridizations, the 5′ and 3′ UTR of *RTE* and *RTE2* were cloned into the pGEM-T Easy Vector System (Promega, Madison, WI) using primers *RTE-UTR* and *RTE2-UTR* (Table S3 in File S1). The 5′ UTR of *RTE* shares 78% identity with *RTE2*, and the 3′ UTR of *RTE* shares 79% identity with *RTE2*. Purified PCR products obtained using primers M13F and M13R were used as templates for synthesizing sense and antisense probes using SP6 and T7 RNA polymerases (Promega), respectively. For each experiment, the 5′ UTR and 3′ UTR RNA probes were mixed in equal ratios and used for hybridizations. The full-length *RTE2* antisense probe was subjected to carbonate hydrolysis prior to its use. Seedling roots and young inflorescences were fixed in a 4% paraformaldehyde solution, dehydrated in ethanol, and embedded in paraplast. Hybridizations were conducted at 59° overnight. After several washes and treatment with anti-DIG antibody, signals of DIG-labeled probes were detected using NBT/BCIP (Promega), and images were acquired using a Leica DM5500B microscope.

Transient expression in tobacco

To create the *35S::RTE2:YFP* construct, the *RTE2* coding sequence (without stop codon) was PCR amplified and cloned in *pBJ36+2x35S*$_{pro\text{-}YFP}$. The resulting plasmid was digested with *Not*I and the *2x35S-RTE2-YFP* cassette was subcloned into the *Not*I sites of pMLBART. Expression plasmids for 35S-RTE-YFP and 35S-YFP were described previously

(Chatterjee *et al.* 2014). Plasmids were transformed into *Agrobacterium* and used for transient expression in tobacco as described previously (Chatterjee *et al.* 2014). An *mCHERRY*-labeled nuclear marker containing the maize BAF1 transcription factor (Gallavotti *et al.* 2011) was cloned into pEarlyGate104-mCHERRY (Gutierrez *et al.* 2009) and co-injected into tobacco. Leaf disks were imaged on a Leica SP5 confocal microscope using 514-nm excitation and 520- to 575-nm emission for YFP, and 594-nm excitation and 610- to 640-nm emission for mCHERRY. Image processing was performed with ImageJ.

Genomic sequences of RTE4 and RTE5

RTE4 and *RTE5* genes shared 98% identity with ambiguous ORFs, possibly due to genomic sequence assembly errors. To determine the correct genomic sequences of *RTE4* and *RTE5*, we amplified *RTE4* from DNA isolated from the OMA 9.41 line that contained chromosome 9 of the maize B73 inbred line (Rines *et al.* 2009). The *RTE5* locus was instead isolated using B73 genomic DNA. The primers used to amplify both genomic sequences are listed in Table S3 in File S1.

cDNA cloning

The ORFs of *RTE* and *RTE2* were PCR amplified from ear cDNA. *RTE3* (KY129660) was isolated from leaf cDNA pools, while *RTE6* (KY129661) was isolated from pollen cDNA pools. Protein sequence analysis was performed using the following databases: http://aramemnon.botanik.uni-koeln.de, www.ebi.ac.uk/interpro, and http://ExPASy.org.

RTE2 complementation test

To complement the *Arabidopsis bor1-3* mutant (Kasai *et al.* 2011), the B73 *RTE2* coding sequence was amplified with Phusion DNA polymerase (NEB) using primers RTE2 *Eco*RI-F1 and RTE2 *Hin*dIII-R1 (Table S2 in File S1). The amplicon was subsequently cloned into pBJ36+2x35S vector. The $35S_{pro}$*:RTE2* cassette was isolated using *Not*I digestion and cloned into the transfer DNA binary vector pMLBART. Homozygous *bor1-3* mutants were propagated by supplementation with 100 μM boric acid and transformed by the floral dip method. Primary transformants containing the $35S_{pro}$*:RTE2* construct were selected on soil with Basta and assessed for the phenotypic rescue of *bor1-3* defects. Complementation of the *bor1-3* mutant with *RTE* was previously described (Chatterjee *et al.* 2014).

Histology and microscopy

Sections of maize shoot apical meristems and young tassels were stained with Toluidine blue (2 min, 0.1% solution in 0.6% boric acid) and Safranin O-Alcian Blue (20 min, 0.02% in 0.1 M Na acetate, pH 5.0). Following a rinse in deionized water, slides were mounted using Permount (Fisher Scientific, Pittsburgh, PA) and visualized using a Leica DM5500B microscope.

Data availability

All materials generated in this study are available upon request. The authors state that all data necessary for confirming the conclusions presented in the article are represented fully within the article.

Results

Identification of RTE-like genes in maize

To identify additional members of the boron efflux transporter family that may play a role in transport and distribution of the microelement, we discovered five predicted boron transporter genes in the maize genome. Based on sequence similarity to the *RTE* gene, these genes were named *RTE2* (*GRMZM2G082203*), *RTE3* (*GRMZM2G051753*), *RTE4* (*GRMZM2G374989*), *RTE5* (*GRMZM2G302559*), and *RTE6* (*GRMZM2G454327*).

To better understand the evolutionary relationship between the maize boron transporter genes and previously characterized boron transporters, a phylogenetic analysis of the predicted protein sequences of 33 boron transporters from different species was performed. Similarly to what we previously reported (Chatterjee *et al.* 2014), the phylogenetic tree clearly separated the boron transporters into two classes (Figure S1A in File S1) that coincide with differences in gene function. Class I contained AtBOR1, AtBOR2, and OsBOR1-like boron transporters, which are essential for efficient xylem loading under boron-deficient conditions (Miwa *et al.* 2006, 2013; Nakagawa *et al.* 2007). Class II, on the other hand, contained members like AtBOR4, TaBOR2, and HvBOR2 which are responsible for tolerance to boron toxicity (Miwa *et al.* 2007; Reid 2007; Sutton *et al.* 2007). RTE and RTE2 belonged to class I, while RTE3, RTE4, RTE5, and RTE6 were found in the class II clade. RTE4, RTE5, and RTE6 were in the same clade and showed a high percentage of identity with OsBOR4, a pollen-specific boron transporter required for pollen germination and tube elongation (Tanaka *et al.* 2013).

Among all family members, *RTE* is most similar to its paralog *RTE2*. Both genes share an identical gene structure and exhibit conserved intron–exon boundaries (Figure 1A) with an overall 94% nucleotide sequence identity in the coding sequence, and 95% identity at the amino acid level (Figure S2 in File S1). *RTE3* showed lower similarity with both *RTE/RTE2* and *RTE4/RTE5/RTE6* groups. *RTE4*, *RTE5*, and *RTE6* showed significant similarity among themselves at the nucleotide level in the coding region (>90%). To confirm the predicted coding sequences of these genes, we isolated full-length cDNAs of *RTE2*, *RTE3*, and *RTE6*. The ORFs of *RTE2*, *RTE3*, and *RTE6* are 2109, 2028, and 2022 bp in length and encode proteins of 702, 675, and 673 aa, respectively (Figure S2 in File S1). *RTE4*, *RTE5*, and *RTE6* reside on extensively duplicated regions on chromosomes 9, 3, and 8, respectively (Figure S3B in File S1). Gene annotation of *RTE4* and *RTE5* in the maize B73v3 genome was ambiguous. To rule out any improper assembly of the highly similar genomic regions of both genes, we first sequenced the entire *RTE4* locus from an oat-maize addition line carrying maize B73 chromosome 9 (Rines *et al.* 2009), and the *RTE5* locus directly from B73 genomic DNA.

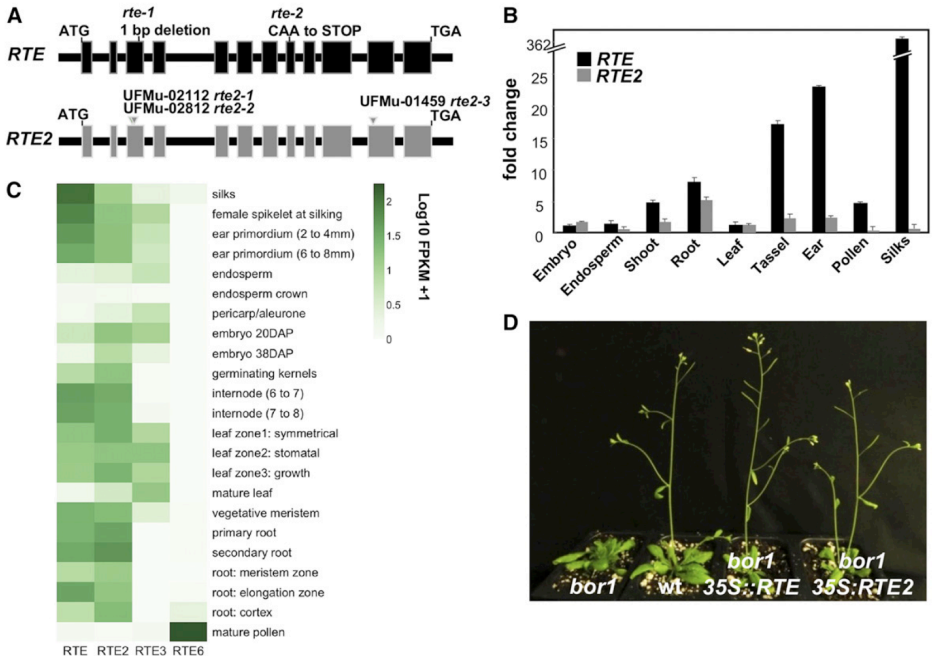

Figure 1 *RTE* and *RTE2* are duplicated genes. (A) *RTE* and *RTE2* mutant alleles used in this study. (B) qRT-PCR analysis of *RTE* and *RTE2* expression in different tissues relative to leaf. (C) Tissue-specific expression of *RTE*, *RTE2*, *RTE3*, and *RTE6* based on RNA-seq data sets from Walley *et al.* (2016). (D) Both RTE and RTE2 rescue the *Arabidopsis bor1* mutant when overexpressed. FPKM, fragments per kilobase of transcript per million mapped reads.

This confirmed that both loci are present in the maize genome on chromosomes 9 and 3, respectively. However, after several attempts we were not able to isolate full-length ORFs of either gene. Based on sequence comparison with the experimentally determined *RTE6* coding sequence, we noticed that *RTE4* had a single base pair deletion in the predicted fourth exon (position +501). Similarly, when compared with *RTE6*, we determined that a stop codon was present in the predicted fifth exon of *RTE5* (position +586). This suggests that both *RTE4* and *RTE5* are likely pseudogenes, and we removed them from our subsequent analysis. All RTE protein family members are predicted antiporters and share a similar structure containing 12 transmembrane domains (Takano *et al.* 2002; Chatterjee *et al.* 2014) (Figure S2 in File S1).

qRT-PCR was performed to assess the tissue-specific expression pattern of all *RTE* family members. The transcript abundance of the *RTE* family members differed in terms of tissue specificity (Figure 1, B and C, and Figure S1C in File S1). *RTE* mRNA was present in all the tissues examined including leaf, root, ear, tassel, and pollen, but was most abundant in ears and silks. Interestingly, *RTE2* showed the highest expression in roots among all tissue tested. On the other hand, *RTE3* was expressed at highest levels in leaves while *RTE6* transcripts were predominantly present in pollen, in accordance with the phylogenetic grouping. We verified the relative expression of the *RTE* family genes in RNA-seq data sets from published sources (Figure 1C) and those agreed well with our qRT-PCR data (Walley *et al.* 2016).

RTE2 is a functional ortholog of the Arabidopsis boron transporter BOR1

RTE2 encodes a boron transporter highly similar to RTE. Analysis of the genomic regions of *RTE* and *RTE2* showed strong colinearity and evidence that the two genes resided in duplicated regions of chromosome 1 and 3, respectively (Figure 1 and Figure S3A in File S1). We therefore wondered if RTE2 played a similar role to RTE in maize development. To investigate the function of RTE2 in maize, we identified three independent transposon insertions, two in the 3rd exon (UFMu-02112 and UFMu-02812) and one in the 11th exon of *RTE2* (UFMu-01459; Figure 1A). We renamed these insertions as *rte2-1*, *rte2-2*, and *rte2-3*, respectively. Each insertion was predicted to completely disrupt the function of RTE2, yet none of the three insertion lines showed any vegetative or reproductive developmental defects in the shoot, even when grown in boron-deficient conditions. We checked if *RTE2* was still expressed in homozygous insertion lines. While we could recover full-length *RTE2* transcripts in all siblings without insertions, we failed to do so for all *rte2* alleles after several attempts (data not shown). *RTE2* expression is still detectable in these insertion lines but we only recovered aberrantly spliced transcripts and transcripts containing the transposon

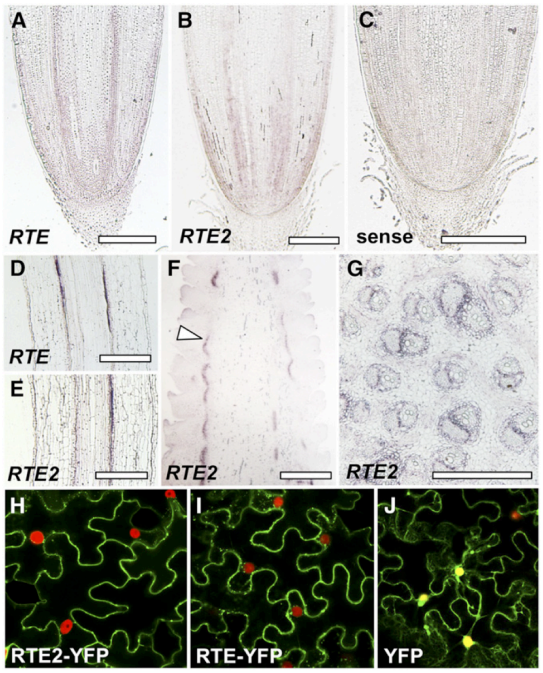

Figure 2 Expression and subcellular localization analysis of RTE and RTE2. *In situ* hybridizations of longitudinal sections of seedling roots showing *RTE* and *RTE2* expression in (A and B) root tips and (D and E) vasculature. (C) *RTE2* sense control. (F) Longitudinal section of an immature ear showing *RTE2* expression in vasculature (arrowhead). (G) Stem cross section. Bar, 500 μm. (H–J) Confocal images of tobacco epidermal cells expressing RTE2-YFP, RTE-YFP, YFP control, and the nuclear marker BAF1-mCHERRY (Gallavotti *et al.* 2011).

(Figure S4 in File S1). These results suggest that all *rte2* alleles are likely functional null.

We previously demonstrated that *RTE* is a functional ortholog of *AtBOR1* (Chatterjee *et al.* 2014). To assess whether RTE2 also shares a similar role during development and if any of the amino acids that differed with RTE could impair its function, we transformed the maize *RTE2* gene under the control of the 35S promoter into the *Arabidopsis bor1-3* mutant (Kasai *et al.* 2011). All vegetative and reproductive defects of *bor1-3* plants such as loss of apical dominance and reduced fertility were completely rescued in ~40% of the 38 independent lines overexpressing RTE2 (Figure 1D and Table S4 in File S1). We checked the expression levels of *RTE2* in a few representative *Arabidopsis* lines, and the level of phenotypic rescue correlated with higher expression levels of the transgene (Figure S4B in File S1). We also measured boron concentration in a subset of fully and partially rescued lines and observed >100% higher levels in leaves when compared to the *Arabidopsis bor1* mutant in both cases (Table S1 in File S1). Altogether these results indicated that *RTE2* encodes a functional boron transporter and can complement the developmental and fertility defects of the *Arabidopsis bor1-3* mutant.

To further understand if expression differences may explain the lack of a mutant phenotype in *rte2* single mutants we performed *in situ* hybridizations in root and inflorescence tissues using antisense probes specific to the 5′ and 3′ UTR regions, as well as full-length *RTE2* probe. Longitudinal sections of roots from 5-day-old seedlings showed identical expression of *RTE* and *RTE2* in the vasculature and root tips (Figure 2, A–E). Similarly, in longitudinal sections of developing inflorescences, *RTE2* transcripts localized to vasculature-surrounding regions (Figure 2, F and G) in an identical fashion to what we previously observed with *RTE* (Chatterjee *et al.* 2014).

We also checked RTE2 subcellular localization. RTE2-YFP was predominantly localized to the plasma membrane by confocal imaging of tobacco leaves in transient expression assays (Figure 2, H–J). The observed localization was identical to what we previously reported for RTE (Chatterjee *et al.* 2014). Altogether, these results indicate that RTE2 and RTE share similar functions in maize development.

RTE and RTE2 are required for maize growth in boron-deficient conditions

In *rte* plants, tassels fail to produce branches and spikelets while ears remain small and show widespread cell death (Chatterjee *et al.* 2014). We therefore generated *rte;rte2* double mutant plants which showed a strong enhancement of the *rte* single mutant phenotype in soils with poor boron content (0.35 ppm, Rutgers field; Table S2 in File S1). *rte;rte2* double mutant plants showed stunted growth (Figure 3, A and B), with leaves displaying narrow white stripes along their length which subsequently widened and became papery and translucent. *rte;rte2* plants also showed rudimentary undeveloped ear-like structures (Figure 3C) and did not develop beyond 10–15 cm, eventually dying off after producing ~7–8 leaves (Figure 3, F and G). These plants showed a 50% decrease in leaf boron content when compared to wild type (Table S1 in File S1). However, when grown in soil with adequate boron content; such as greenhouse soil or in the fields of Molokai, Hawaii (0.20 mg/liter and 2.35 ppm, respectively; Table S2 in File S1); *rte;rte2* double mutants did not show any vegetative defects, and resembled single *rte* mutants grown under the same conditions (Figure S5 in File S1).

However, Rutgers and Molokai soils differ for various parameters, not only for boron concentration (Table S2 in File S1). To unequivocally show that the *rte;rte2* double mutant defects were caused by inadequate boron levels in the soil, we grew double mutant plants in pots containing soil from Rutgers, and watered them with 200 μM boric acid, a concentration that we previously showed being sufficient to fully rescue the vegetative and reproductive defects of *rte* mutants without causing toxicity symptoms in normal plants (Chatterjee *et al.* 2014). Double mutant plants watered with boric acid did not show any of the vegetative phenotypes observed in control plants. While control *rte;rte2* plants

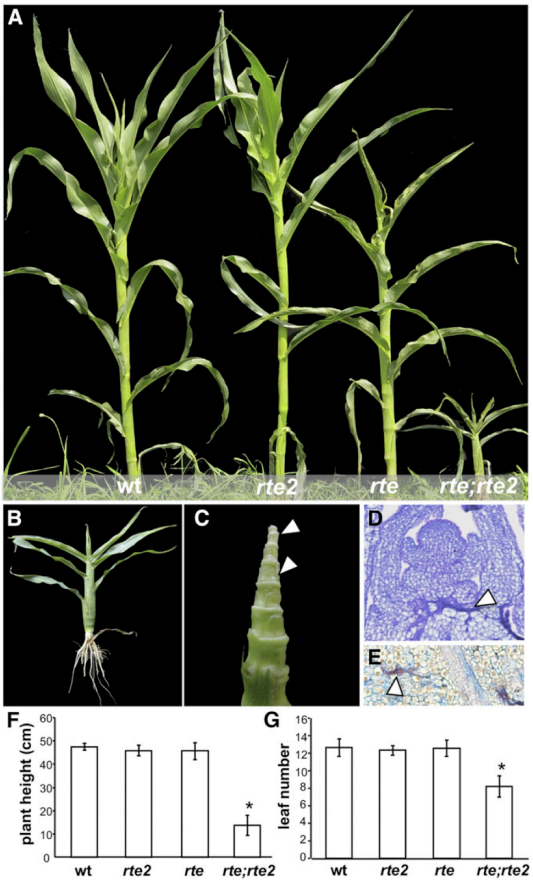

Figure 3 Genetic interaction between *rte* and *rte2* mutants. (A) Phenotype of wild type, *rte2-2*, *rte-1*, and double *rte-1;rte2-2* mutants grown in boron-deficient soil. (B and C) *rte;rte2* double mutants are short in stature and showed rudimentary ear-like structures (arrowheads). (D) Longitudinal section of shoot tips from *rte;rte2* double mutants stained with Toluidine blue, showing tissue anomalies (arrowhead) in the stem. (E) Longitudinal section of shoot stained with Safranin O-Alcian Blue. Lignified red patches (arrowhead) are visible. (F) Average plant height (n = 10, t-test, * $P <$ 0.0001). (G) Average number of leaves (n = 10, t-test, * $P < 0.0001$). Error bars indicate SD. wt, wild type.

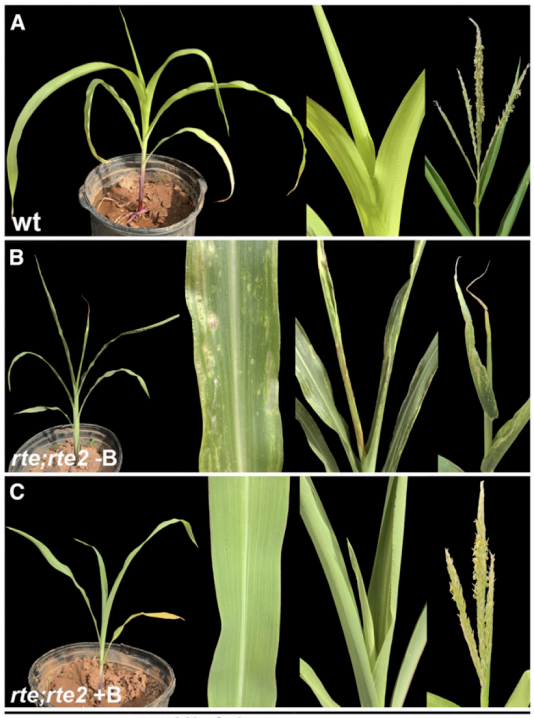

D	total N of plants	average µg of B/g of DW
wild type -B	2	16.6
wild type +B	3	74.5
rte;rte2 -B	5	12.7*
rte;rte2 +B	4	45.4*

Figure 4 (A–C) Boric acid rescue of the double *rte-1;rte2-2* mutant phenotype. Zoomed in portion of leaf lamina, top leaves, and mature tassels are visible. (D) Quantification of boron levels in treated and control plants (* $P < 0.01$, comparison within the same genotype). B/g, boron per gram; DW, dry weight.

already showed severe defects such as broad necrotic lesions and rolled up leaves 40 days after planting, those defects were not visible in *rte;rte2* plants supplemented with boric acid and those plants eventually produced fully formed and fertile tassels (Figure 4; n = 6). We then measured boron levels in treated and control plants. In *rte;rte2*-treated plants, the amount of boron was >200% higher than in untreated plants (Figure 4D). We also quantified the level of boron in both control and treated soils, and we determined that in pots watered with boric acid the concentration of boron was more than four times higher compared to control pots after treatment (Table S2 in File S1). These results unambiguously show that the defects observed in *rte;rte2* mutants are due to lack of adequate boron supply to growing tissues.

To understand how shoots of single *rte* or *rte;rte2* double mutants were affected in boron-deficient conditions, we analyzed different developmental stages. Shoot tips of wild type, *rte*, *rte2*, and *rte;rte2* were collected from 3- to 5-week-old plants grown in Rutgers fields. At 3 weeks, wild-type, *rte*, *rte2*, and *rte;rte2* plants showed a normal developing shoot apical meristem and leaf primordia (Figure 5, A–D). As development progressed, wild-type, *rte*, and *rte2* plants transitioned normally to reproductive development. However, *rte;rte2* doubled mutants began showing several lesions in the stem ground tissue (Figure 5, E–H and L). Staining with Safranin O-Alcian Blue suggested that those lesions corresponded to patches of lignified tissues (Figure 4E and Figure 5, H and L). At 5 weeks, wild type, *rte*, and *rte2*

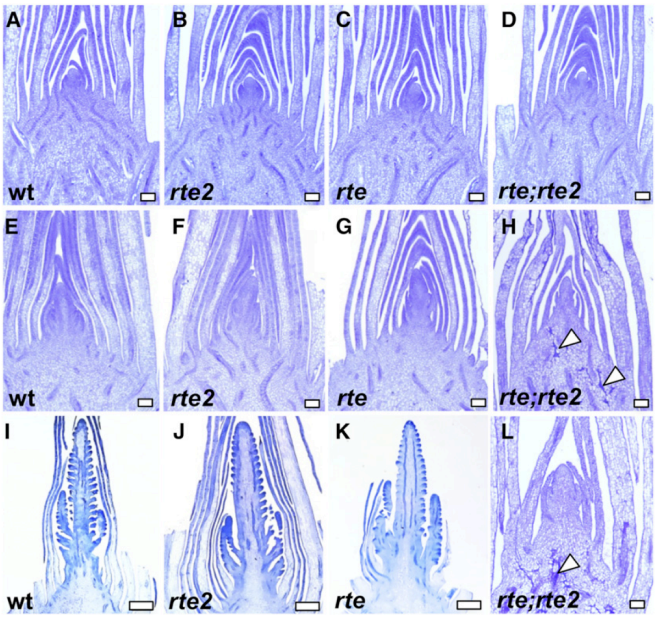

Figure 5 Longitudinal sections of shoot apical meristems and inflorescence meristems at different stages of development. (A–D) 3-week-old shoot tip showing shoot apical meristem and developing leaf primordia, (E–H) 4-week-old shoot tips at transition stage, and (I–L) 5-week-old shoot tips showing developing tassels in wild type, *rte*, and *rte2*. *rte;rte2* double mutant failed to grow. Arrowheads point to ground tissue lesions. (A–H and L) Bar, 100 μm. (I–K) Bar, 1000 μm. wt, wild type.

mutants showed initiation of several axillary meristems in immature tassels. However, the shoot apical meristem of *rte;rte*2 double mutants appeared arrested (Figure 5, I–L, and Figure S5 in File S1). Eventually, wild-type and *rte2* plants produced fully fertile inflorescences, while *rte* mutants showed characteristic small, sterile ears with brown tips (Chatterjee *et al.* 2014). Although single *rte2* mutants did not show any vegetative or reproductive phenotype in the shoots, a subtle phenotype in primary root development was evident in young seedlings (Figure 6). The primary roots of *rte2* seedlings were significantly shorter than wild-type or *rte* single mutant seedlings. This phenotype was more extreme in roots of *rte;rte2* double mutants which appeared significantly shorter and generated fewer lateral and seminal roots (Figure 6).

Overall, these results demonstrate that the disruption of *RTE2* strongly enhanced the phenotype of single *rte* mutants, suggesting that *RTE* and *RTE2* act synergistically to sustain maize growth in boron-deficient conditions.

Discussion

We previously demonstrated that *RTE* encodes a functional coortholog of the *Arabidopsis* efflux transporter BOR1 (Chatterjee *et al.* 2014). In this study, we identified three additional boron transporter genes in the maize genome (*RTE2*, *RTE3*, and *RTE6*) that likely contribute to boron transport and distribution during maize development in different tissues.

Boron transporter genes vary in number, function, as well as expression in different plant species. Among the different family members, some genes have been reported to provide tolerance to boron deficiency, whereas others are known to prevent toxicity, and those genes belong to class I and class II, respectively (Miwa *et al.* 2006, 2007; Sutton *et al.* 2007; Pallotta *et al.* 2014). In several instances, copy number variation in boron transporters has been associated with tolerance to high levels of boron in soils. Some barley varieties have tandem copies for *BOR1*-like (*Bot1*) genes (Sutton *et al.* 2007), whereas different landraces in wheat show variation in *Bot-B5/D5* alleles due to insertions of repetitive sequences in promoter regions or deletions in exons (Pallotta *et al.* 2014). These genes all belong to class II and are phylogenetically related to *RTE3*, suggesting that increasing the number of *RTE3* copies may produce maize with tolerance to high boron soils.

Homologous boron transporters in various species have also been reported to show cell type-specific expression patterns. For example, *OsBOR4* expression is mainly restricted to pollen, as is the expression of *Arabidopsis BOR6* and *BOR7* (Becker *et al.* 2003; Bock *et al.* 2006). In addition to differences in transcriptional regulation, boron transporters are also differentially regulated at the post-transcriptional level (Takano *et al.* 2005, 2010; Nakagawa *et al.* 2007; Leaungthitikanchana *et al.* 2013). BOR1 abundance at the plasma membrane is regulated via the endosomal/vacuolar recycling pathway whereby its activity at the plasma membrane is decreased or increased in high or low boron conditions, respectively (Takano *et al.* 2010; Kasai *et al.* 2011; Yoshinari *et al.* 2012). BOR2 was also reported to be regulated in the same fashion (Miwa *et al.* 2013). In rice, expression of *OsBOR1* changes according to fluctuations of boron supply in the medium (Nakagawa *et al.* 2007). Maize *RTE*-like genes

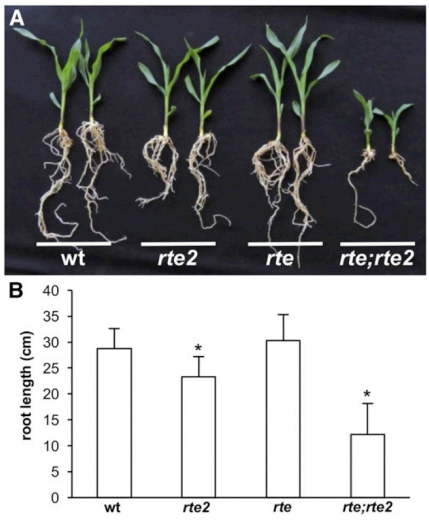

Figure 6 (A) Root phenotype of 3-week-old wild type, *rte*, *rte2*, and *rte; rte2* grown in boron-deficient soil. (B) Average length of primary roots (*t*-test between wild type, *rte2*, and *rte;rte2*, * $P < 0.001$). Error bars represent SD. wt, wild type.

showed notable tissue-specific expression differences (Figure 1). *RTE*, *RTE2*, and *RTE3* were expressed in all tissues examined, however each gene was preferentially expressed in certain tissue types. Expression of *RTE* was most abundant in ears and silks (Chatterjee *et al.* 2014), *RTE2* in roots, and *RTE3* in leaves. *RTE6* was expressed at very low levels in most tissues but was extremely abundant in pollen, consistent with it belonging to the same clade as *OsBOR4*. Overall, the phylogenetic grouping of each member is consistent with expression specificity in various species, suggesting that family members belonging to the same clades carry out specific functions in different tissues.

RTE2 encodes a protein similar to its paralog *RTE* and can fully complement the *Arabidopsis bor1* mutant (Figure 1). *In situ* hybridizations of both *RTE* and *RTE2* in maize roots and inflorescences showed an essentially identical expression pattern (Figure 2). Surprisingly, transposon insertions in *RTE2* did not show any vegetative or inflorescence defects. However, in young seedlings, single *rte2* mutants showed a slight reduction in root length when grown in boron-deficient soil (Figure 6). This suggested a subtle difference in the function of RTE and RTE2 and, together with slightly higher expression levels of *RTE2* in roots compared to other tissue, indicates that *RTE2* main function may reside in roots. A comparable situation has been described for *Arabidopsis bor2* mutants, whose root growth is affected under low boron conditions. *BOR2* is a close paralog of *BOR1* and both share 90% amino acid sequence identity (Miwa *et al.* 2013). By using fluorescent marker lines, BOR2 and BOR1 expression was reported to differ in roots, with stronger expression of BOR2 observed in lateral root caps and epidermis; while BOR1 was predominantly expressed in the root meristem, transition, and elongation zones, but not in lateral root caps. Double *bor1;bor2* mutants show more severe growth defects than either single mutant, suggesting that BOR1 and BOR2 have partially overlapping roles in shoot and root growth when grown in boron-limiting conditions. This is similar to the synergistic interaction we observed in *rte;rte2* mutants. *rte;rte2* double mutants remained undeveloped, produced only a few leaves, and died after 4–6 weeks (Figure 3). This phenotype, visible in boron-poor soils (Rutgers) but not in nutrient-rich soils (Molokai), could be fully rescued by applications of boric acid.

The duplication events originating paralogous genes in each species are independent of each other (Figure S1 in File S1). *RTE* and *RTE2* belong to maize 1 and 2 subgenomes, respectively, from the most recent maize whole-genome duplication that happened 5–12 MYA (Schnable *et al.* 2011; Hughes *et al.* 2014); while *BOR1* and *BOR2* are located on chromosomes 2 and 3, respectively, in duplicated regions possibly arisen from a more ancient whole-genome duplication event (Arabidopsis Genome Initiative 2000; Miwa *et al.* 2013). This different evolutionary history is reflected by a significantly higher identity between the paralogous proteins in maize than in *Arabidopsis* (95% *vs.* 90%). It is intriguing that a similar fate of paralogous genes is observed in two distantly related species for corresponding orthologs. While the expression differences of BOR1 and BOR2 suggest a case of subfunctionalization following a whole-genome duplication event (Miwa *et al.* 2013), we could not detect significant differences between *RTE* and *RTE2* expression by *in situ* hybridizations. However, *rte2* mutants have a subtle-root phenotype and it is therefore possible that *RTE2* is a subfunctionalized gene similarly to *BOR2* (Hughes *et al.* 2014). RTE and RTE2 protein localization may indeed reveal subtle differences that could explain the root *rte2* phenotype. Another possible scenario is that *RTE2* will eventually become an entirely nonfunctional gene, given that RTE in *rte2* mutants is sufficient for normal development.

Altogether, our current and previous results suggest that, in normal conditions, RTE is the main boron transporter in maize and the loss of its function severely impairs maize fertility in conditions of both adequate and low boron availability (Chatterjee *et al.* 2014). RTE2 function, on the other hand, can be lost without significant repercussion on development and reproduction even in low boron conditions, presumably due to RTE function. When RTE function is lost, *RTE2*, which is highly expressed in roots, can supply enough boron to shoot tissues to allow plants to grow and form inflorescences, albeit severely compromised. However, when both gene functions are lost, diffusion and channel proteins cannot supply enough boron to sustain rapidly growing tissues in conditions of low boron availability. Indeed, in the current model of boron transport, BOR1-like proteins are required for the export of negatively charged borate from root endodermal cells to supply boron to xylem elements (Takano *et al.* 2008; Miwa and Fujiwara 2010). The severity of the *rte;rte2* double mutant phenotype is very similar to that reported for single *tls1*

mutants grown in poor soils, which supports a two-step process for boron transport in maize whereby both *RTE* and *RTE2* function downstream of *TLS1* in boron uptake and loading in the root xylem (Miwa and Fujiwara 2010; Durbak *et al.* 2014). It is important to point out though that *rte;rte2* double mutants are fully complemented by boric acid watering. Three possibilities could explain this result: *rte2* mutants may not be completely null, additional not-yet-identified boron transporters may be expressed in roots of the genetic background used in our experiments, or diffusion and facilitated transport mechanisms may be able to overcome active boron transport deficiencies. In summary, our results show that under boron-deficient conditions RTE and RTE2 work synergistically to provide boron to support maize growth during vegetative and reproductive development.

Acknowledgments

We are grateful to Paula McSteen, Michaela Matthes, Kimble Ashten, and the Missouri University Plant and Soil Analysis Facility for support with boron measurements; Nelson Garcia for providing oat-maize addition lines; Marc Probasco for greenhouse and field care; Zara Tabi for Figure 2, F and G; and the Maize Genetics Cooperation Stock Center for Uniform-Mu seeds. Q.L. was supported by the China Scholarship Council. This research was supported by the National Science Foundation (IOS-1114484 and IOS-1546873) to A.G.

Literature Cited

Agarwala, S. C., P. N. Sharma, C. Chatterjee, and C. P. Sharma, 1981 Development and enzymatic changes during pollen development in boron deficient maize plants. J. Plant Nutr. 3: 329–336.

Arabidopsis Genome Initiative, 2000 Analysis of the genome sequence of the flowering plant Arabidopsis thaliana. Nature 408: 796–815.

Becker, J. D., L. C. Boavida, J. Carneiro, M. Haury, and J. A. Feijo, 2003 Transcriptional profiling of Arabidopsis tissues reveals the unique characteristics of the pollen transcriptome. Plant Physiol. 133: 713–725.

Bock, K. W., D. Honys, J. M. Ward, S. Padmanaban, E. P. Nawrocki *et al.*, 2006 Integrating membrane transport with male gametophyte development and function through transcriptomics. Plant Physiol. 140: 1151–1168.

Brown, P. H., N. Bellaloui, M. A. Wimmer, E. S. Bassil, J. Ruiz *et al.*, 2002 Boron in plant biology. Plant Biol. 4: 205–223.

Canon, P., F. Aquea, A. R. H. de la Guardia, and P. Arce-Johnson, 2013 Functional characterization of *Citrus macrophylla BOR1* as a boron transporter. Physiol. Plant 149: 329–339.

Chatterjee, M., Z. Tabi, M. Galli, S. Malcomber, A. Buck *et al.*, 2014 The boron efflux transporter ROTTEN EAR is required for maize inflorescence development and fertility. Plant Cell 26: 2962–2977.

Dordas, C., and P. H. Brown, 2001 Permeability and the mechanism of transport of boric acid across the plasma membrane of *Xenopus laevis* oocytes. Biol. Trace Elem. Res. 81: 127–139.

Durbak, A. R., K. A. Phillips, S. Pike, M. A. O'Neill, J. Mares *et al.*, 2014 Transport of boron by the *tassel-less1* aquaporin is critical for vegetative and reproductive development in maize. Plant Cell 26: 2978–2995.

Edgar, R. C., 2004 MUSCLE: multiple sequence alignment with high accuracy and high throughput. Nucleic Acids Res. 32: 1792–1797.

Gallavotti, A., S. Malcomber, C. Gaines, S. Stanfield, C. Whipple *et al.*, 2011 BARREN STALK FASTIGIATE1 is an AT-hook protein required for the formation of maize ears. Plant Cell 23: 1756–1771.

Gaujoux, R., and C. Seoighe, 2010 A flexible R package for nonnegative matrix factorization. BMC Bioinformatics 11: 367.

Gupta, U. C., Y. W. Jame, C. A. Campbell, A. J. Leyshon, and W. Nicholaichuk, 1985 Boron toxicity and deficiency: a review. Can. J. Soil Sci. 65: 381–409.

Gutierrez, R., J. J. Lindeboom, A. R. Paredez, A. M. Emons, and D. W. Ehrhardt, 2009 *Arabidopsis* cortical microtubules position cellulose synthase delivery to the plasma membrane and interact with cellulose synthase trafficking compartments. Nat. Cell Biol. 11: 797–806.

Hayes, J. E., and R. J. Reid, 2004 Boron tolerance in barley is mediated by efflux of boron from the roots. Plant Physiol. 136: 3376–3382.

Hayes, J. E., M. Pallotta, M. Garcia, M. T. Oz, J. Rongala *et al.*, 2015 Diversity in boron toxicity tolerance of Australian barley (*Hordeum vulgare* L.) genotypes. BMC Plant Biol. 15: 231.

Hu, H. N., P. H. Brown, and J. M. Labavitch, 1996 Species variability in boron requirement is correlated with cell wall pectin. J. Exp. Bot. 47: 227–232.

Hughes, T. E., J. A. Langdale, and S. Kelly, 2014 The impact of widespread regulatory neofunctionalization on homeolog gene evolution following whole-genome duplication in maize. Genome Res. 24: 1348–1355.

Kasai, K., J. Takano, K. Miwa, A. Toyoda, and T. Fujiwara, 2011 High boron-induced Ubiquitination regulates vacuolar sorting of the BOR1 borate transporter in *Arabidopsis thaliana*. J. Biol. Chem. 286: 6175–6183.

Kobayashi, M., T. Matoh, and J. Azuma, 1996 Two chains of rhamnogalacturonan II are cross-linked by borate-diol ester bonds in higher plant cell walls. Plant Physiol. 110: 1017–1020.

Leaungthitikanchana, S., T. Fujibe, M. Tanaka, S. L. Wang, N. Sotta *et al.*, 2013 Differential expression of three *BOR1* genes corresponding to different genomes in response to boron conditions in hexaploid wheat (*Triticum aestivum* L.). Plant Cell Physiol. 54: 1056–1063.

Leonard, A., B. Holloway, M. Guo, M. Rupe, G. X. Yu *et al.*, 2014 *Tassel-less1* encodes a boron channel protein required for inflorescence development in maize. Plant Cell Physiol. 55: 1044–1054.

Liu, K., L. L. Liu, Y. L. Ren, Z. Q. Wang, K. N. Zhou *et al.*, 2015 *Dwarf* and *tiller-enhancing 1* regulates growth and development by influencing boron uptake in boron limited conditions in rice. Plant Sci. 236: 18–28.

Livak, K. J., and T. D. Schmittgen, 2001 Analysis of relative gene expression data using real-time quantitative PCR and the 2 (-Delta Delta C(T)) method. Methods 25: 402–408.

Lordkaew, S., B. Dell, S. Jamjod, and B. Rerkasem, 2011 Boron deficiency in maize. Plant Soil 342: 207–220.

Lyons, E., B. Pedersen, J. Kane, M. Alam, R. Ming *et al.*, 2008 Finding and comparing syntenic regions among Arabidopsis and the outgroups papaya, poplar, and grape: CoGe with rosids. Plant Physiol. 148: 1772–1781.

Mickelbart, M. V., P. M. Hasegawa, and J. Bailey-Serres, 2015 Genetic mechanisms of abiotic stress tolerance that translate to crop yield stability. Nat. Rev. Genet. 16: 237–251.

Miwa, K., and T. Fujiwara, 2010 Boron transport in plants: co-ordinated regulation of transporters. Ann. Bot. 105: 1103–1108.

Miwa, K., J. Takano, and T. Fujiwara, 2006 Improvement of seed yields under boron-limiting conditions through overexpression

of BOR1, a boron transporter for xylem loading, in *Arabidopsis thaliana*. Plant J. 46: 1084–1091.

Miwa, K., J. Takano, H. Omori, M. Seki, K. Shinozaki *et al.*, 2007 Plants tolerant of high boron levels. Science 318: 1417.

Miwa, K., S. Wakuta, S. Takada, K. Ide, J. Takano *et al.*, 2013 Roles of BOR2, a boron exporter, in cross linking of rhamnogalacturonan II and root elongation under boron limitation in Arabidopsis. Plant Physiol. 163: 1699–1709.

Nakagawa, Y., H. Hanaoka, M. Kobayashi, K. Miyoshi, K. Miwa *et al.*, 2007 Cell-type specificity of the expression of Os *BOR1*, a rice efflux boron transporter gene, is regulated in response to boron availability for efficient boron uptake and xylem loading. Plant Cell 19: 2624–2635.

Noguchi, K., M. Yasumori, T. Imai, S. Naito, T. Matsunaga *et al.*, 1997 bor1–1, an Arabidopsis thaliana mutant that requires a high level of boron. Plant Physiol. 115: 901–906.

O'Neill, M. A., D. Warrenfeltz, K. Kates, P. Pellerin, T. Doco *et al.*, 1996 Rhamnogalacturonan-II, a pectic polysaccharide in the walls of growing plant cell, forms a dimer that is covalently cross-linked by a borate ester. *In vitro* conditions for the formation and hydrolysis of the dimer. J. Biol. Chem. 271: 22923–22930.

O'Neill, M. A., S. Eberhard, P. Albersheim, and A. G. Darvill, 2001 Requirement of borate cross-linking of cell wall rhamnogalacturonan II for *Arabidopsis* growth. Science 294: 846–849.

Pallotta, M., T. Schnurbusch, J. Hayes, A. Hay, U. Baumann *et al.*, 2014 Molecular basis of adaptation to high soil boron in wheat landraces and elite cultivars. Nature 514: 88–91.

Perez-Castro, R., K. Kasai, F. Gainza-Cortes, S. Ruiz-Lara, J. A. Casaretto *et al.*, 2012 VvBOR1, the grapevine ortholog of AtBOR1, encodes an efflux boron transporter that is differentially expressed throughout reproductive development of *Vitis vinifera* L. Plant Cell Physiol. 53: 485–494.

Raven, J. A., 1980 Short-distance and long-distance transport of boric-acid in plants. New Phytol. 84: 231–249.

Reid, R., 2007 Identification of boron transporter genes likely to be responsible for tolerance to boron toxicity in wheat and barley. Plant Cell Physiol. 48: 1673–1678.

Rines, H. W., R. L. Phillips, R. G. Kynast, R. J. Okagaki, M. W. Galatowitsch *et al.*, 2009 Addition of individual chromosomes of maize inbreds B73 and Mo17 to oat cultivars Starter and Sun II: maize chromosome retention, transmission, and plant phenotype. Theor. Appl. Genet. 119: 1255–1264.

Schnable, J. C., N. M. Springer, and M. Freeling, 2011 Differentiation of the maize subgenomes by genome dominance and both ancient and ongoing gene loss. Proc. Natl. Acad. Sci. USA 108: 4069–4074.

Schnurbusch, T., J. Hayes, and T. Sutton, 2010 Boron toxicity tolerance in wheat and barley: Australian perspectives. Breed. Sci. 60: 297–304.

Settles, A. M., D. R. Holding, B. C. Tan, S. P. Latshaw, J. Liu *et al.*, 2007 Sequence-indexed mutations in maize using the UniformMu transposon-tagging population. BMC Genomics 8: 116.

Shelp, B. J., E. Marentes, A. M. Kitheka, and P. Vivekanandan, 1995 Boron mobility in plants. Physiol. Plant. 94: 356–361.

Shorrocks, V. M., 1997 The occurrence and correction of boron deficiency. Plant Soil 193: 121–148.

Stangoulis, J. C. R., P. H. Brown, N. Bellaloui, R. J. Reid, and R. D. Graham, 2001 The efficiency of boron utilisation in canola. Aust. J. Plant Physiol. 28: 1109–1114.

Sun, J. H., L. Shi, C. Y. Zhang, and F. S. Xu, 2012 Cloning and characterization of boron transporters in *Brassica napus*. Mol. Biol. Rep. 39: 1963–1973.

Sutton, T., U. Baumann, J. Hayes, N. C. Collins, B. J. Shi *et al.*, 2007 Boron-toxicity tolerance in barley arising from efflux transporter amplification. Science 318: 1446–1449.

Takano, J., K. Noguchi, M. Yasumori, M. Kobayashi, Z. Gajdos *et al.*, 2002 *Arabidopsis* boron transporter for xylem loading. Nature 420: 337–340.

Takano, J., K. Miwa, L. Yuan, N. von Wiren, and T. Fujiwara, 2005 Endocytosis and degradation of BOR1, a boron transporter of *Arabidopsis thaliana*, regulated by boron availability. Proc. Natl. Acad. Sci. USA 102: 12276–12281.

Takano, J., M. Wada, U. Ludewig, G. Schaaf, N. von Wiren *et al.*, 2006 The *Arabidopsis* major intrinsic protein NIP5;1 is essential for efficient boron uptake and plant development under boron limitation. Plant Cell 18: 1498–1509.

Takano, J., K. Miwa, and T. Fujiwara, 2008 Boron transport mechanisms: collaboration of channels and transporters. Trends Plant Sci. 13: 451–457.

Takano, J., M. Tanaka, A. Toyoda, K. Miwa, K. Kasai *et al.*, 2010 Polar localization and degradation of *Arabidopsis* boron transporters through distinct trafficking pathways. Proc. Natl. Acad. Sci. USA 107: 5220–5225.

Tamura, K., G. Stecher, D. Peterson, A. Filipski, and S. Kumar, 2013 MEGA6: molecular evolutionary genetics analysis version 6.0. Mol. Biol. Evol. 30: 2725–2729.

Tanaka, M., I. S. Wallace, J. Takano, D. M. Roberts, and T. Fujiwara, 2008 NIP6;1 is a boric acid channel for preferential transport of boron to growing shoot tissues in *Arabidopsis*. Plant Cell 20: 2860–2875.

Tanaka, N., S. Uraguchi, A. Saito, M. Kajikawa, K. Kasai *et al.*, 2013 Roles of pollen-specific boron efflux transporter, OsBOR4, in the rice fertilization process. Plant Cell Physiol. 54: 2011–2019.

Walley, J. W., R. C. Sartor, Z. Shen, R. J. Schmitz, K. J. Wu *et al.*, 2016 Integration of omic networks in a developmental atlas of maize. Science 353: 814–818.

Yoshinari, A., K. Kasai, T. Fujiwara, S. Naito, and J. Takano, 2012 Polar localization and endocytic degradation of a boron transporter, BOR1, is dependent on specific tyrosine residues. Plant Signal. Behav. 7: 46–49.

Communicating editor: K. Bomblies

Figure S1

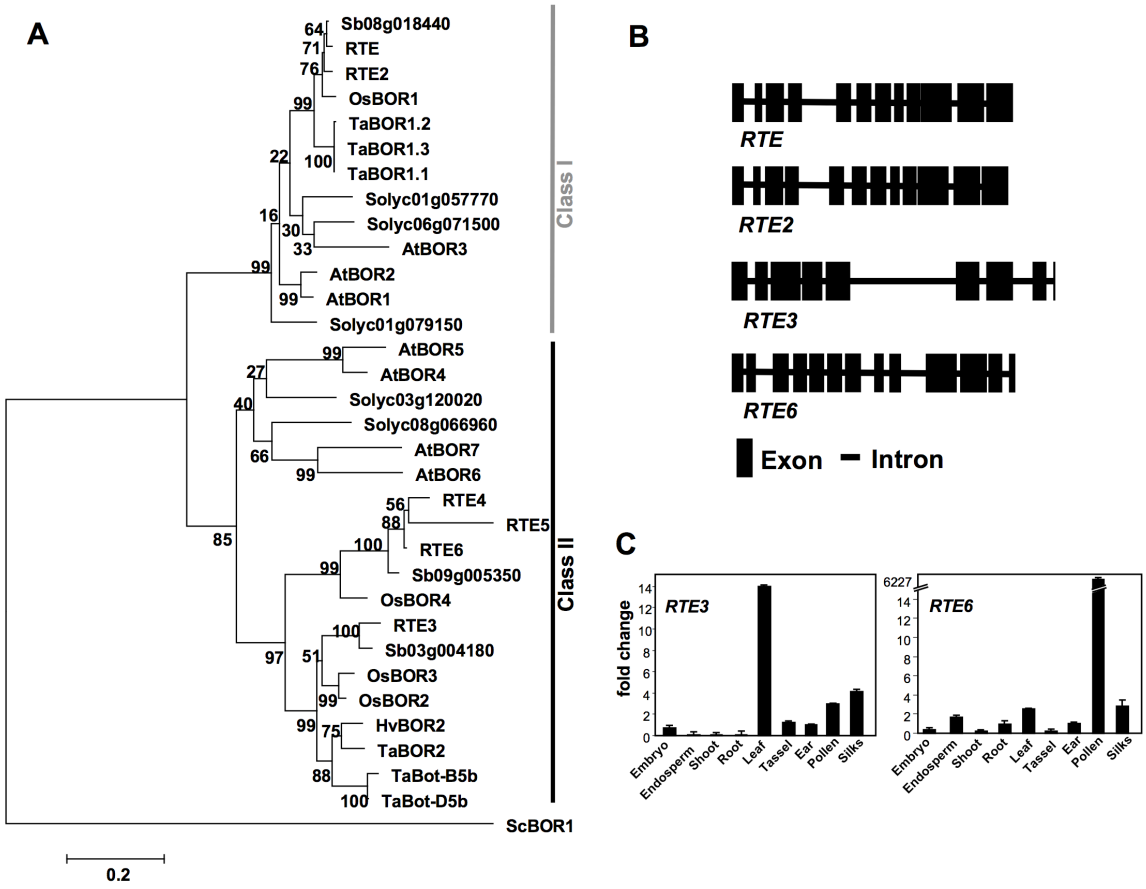

Figure S1. Maximum Likelihood phylogenetic analysis of boron transporters [A]. Bootstrap values based on 1000 replicates are shown. The yeast boron transporter ScBOR1 was used as an outgroup. At, *Arabidopsis thaliana*; Solyc, *Solanum lycopersicum*; Os, *Oryza sativa* ; Sb, *Sorghum bicolor*; Hv, *Hordeum vulgare*, and Ta, *Triticum aestivum*. The *RTE* family of maize boron transporters [B]. Schematic diagram showing the gene structure of *RTE*, *RTE2*, *RTE3* and *RTE6*. Quantitative RT-PCR analysis in different tissues (fold change relative to ear) [C].

Figure S2

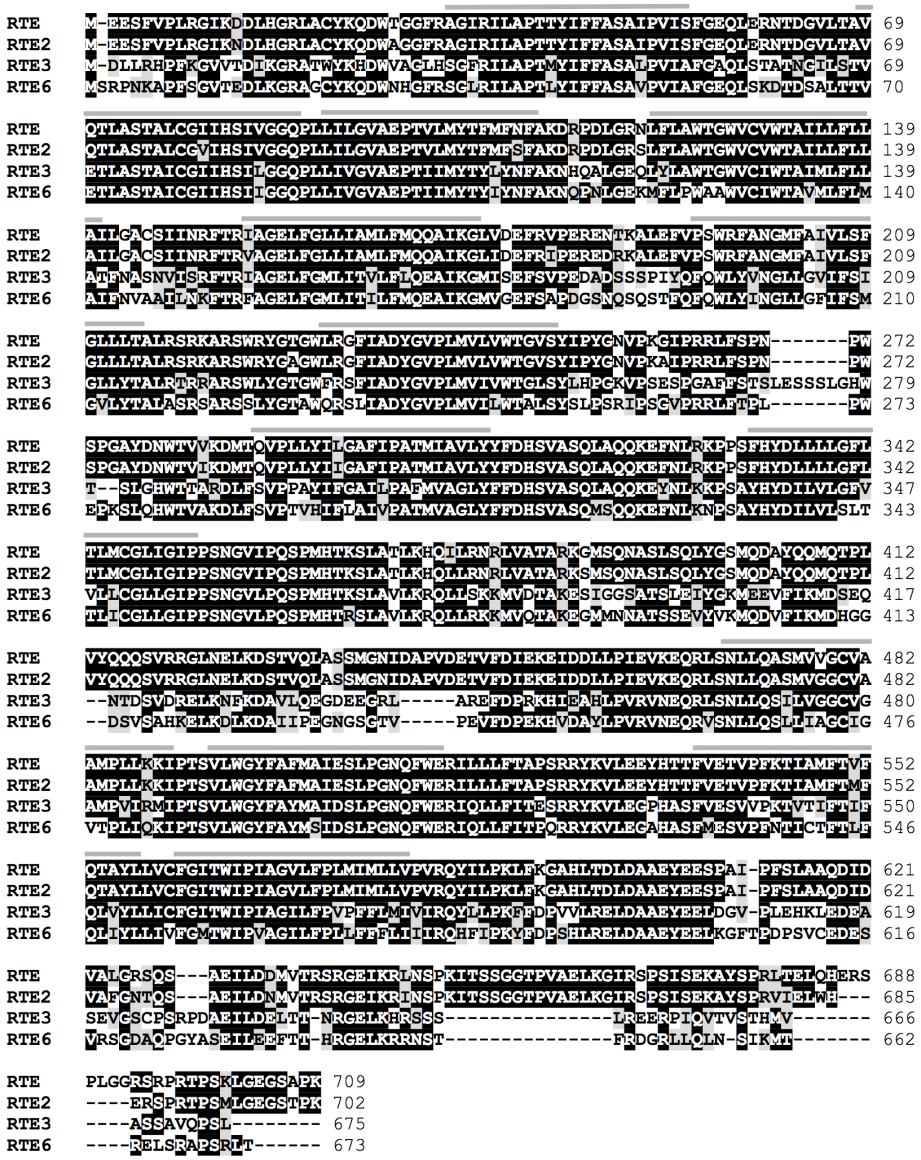

Figure S2. Alignment of RTE amino acid sequence with RTE2,RTE3 and RTE6. Black boxes indicate identical residues whereas grey boxes indicate similar residues. Light grey bars, putative transmembrane domains as predicted by aramemnon.botanik.uni-koeln.de.

Figure S3

Figure S3. Comparison between chromosome 1:149247320-149401183 containing the *RTE* gene and chromosome 3:128040133-128193930 containing the *RTE2* gene [B]. Sequence comparison between chromosome 9:153632461-1537888961 containing *RTE4*, chromosome 3:183017037-183171804 containing *RTE5,* and chromosome 8:79864709-80015561 containing *RTE6* [C]. Red rectangular boxes represent high-scoring segment pairs whereas red shaded areas connecting the segments represent regions of sequence similarity.

Figure S4

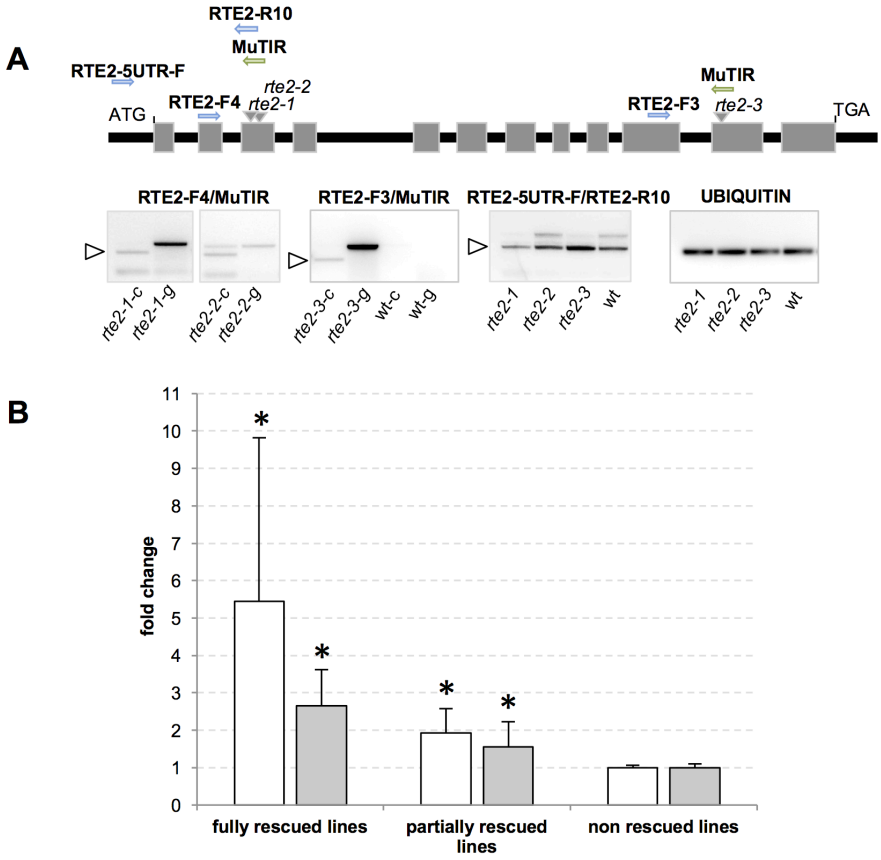

Figure S4. Expression analysis of *RTE2* insertion lines by RT-PCR [A]. Schematic diagram of *RTE2* gene structure with arrows indicating primers used in the analysis. C, cDNA; g, genomic DNA. White arrowheads, expected cDNA product. Quantitative RT-PCR of representative Arabidopsis *bor-1* lines overexpressing *RTE2* (* p≤0.05; n=6 technical replicates; error bars, standard deviation) [B].

Figure S5

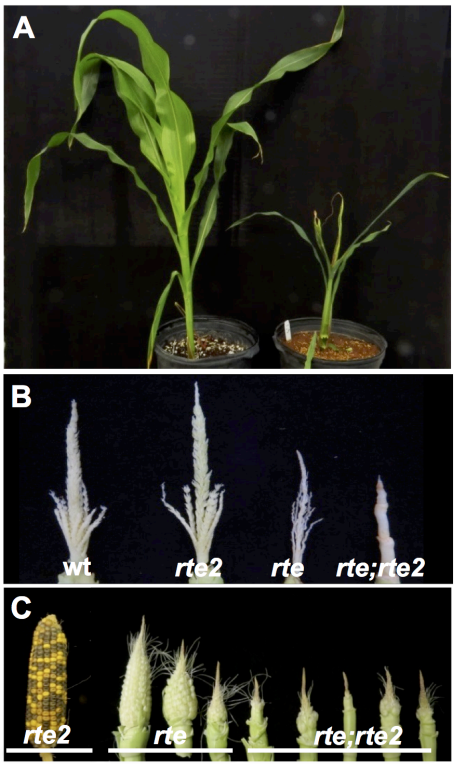

Figure S5. Phenotype of *rte;rte2* double mutants growing in greenhouse soilless mix (left) and boron-deficient Rutgers field soil (right) [A]. In Rutgers field soil**,** wild-type and *rte2* plants showed normal tassel development with fertile spikelets [B], while *rte* failed to produced any spikelets and *rte;rte2* double mutant plants displayed growth arrest. Ear phenotype of *rte2*, *rte* and *rte;rte2* double mutants grown in potting soil [C]**.**

Table S1: B measurements by ICP-OES in leaves.

Arabidopsis	total N of lines	average μg of B/g of DW
fully rescued lines	4	110*
partially rescued lines	3	100.5
bor1-3	1	38.4*

maize	total N of plants	average μg of B/g of DW
wild type	12	22.8*
rte2	6	16.1
rte	13	15.1
rte;rte2	14	11.05*

*$p<0.05$

Table S2: Soil analysis.

	pH	B (ppm)	Ca (pounds/acre)
Molokai field	5.34 (strongly acidic)	2.35 (adequate)	3350 (above optimum)
Rutgers field (Figure 3)	5.9 (moderately acidic)	0.35 (low)	1299 (below optimum)
Greenhouse soilless potting mix (Figure S6)	6.07 (optimum)	0.20 mg/L (optimum)	131.5 mg/L (medium)
Rutgers soil +B (Figure 4)	5.99 (moderately acidic)	4.26 (adequate)	2820 (above optimum)
Rutgers soil –B (Figure 4)	5.8 (moderately acidic)	0.93 (adequate)	3042 (above optimum)

	P (pounds/acre)	K (pounds/acre)	Mg (pounds/acre)
Molokai field	593 (above optimum)	1193 (above optimum)	1086 (above optimum)
Rutgers field (Figure 3)	335 (above optimum)	334.5 (above optimum)	291.5 (optimum)
Greenhouse soilless potting mix (Figure S6)	38.8 mg/L (above optimum)	86 mg/L (medium)	33.4 mg/L (medium)
Rutgers soil +B (Figure 4)	354 (above optimum)	430 (above optimum)	604 (above optimum)
Rutgers soil –B (Figure 4)	356 (above optimum)	414 (above optimum)	673 (above optimum)

Table S3: List of primers used.

PRIMERS	SEQUENCE 5'-3'	PURPOSE
RTE-RT	For: GAGGGAGAAGCAGGCCTAGGA Rev: TGATGGCCAGTAACCCAGTAGTTG	Real-time PCR
RTE2-RT	For: GCAAGGGCCTCACTTCACAC Rev: CACGAAGCTCTCCTCCATTGAAG	Real-time PCR
RTE3-RT	For: GTGACAGTGAGCACGCATATGG Rev: CAGTATTCACATCAACGGAGTGCA	Real-time PCR
RTE4-RT	For: TGTGTTTCTTGTTCTCATACCATGG Rev: AATGCCAAGAAGACCACACCAC	Real-time PCR
RTE5-RT	For: ATGATGAACCCAGTGGTGACAG Rev: GCGGTCCAAGAGCACGAC	Real-time PCR
RTE6-RT	For: GGTCATCGCTATATGGCACTGC Rev: GCTTGGCAATGAATATGACAATGC	Real-time PCR
Ubi-RT	For: GAGTGCCCCAACGCCGAGTG Rev: CTACGCCTGCTGGTTGTAGACGTA	Real-time PCR
18S	For: CCAGCGATCGTTTATTGCTT Rev: AGTCTTTCCTCTGCGACCAG	Real-time PCR in At
RTE2-RT	For: GCTAGAGTTTGTTCCATCATGGCG Rev: GTGGAACACCATAGTCAGCGATGAAG	Real-time PCR in At
RTE-5UTR	For: TTCCGTGTGCTCAGCTCA Rev: GCCAGTCGGAGTGTCAAGTG	In situ
RTE2-5UTR	For: GGACCTTGCCGTTCTCTCC Rev: TCTCCCACTCCGGGTGTG	In situ
RTE-3UTR	For: GGTGAAGGCTCGGCACCAAAGTG Rev: GAGTAGTTACTCTAATATTTCTG	In situ
RTE2-3UTR	For: CCTAGGACGCCGTCCATGCTG Rev: GCCACTCTAATATTCTGCTAG	In situ
F-RTE1-XhoI	GTCTCGAGATGGAGGAGAGCTTCGTGC	RTE1 CDS
R-RTE1-XbaI	GTTCTAGATCACTTTGGTGCCGAGC	
F-RTE2-XhoI	GTCTCGAGATGGAGGAGAGCTTCGTGC	RTE2 CDS
R-RTE2-XbaI	GTTCTAGATCACTTTGGTGTTGAGCCTT	
F-RTE3-XhoI	GTCTCGAGATGGATCTACTGAGACACCC	RTE3 CDS
R-RTE3-XbaI	GTTCTAGATCACAGGCTTGGCTGAAC	

F-RTE6-Hind	GTAAGCTTATGTCGAGACCTAATAAAGCTCC	RTE6 CDS
R-RTE6-Xbal	GTTCTAGATCATGTAAGCCGAGAAGGAG	
F-RTE5-GE	ATGATGAACCCAGTGGTGAC	RTE5 B73 genomic
R-RTE5-GE	TCATGTAAGCCAAGAAGGAAC	
F-RTE4 -GE	ATGATGAACCCAGTGGTGAC	RTE4 OMA genomic
R-RTE4-xba	GTTCTAGATCAGTACCTAAAATGAGTTGC	
RTE2EcoRI-F1	For: AGTGAATTCATGGAGGAGAGCTTCGTGCCCTTG	*35S::RTE2* complementation
RTE2HindIII-R1	Rev: GACAAGCTTTCACTTTGGTGTTGAGCCTTCACC	

Table S4: Complementation of *Arabidopsis bor1-3* mutant with maize *RTE2*.

Lines	Degree of complementation	Phenotype of T1 plants
1	Fully rescued	Fertile and growth similar to wild-type
2	Fully rescued	Fertile and growth similar to wild-type
3	Fully rescued	Fertile and growth similar to wild-type
4	Partially rescued	Mix of fertile and empty siliques
5	Not rescued	No seeds, bushy and tall
6	Partially rescued	Mix of fertile and empty siliques
7	Partially rescued	Mix of fertile and empty siliques
8	Partially rescued	Mix of fertile and empty siliques
9	Not rescued	Bushy plant similar to *bor1-3* mutant
10	Not rescued	No seeds, bushy and tall
11	Not rescued	Bushy plant similar to *bor1-3* mutant
12	Not rescued	Bushy plant similar to *bor1-3* mutant
13	Partially rescued	Mix of fertile and empty siliques
14	Not rescued	Bushy plant similar to *bor1-3* mutant
15	Fully rescued	Fertile and growth similar to wild-type
16	Fully rescued	Fertile and growth similar to wild-type
17	Partially rescued	Mix of fertile and empty siliques
18	Not rescued	Bushy plant similar to *bor1-3* mutant
19	Fully rescued	Fertile and growth similar to wild-type
20	Partially rescued	Mix of fertile and empty siliques
21	Fully rescued	Fertile and growth similar to wild-type
22	Not rescued	Bushy plant similar to *bor1-3* mutant
23	Fully rescued	Fertile and growth similar to wild-type
24	Fully rescued	Fertile and growth similar to wild-type
25	Not rescued	Bushy plant similar to *bor1-3* mutant
26	Partially rescued	Mix of fertile and empty siliques
27	Partially rescued	Mix of fertile and empty siliques
28	Partially rescued	Mix of fertile and empty siliques
29	Not rescued	Bushy plant similar to *bor1-3* mutant
30	Not rescued	Bushy plant similar to *bor1-3* mutant
31	Fully rescued	Fertile and growth similar to wild-type
32	Fully rescued	Fertile and growth similar to wild-type
33	Fully rescued	Fertile and growth similar to wild-type
34	Partially rescued	Mix of fertile and empty siliques
35	Not rescued	Bushy plant similar to *bor1-3* mutant
36	Fully rescued	Fertile and growth similar to wild-type
37	Fully rescued	Fertile and growth similar to wild-type
38	Fully rescued	Fertile and growth similar to wild-type

CHAPTER THREE

NEEDLE1 (NDL1) ENCODES A MITOCHONDRIA LOCALIZED PROTEASE REQUIRED FOR THERMOTOLERANCE OF MAIZE GROWTH

Abstract

Plant axillary meristems (AMs) are groups of stem cells initiated at the axils of leaves during post-embryonic development. AMs are ultimately responsible for the production of branches, lateral organs and stems, thus they directly shape plant architecture and affect crop yield. The previous identification of several mutants showing defects in inflorescence development has shed light on the essential role of the plant hormone auxin in regulating maize AM initiation. Here we characterized and cloned *needle1* (*ndl1*), a temperature sensitive mutant displaying strong genetic interactions with several auxin-related mutants. Interestingly, we demonstrate that *NDL1* encodes a metallo-protease localized to mitochondria. Further analysis indicates that together with the hyperaccumulation of reactive oxygen species (ROS), *ndl1* mutant inflorescences show the up-regulation of many genes involved in stress responses and mitochondrial retrograde regulation (MRR). These findings uncovered an essential pathway that coordinates meristem redox status with the hormonal control of reproductive organogenesis, and regulates overall maize growth.

Introduction

Plant developmental plasticity depends on the life-long maintenance of stem cells called meristems, group of cells that retain the ability to proliferate as well as to differentiate functional progeny (de Jong and Leyser, 2012; Greb and Lohmann, 2016; Laux, 2003). Plants produce different types of meristems throughout their lifecycle. In particular, shoot architecture in higher plants is established by apical meristems, shoot apical meristems (SAMs) and inflorescence meristems (IMs), and axillary meristems (AMs), initiating at the axils of true or modified leaves. In crop species such as maize, IM and AM activity determines the architecture of its inflorescences thus directly impacting yield (Bommert et al., 2013b). Meristem function is heavily influenced by the activity of phytohormones and by environmental factors such as light, temperature and stresses (Pfeiffer et al., 2017). For example, when grown in drought and heat stress condition, grain crops have defective floral initiation and show delayed flowering dramatically reducing yield (Barnabas et al., 2008).

Auxins are a group of phytohormones that play essential roles in plant growth and development and are essential for organogenesis. In the past few decades, the molecular characterization of several auxin mutants showing defects in meristem formation and development highlighted the importance of auxin in regulating plant shoot architecture. In Arabidopsis, mutants defective in inflorescence development are characterized by the pin-formed phenotype whereby no floral meristem, a type of AM, is initiated. Pin-like mutants such as *pinformed1* (*pin1*), *pinoid* (*pid*), *monopteros* (*mp*), and *yucca* (*yuc*) are affected in

auxin transport, signaling and biosynthesis, respectively (Bennett et al., 1995; Cheng et al., 2006; Gälweiler et al., 1998; Przemeck et al., 1996). In maize, mutants defective in AM initiation and development are generally characterized by a reduction in spikelets (grass specific structures containing florets) and branches in its inflorescences, the tassel and the ear. Molecular analysis indicates that the defects observed in several of these mutants are caused by mutations in genes regulating auxin function. *VANISHING TASSEL2* (*VT2*) and *SPARSE INFLORESCENCE1* (*SPI1*) encode the co-orthologs of TRYPTOPHAN AMINOTRANSFERASE 1 (TAA1) and YUCCA4 (YUC4) in Arabidopsis, respectively, and function in the best characterized auxin biosynthetic pathway in plants (Gallavotti et al., 2008a; Phillips et al., 2011; Stepanova et al., 2008; Zhao et al., 2001). BARREN INFLORESCENCE1 (BIF1) and BARREN INFLORESCENCE4 (BIF4) are members of the AUXIN/INDOLE3 ACETIC ACIDs (Aux/IAAs) family, a group of essential proteins functioning as negative regulators of auxin signaling (Barazesh and McSteen, 2008; Galli et al., 2015). *BARREN INFLORESCENCE2* (*BIF2*) encodes a serine/threonine protein kinase, homologous to Arabidopsis PID, that regulates auxin polar transport by phosphorylation of PIN efflux transport proteins (McSteen et al., 2007; Skirpan et al., 2009). Moreover, analysis of widely-used reporter lines for auxin response and polar transport suggests that the creation of PIN1-mediated local auxin concentration gradients is necessary for plant organ formation in both Arabidopsis and maize (Benková et al., 2003; Gallavotti et al., 2008b; Heisler et al., 2005). Interestingly, recent evidences suggest that auxin minima also play an essential

role in regulating axillary meristem formation (Hofmann, 2014; Qi et al., 2014). Thus the dynamic regulation of auxin is crucial for inflorescence development and is necessary for establishing the species-specific patterning of organ formation in inflorescences.

Here we characterize a new temperature sensitive maize mutant called *needle1* (*ndl1*) with striking phenotypic similarities with the auxin-related mutants mentioned above, and showing a strong genetic interaction with several auxin-related mutants such as *Bif1* and *spi1*. Surprisingly, *NDL1* encodes a mitochondrial localized ATP-dependent zinc metalloprotease belonging to the FTSH (Filamentation Temperature Sensitive H) family, originally identified in *E. coli* (Begg et al., 1992; Santos and De Almeida, 1975). *ndl1* mutants show ROS hyperaccumulation and strong up-regulation of many genes involved in stress responses. We show that these conditions affect auxin homeostasis and consequently reproductive organogenesis, indicating a functional link between meristem redox status and auxin in regulating maize inflorescence architecture.

RESULTS

ndl1 (needle1) is a temperature-sensitive mutant affected in the early stages of reproductive organogenesis

The *ndl1* mutant was originally identified in ethyl methanesulfonate (EMS) mutagenesis screens for new mutations affecting maize inflorescence development. Segregation in M2 populations indicated that the mutant was caused by a single recessive mutation. After introgression in a homogeneous B73 background, *ndl1* plants showed abnormal inflorescence development, showing tassels with fewer branches and spikelets (Fig. 1a-d and Fig. 2c-d) while ears were only slightly shorter with occasional disorganized rows of kernels (Fig. 2a, b and 2e).

We noticed that in fields and greenhouse growth conditions, the *ndl1* tassel phenotype showed variable expressivity, ranging from very thin tassels with no branches and no spikelets to tassels with fewer branches and spikelets (Fig. 1a-d). Several evidences suggested that the phenotype severity was influenced by temperature. The appearance of a strong phenotype (no branches and spikelets) always correlated with field plantings in warmer temperatures in late Spring (Fig. 3a,b). To test the hypothesis that temperature was therefore a factor influencing the expressivity of the *ndl1* phenotype, we grew *ndl1* plants in long day conditions (16 hours light-8 hours dark) in a controlled growth chamber in mild (24°C day-20°C night) and high temperature (32°C day-28°C night). Over 30% of *ndl1* plants arrested growth after producing a few leaves when grown at high temperature. The remaining mutants produced tassels with a significantly reduced

number of branches (Fig. 3c-h). None of the above phenotypes were instead observed in the mild temperature regime.

The inflorescence phenotype of *ndl1* mutants was reminiscent of mutants affected in AM development in inflorescences, such as the semi-dominant *Bif1* and *Bif4* mutants affected in auxin signaling (Galli et al., 2015). To determine whether AM initiation or maintenance was impaired, we used Scanning Electron Microscopy (SEM) to analyze the early stages of *ndl1* tassel and ear development. In normal plants, the inflorescence meristem (IM) gives rise to a series of reproductive axillary meristems (AMs), which eventually produce the spikelets and their florets (Fig. 1e). In *ndl1* tassels showing a strong phenotype, no AM was visible (Fig. 1h), whereas in weak mutants the regular initiation and arrangements of AMs along the inflorescence axis was visibly disrupted (Fig. 1f and Fig. 1g). In *ndl1* ears, we noticed milder defects in AM initiation compared to tassels but some IMs showed slight fasciation (Fig. 2b). Altogether these results suggested that *NDL1* functions in AMs initiation as well as in IM maintenance.

To better characterize the molecular defects of *ndl1* plants, we used RNA *in situ* hybridizations with a series of known marker genes. Normally in maize inflorescences, the early steps of primordia initiation occur at the peripheral zone of IMs. Suppressed bracts (SBs) are the first visible primordia and subtend newly initiating AMs. Boundary domains between the newly forming AMs and the inflorescence axis are established very early in development by the function of boundary genes such as *BARREN STALK1* (*BA1*) to prevent fusion defects (Gallavotti et al., 2004; Galli et al., 2015). We used antisense probes for the maize

ZYB15, *BA1* and *ARF4* genes whose expression marks SBs, BDs and meristems, respectively (Fig. 1i, k and m) to analyze the early steps in reproductive organogenesis of *ndl1* tassels. In *ndl1* immature tassels, the regular expression patterns of *ZYB15* and *BA1* were disrupted in the peripheral zone of IMs (Fig. 1i, j, m and n). Similarly, *ARF4*, whose expression is normally observed both in the IM and in the peripheral zone marking newly forming primordia, was normally expressed in *ndl1* IM but not in its peripheral zone (Fig. 1k, l; (Galli et al., 2015). These results indicate that in *ndl1* mutants the early steps of tassel organogenesis leading to initiating SBs and AMs were disrupted, while the IM per se appeared unaffected, at least in early stages of development.

Previous studies showed that polar auxin transport is necessary for maize AM initiation and inflorescence patterning (Gallavotti et al., 2008b). *ZmPIN1a* encodes a membrane-localized auxin efflux transporter whose upregulation at the peripheral zone of IMs marks newly initiating primordia (Gallavotti et al., 2008b). We used confocal microscopy to monitor the expression of ZmPIN1a:YFP in wild type and *ndl1* immature tassels. A strong up-regulation of ZmPIN1a:YFP was detected on the flank of wild type IMs, which overlapped with SB and AM initiation sites (Fig. 1o), as previously reported, whereas in the *ndl1* tassels with a severe phenotype this patterning was completely absent (Fig. 1p; n=3). Overall, our results indicate that *NDL1* is essential for the early stages of maize reproductive organogenesis.

ndl1 mutants enhance the inflorescence phenotype of auxin-related mutants

The phenotypic resemblance of *ndl1* and previously reported mutants with altered auxin transport, signaling or biosynthesis as well as the analysis of ZmPIN1a:YFP suggested that *NDL1* function may also affect these pathways (Barazesh and McSteen, 2008; Gallavotti et al., 2008a; Gallavotti et al., 2008b; Galli et al., 2015; McSteen et al., 2007; Phillips et al., 2011). To investigate this hypothesis, we checked the genetic interaction between *ndl1* and different auxin-related mutants, such as *Bif1* and *Bif4*, *spi1* and *bif2*, affected in auxin signaling, biosynthesis and transport, respectively (Barazesh and McSteen, 2008; Gallavotti et al., 2008a; Galli et al., 2015; McSteen et al., 2007). The strongest genetic interaction was observed between *ndl1* and *Bif1*, and between *ndl1* and *spi1*. *ndl1* enhanced the phenotype of *Bif1/+* and *spi1/spi1* mutants in both tassels and ears (Fig. 4). Quantitative analysis of mature tassels showed a significant reduction in branch and spikelet-pair number compared with single mutants (Fig. 5). Furthermore, we observed long barren tips in double mutants' ears only (Fig. 4g-l). A similar phenotype was also observed in *Bif4/+;ndl1/ndl1* mutants (Fig. 6e). However, *ndl1* could not significantly enhance the tassel phenotype of *Bif4/+* plants (Fig. 6a-d, f, g). Moreover, we analyzed the phenotype of *bif2/bif2;ndl1/ndl1* double mutants, which produced tassels and ears with a similar phenotype with *bif2* single mutants (Fig. 7a-e, g and h). However, the main rachis of double mutant tassel was significant thinner than *bif2* mutants, but comparable with *ndl1* mutants (Fig. 7f), suggesting a more complex genetic connection. The phenotypic similarities

between *ndl1* and auxin-related mutants and the fact that most double mutants displayed synergistic interactions suggested a functional link between *NDL1* and auxin in regulating maize inflorescence development.

NDL1 encodes a mitochondria localized FTSH protein

The originally isolated *ndl1* reference allele (*ndl1-ref*) was initially mapped to chromosome 8 using a Bulked Segregant Analysis (BSA) approach using a high-throughput SNP genotyping platform on an M3 segregating population (Gallavotti and Whipple, 2015). To further define the map position of *NDL1,* we constructed a fine-mapping F2 population by crossing *ndl1-ref* from the original M2 genetic background to the B73 inbred line, as well as analyzed a smaller M4 population. By screening both mapping populations including 477 and 32 *ndl1* individuals, respectively, we mapped *ndl1* to a 1.2 Mb window (B73v2) between markers CYP450 (2R/1018chr) and KIP (1R/1018chr) including 27 predicted genes (Fig. 8a). Since an obvious candidate gene was not identified in this list, we performed a complementary mapping approach called Bulked Segregant RNA-seq analysis (Liu et al., 2012) . We prepared 3 bulked samples of immature tassels (0.5-1cm) for RNA-seq analysis including *ndl1* severe mutant and wild type samples from F2 segregating populations, as well as tassels from OH43, the original EMS treated genetic background. To prevent accidental sampling of mutant tassels within the wild type bulked sample due to variable expressivity, we genotyped each wild type individual using flanking markers TP and 49T19 (see Table 1), thus only homozygous wild type plants would be bulked.

High-throughput sequencing of these samples generated 28M, 45M and 28M 100-bp single end reads that were mapped to the B73v2 genome. By searching the aligned transcripts within the mapping window, an A to T transversion present only in the *ndl1* transcripts was identified in the coding region of gene model *GRMZM2G038401*, encoding a FILAMENTOUS TEMPERATURE SENSITIVE H10 protein (ZmFTSH10). The resulting amino acid substitution (Isoleucine 541 to Phenylalanine) occurred in a highly conserved amino acid from prokaryotic to eukaryotic organisms, where it invariably is an Isoleucine or Leucine residue (Fig. 9a). To exclude the possibility that this SNP was a polymorphism due to extensive genetic diversity existing in maize germplasms, we sequenced the candidate gene in 29 maize inbred lines along with a teosinte sample, the wild progenitor of modern maize. We further checked more than 300 maize inbred lines for SNPs in *GRMZM2G038401*. Based on this analysis, the A>T SNP was only present in the *ndl1* mutants, suggesting that the SNP was a mutation rather than an extant polymorphism (Fig. 9b).

To confirm that *ZmFTSH10/GRMZM2G038401* corresponded to *NDL1*, we undertook two complementary approaches. As the *ndl1-ref* was the only allele available, we created null mutations in *ZmFTSH10* using CRISPR/Cas9 gene-editing technology with a gRNA designed to target exon 5 (Fig. 8b). The genome editing vector was transformed into immature embryos by *Agrobacterium*-mediated transformation and regenerated plants were crossed to *ndl1* homozygous mutants. We observed a barren tassel phenotype in the resulting F1s, which carried heterozygous *ndl1-ref* mutation, in several individual

plants (Fig. 8k-m and Fig. 10a and b). Sequencing of *ZmFTSH10* in these plants identified 4 frame-shift deletions and insertions (Fig. 10c). Additionally, we introgressed a *pFTSH10::FTSH10-3xHA-YFP* construct into *ndl1* homozygous mutants. Four independent events carrying this construct and expressing a NDL1-YFP fusion protein were capable of fully complementing the *ndl1* phenotype (Fig. 8d-j and Fig. 11). Overall, these complementary approaches confirmed that *NDL1* corresponds to *ZmFTSH10/GRMZM2G038401*.

NDL1 is a mitochondria-localized protease

FTSHs are ATP-dependent metalloproteases belonging to the AAA (ATPases associated with diverse cellular activities) protein family (Ogura et al., 1991). FTSHs are bifunctional enzymes achieving proteolytic activity as well as chaperone-like activity, which are crucial for protein quality control (Bieniossek et al., 2006; Kolodziejczak et al., 2002; Leonhard et al., 1999; Neuwald et al., 1999; Ogura and Wilkinson, 2001). In yeast, three copies of FTSH proteins have been identified and they are grouped into the m-AAA and i-AAA class, both localized in the inner membrane system of mitochondria. YTA10 and YTA12 belong to the m-AAA class, with the active site facing the mitochondria matrix, whereas the i-AAA YME1 exposes its catalytic sites to the inner membrane space (Tauer et al., 1994). Arabidopsis contains 12 FTSH proteins, four of which are targeted to mitochondria, including two m-AAA proteases AtFTSH3 and AtFTSH10 and two i-AAA proteases AtFTSH4 and AtFTSH11 (Sakamoto et al., 2003; Sokolenko et al., 2002; Urantowka et al., 2005). Neighbour-joining analysis placed ZmFTSH10

within the clade of mitochondrial localized m-AAA proteases, including AtFTSH3 and AtFTSH10, YTA10 and YTA12 (Fig. 12). In addition, we identified two truncated proteins, ZmFTSH3A and ZmFTSH3B, in the maize genome, sharing about 300 similar amino acids with the N-terminal portion of ZmFTSH10 (Fig. 13). Based on this analysis, *NDL1/ZmFTSH10* appears the only putative functional maize ortholog of *AtFTSH3* and *AtFTSH10*. NDL1 shared 74% and 71% identity and 82% and 78% similarity with AtFTSH3 and AtFTSH10, respectively. As expected, staining with a Mito tracker colocalized with the NDL1-YFP signal in maize transgenic lines, indicating that NDL1 was targeted to mitochondria, consistent with the reported subcellular localization of AtFTSH3 and AtFTSH10 (Fig. 14a-c) (Sakamoto et al., 2003).

NDL1 contains several conserved domains shared by the FTSH protein family (Fig. 8c). A putative mitochondria target peptide was identified at the N-terminal of NDL1, followed by an FTSH extracellular domain. The middle domain of NDL1 contained Walker A and Walker B motifs, and a Second Region of Homology (SRH) motif, which are crucial for ATPase function (Karata et al., 2001). A Zn^{2+} binding motif HEXXH, a conserved feature of this class of metalloproteases (Leonhard et al., 1996), was also found at the C-terminal of NDL1. The I541F mutation of the *ndl1-ref* mutant was located in a variable stretch of amino acids between the SRH and HEXXC motifs. We therefore measured the effect of this mutation on the protein function by assaying the ATPase activity of NDL1 and NDL1-REF proteins. According to our results, the I541F mutation significantly decreased NDL1 ATPase activity (Fig. 9c). By confocal analysis of the NDL1-YFP

protein, we determined that NDL1 is expressed in essentially every cell (Fig. 15a-c), and accordingly, quantitative real-time PCR in different tissues showed that *NDL1* transcripts were detected in all tissues examined (Fig. 15d).

Since in Arabidopsis two putative orthologous genes were present, we obtained double mutant combinations of *AtFTSH3* and *AtFTSH10* for functional analysis. We first obtained a T-DNA insertion line in *AtFTSH3* (SALK_037144) and confirmed that *AtFTSH3* expression was completely knocked-out (Fig. 16a and b). Subsequently, since no *AtFSTH10* knockout lines were available, we employed CRISPR/Cas9 gene-editing technology to target *AtFTSH10* in the *ftsh3* insertion line background. After self-crossing the T0 plants, we obtained several T1 lines, and among them, we followed one line carrying a 4 base pair deletion in the coding region of *AtFTSH10* (Fig. 16a). Interestingly, no significant visible morphological change was observed in the shoot of *Atftsh3;Atftsh10* double mutants, except that the double mutant plants showed a reduction in primary root length when compared with wild type, a result consistent with a recent report using a different *Atftsh3;Atftsh10* double mutant combination (Kolodziejczak et al., 2018) (Fig. 16c). We therefore checked whether *ndl1* mutants also showed a similar phenotype in roots and determined that *ndl1* mutants displayed significantly shorter primary roots (Fig. 16 d-e). These results suggest that the function of m-AAAs is at least partially conserved from Arabidopsis to maize.

***ndl1* is defective in respiration complexes and ROS homeostasis.**

It has been previously determined that AtFTSH3, AtFTSH10 and AtFTSH4 are required for the stability and assembly of the mitochondrial oxidative

phosphorylation (OXPHOS) complexes. In *Atftsh3;Atftsh10* mutants, the activities of complex I (CI) and V (CV) are significantly reduced, while complex IV (CIV) activity is identical to wild type (Kolodziejczak et al., 2018; Marta et al., 2007). Most mitochondrial proteins, including m-AAA proteases, are encoded in the nucleus. Thus, the communication between mitochondria and nuclear transcription known as the mitochondrial retrograde regulation (MRR) is critical to coordinate nuclear and organellar activities to maintain cell function, especially in stress or mitochondrial dysfunction conditions (Kerchev et al., 2014; Rhoads and Subbaiah, 2007; Woodson and Chory, 2008). The Mitochondrial Dysfunction Stimulon (MDS) is a set of nuclear genes that respond to mitochondrial defects (De Clercq et al., 2013), among which the best characterized gene is *ALTERNATIVE OXIDASE 1a* (*AOX1a*) that encodes a cyanide-insensitive terminal oxidase (Møller, 2001). Previous studies showed that in tassels of maize CI- and CIV-deficient mutants, high expression of two genes, *ZmAOX2* (*GRMZM2G125669)* and *ZmAOX3* (*GRMZM2G074743*) was detected, respectively, indicating that the expression pattern of different AOX genes serve as marker for specific mitochondrial defects (Karpova et al., 2002). We therefore performed qRT-PCR analysis of these markers using immature tassels of *ndl1*, wild type and *Bif1;Bif4* double heterozygous mutants. High expression of *ZmAOX2* was observed in *ndl1* mutants, whereas no difference was detected in *Bif1;Bif4* mutants, which exhibit a striking similar phenotype to *ndl1* severe mutants (Galli et al. 2015; Fig. 14d). However, the expression level of *ZmAOX3* in *ndl1* and *Bif1;Bif4* tassels were comparable to wild type (Fig. 14d). These results

suggest that the mitochondria complex I function is impaired in *ndl1* tassels and are consistent with the *ftsh3;ftsh10* analysis in Arabidopsis. Specific up-regulation of another MDS gene, *HSP20* (*GRMZM2G135960*), supported the conclusion that OXPHOS complexes were damaged in *ndl1* tassels (Fig. 14d).

Mitochondria are the main source of reactive oxygen species (ROS). OXPHOS complexes defects usually increase ROS production (Kirkinezos and Moraes, 2001). It was previously reported that AtFTSH4 influences OXPHOS complex activity and that inactivation of *AtFTSH4* results in elevated levels of ROS (Gibala et al., 2009; Zhang et al., 2014). To determine if high levels of ROS were also produced in *ndl1* mutants, 3,3'-diaminobenzidine (DAB) staining was performed to examine hydrogen peroxide (H_2O_2) levels in immature tassels. Unusual accumulation of H_2O_2 was detected at the tip of *ndl1* tassels displaying a strong phenotype (Fig. 14e-i). However, no significant increase was found in wild type or *Bif1;Bif4* tassels (Fig. 14f), indicating that the *ndl1* mutation specifically up-regulates ROS production, consistent with the hypothesis that NDL1 functions in maintaining OXPHOS complex activities.

NDL1 **controls maize inflorescence development by regulating endogenous auxin levels**

The synergistic interaction and phenotypic similarity between *ndl1* and several auxin mutants suggested that *NDL1* may regulate maize inflorescence development via cross-talk with auxin-related pathways. In particular, the strong genetic interactions observed with *Bif1* (Fig. 4, 5), which encodes a stabilized

Aux/IAA protein insensitive to auxin-induced degradation (Galli et al., 2015), and with *spi1*, an auxin biosynthetic mutant, suggested that the levels of free auxin may be decreased in *ndl1* mutant IMs, and that may be the cause of the early defects in organogenesis. To verify this hypothesis, we crossed *ndl1* to the auxin signaling marker line DII-VENUS, a marker for endogenous auxin levels. The nuclear DII-VENUS marker is based on the degron domain of Aux/IAA proteins, whose degradation is controlled by auxin levels in cells (Brunoud et al., 2012; Mir et al., 2017). In wild type immature tassels, low expression of DII-NENUS was detected in the IM indicating high concentration of auxin. In *ndl1* tassels, however, the DII-VENUS signal was much stronger than in wild type, indicating lower levels of auxin in *ndl1* IMs and in particular in the peripheral zone (Fig. 17; n=3). These results are consistent with the genetic analysis and support the hypothesis that lower auxin levels in *ndl1* IMs may perturb the auxin-driven initiation of lateral primordia.

Discussion

In crop species like maize, inflorescences are a major source of yield, therefore mutations affecting inflorescence development greatly impact productivity. Previously identified genes responsible for barren inflorescence phenotypes when mutated, such as *SPI1*, *VT2*, *BIF1*, *BIF2*, and *BIF4*, are all directly involved in regulating auxin function (Gallavotti et al., 2008a; Galli et al., 2015; McSteen et al., 2007; Phillips et al., 2011). Here we characterized *ndl1*, a new barren mutant displaying synergistic interaction with many of the auxin mutants mentioned above, caused by a mutation in a mitochondrial localized protease highly conserved from prokaryotic to eukaryotic organisms. The characterization and identification of *ndl1* uncovered another pathway that coordinates intracellular redox status with hormonal pathways to regulate plant developmental processes.

NDL1 encodes a mitochondrial localized m-AAA protease belonging to the FTSH family. Mitochondria are best known for sustaining cellular ATP supply through oxidative phosphorylation and the tricarboxylic acid cycle (TCAC). Recently, mounting evidences highlighted mitochondria as major players in stress response (Van Aken et al., 2009) as well as multiple other metabolic processes (Millar et al., 2011). Moreover, several studies suggested chemical and genetic perturbation of mitochondria could affect plant architecture. Prohibitins (PHB) are a group of integral mitochondrial membrane proteins that interact with FTSH proteins to assemble into a high molecular weight complex acting as chaperones in mitochondrial respiratory chain assembly (Van Aken et al., 2007). Both *PHB3* knockout line and overexpression line display altered shoot architecture in

Arabidopsis (Van Aken et al., 2007). Arabidopsis FTSH4, a mitochondrial localized i-AAA protease involved in regulating oxidative phosphorylation (OXPHOS) complexes activity, has been reported to influence leaf morphology (Gibala et al., 2009; Hong et al., 2016; Smakowska et al., 2016) and shoot architecture (Zhang et al., 2014) under short day or high temperature conditions. Here we showed that NDL1 is necessary for thermotolerance of inflorescence development, providing another evidence supporting the importance of mitochondria in regulating plant development. Surprisingly, mutations in the Arabidopsis co-orthologous genes *AtFTSH3* and *AtFTSH10* do not affect inflorescence development, but only root development (Kolodziejczak et al., 2018). One possible explanation of this striking difference may be related to the different growth habits of Arabidopsis and maize. In particular, the optimal growth temperature for Columbia (Col-0), a common lab Arabidopsis strain, is much lower than for maize, and *ndl1* mutants only show strong phenotypes in high temperature conditions (Fig. 3). In these conditions, wild type Arabidopsis is severely affected in growth, unless specific tropical strains are used. It would be indeed interesting to test if knocking out *AtFTSH3* and *AtFTSH10* in tropical strains would result in a much stronger shoot phenotype than the root-specific phenotype observed in Col-0.

The precise molecular mechanisms by which mitochondria regulate plant architecture are far from elucidated but MRR, the communication between mitochondria and the nucleus, is likely to be involved in this process. In the *PHB3* knock out and overexpression lines, the up-regulation of several MDS genes was

observed (Van Aken et al., 2007). Our data indicated that an abundance of MDS genes were specific up regulated in *ndl1* mutants (Fig. 14d), including a small heat shock protein (sHSP), *HSP20*, which is known to coordinate MRR with heat stress response (Rhoads et al., 2005). According to our analysis, *ndl1* showed stronger phenotype in high temperature conditions (Fig. 3), indicating that heat stress enhances the mutant phenotype. Although not specifically tested, it is likely that other stresses may influence the severity of the *ndl1* phenotype. It is also worth noticing that when grown at a constant high temperature in a controlled environment *ndl1* mutants are severely impaired in vegetative development as well.

Accumulating evidence suggests that ROS and associated redox regulation have the potential to play crucial roles in shoot development (Schippers et al., 2016). Glutaredoxins (GRXs) are a group of antioxidants that utilize glutathione to reduce protein disulfide bonds and regulate cellular redox status. Arabidopsis mutants lacking *GRXS17* show compromised shoot apical meristems (Knuesting et al., 2015). Moreover, the maize GRX protein ABERRANT PHYLLOTAXY2 (ABHP2) has been shown to regulate shoot meristem size (Yang et al., 2015). Thioredoxins (TRXs) and glutaredoxins (GRXs) are important players in maintaining cellular redox homeostasis by catalyzing disulfide reduction. *ntra* and *ntrab* are two Arabidopsis mutants lacking the NADPH-thioredoxin reductases and *cad2-1* is a mutant with reduced GSH synthesis activity. The triple mutant of *ntra*;*ntrab;cad2-1* showed defective flower and root development, and displayed characteristic pin-formed shoot and shorter primary root (Bashandy et al., 2010),

resembling defects observed in strong *ndl1* mutants. It is interesting to note that auxin metabolism, signaling and transport are highly influenced in the *ntra*;*ntrab;cad2-1* triple mutants and auxin is able to at least partially recue the mutant phenotype, indicating the interplay between redox homeostasis and auxin biology in regulating plant architecture (Bashandy et al., 2010).

One of the possible molecular mechanisms connecting mitochondria redox status to inflorescence architecture is that oxidative stress, a common component of abiotic stresses, causes mitochondrial dysfunction, thus inducing the MRR (Møller, 2001). Oxidative stress is caused by an imbalance between ROS production and scavenging enzymes that causes oxidative damage (Schieber and Chandel, 2014). ROS have been identified as one of the molecules that plant mitochondria signal to the nucleus (Rhoads and Subbaiah, 2007). In *Atftsh4* mutants (Zhang et al., 2014) and *ndl1* mutants (Fig. 14e-i), abnormal accumulation of ROS was detected. Moreover, many ROS scavenger genes were up-regulated in *ndl1* mutant transcriptomes (data not shown), such as genes belonging to the peroxidase and the thioredoxins (TRXs) families. Hence ROS can be considered as an integrator of stresses and mitochondrial perturbation, and as signaling molecules that regulate plant architecture.

There is growing evidence that the crosstalk between ROS and auxin contribute significantly to overall plant development and stress responses. ROS are able to affect different aspects of auxin biology, such as auxin biosynthesis, auxin metabolism, auxin transport, and auxin signaling (Tognetti et al., 2012). One of the well-known examples is that H_2O_2 is able to mediate auxin oxidative

degradation via inducing peroxidase activities (Kawano, 2003; Vatulescu et al., 2004; Zhang et al., 2014), which may provide an explanation for the synergistic interaction of *ndl1* mutants and auxin mutants (Fig. 4, 5, 6, 7). Moreover, by confocal analysis of the DII-VENUS marker line, we showed that auxin concentration was reduced in *ndl1* mutant IMs (Fig. 17). Previous studies indicated that the chemical perturbation of mitochondria could directly affect auxin signaling and stabilized the DII-VENUS signal, providing another evidence in support of our hypothesis (Kerchev et al., 2014).

Overall, the isolation of *ndl1* provides new insights into maize inflorescence development. We showed that NDL1/ZmFTSH10 is essential for maize growth in high temperature, and that *NDL1* may function at the interplay of auxin and ROS pathways. Moreover, we showed that the mitochondrial retrograde regulation pathway was induced in *ndl1* mutants, providing a maize model system to study MRR in addition to the widely used alternative respiration system. Furthermore, the up-regulation of a series of stress related genes and the temperature-sensitive phenotype of *ndl1* mutants suggest that NDL1/ZmFTSH is also involved in maize stress response, thus could be used as a model to study maize stress biology.

Materials and Methods

Plant material and phenotyping

The *ndl1* reference (*ndl1-ref*) allele was generated by EMS mutagenesis in the OH43 background by Gerald Neuffer and obtained by the Maize Genetics Cooperation Stock Center (04HI-A632XOH43GN-173). The mutation was introgressed into B73 with seven backcrosses for phenotypic measurements, unless otherwise noted. *ndl1/ndl1*;*Bif1/+, ndl1/ndl1;Bif4/+* and *ndl1/ndl1;spi1/spi1* double mutants were created by crossing BC2(B73) *ndl1/ndl1* individuals with *Bif1/+, Bif4/+* and *spi1/spi1* respectively, and selfed. Both mutations were in the B73 background. The vegetative phenotype of *ndl1* mutants and double mutants were analyzed at Rutgers University, New Jersey. Student's *t*-test was used to determine statistical significance. The *ndl1* root phenotype experiment was carried out using BC7 *ndl1* mutants (B73) at 30 °C.

The *AtFTSH3* insertion line SALK_037144 was obtained from the Arabidopsis Biological Resource Center (ABRC). Arabidopsis plants were grown on half-strength MS plates at 22 °C with 16hr/8hr light/dark cycles for 7-10 days and transplanted to soil in the growth chamber in a 16hr/8hr light/dark (LD) photoperiod at 22 °C.

Arabidopsis *CRISPR/Cas9* mutagenesis

The gRNA targeting *AtFTSH10* was designed with the on-line tool http://cbi.hzau.edu.cn/cgi-bin/CRISPR. Equal volumes of 100 μM FTSH10-gRNA-F and FTSH10-gRNA-R were mixed, incubated at 65°C for 5

minutes and cooled down to room temperature. The fragments were inserted into the *Bbs*I site of the pX330 vector (AddGene). The *CRISPR* target cassette was subsequently cloned into the HindIII/EcoRI sites of pCAMBIA1300 vector. Arabidopsis transformation was performed by floral dipping (Clough and Bent, 1998).

Positional cloning

For map-based cloning of the *NLD1* locus, we first performed a Bulked Segregant Analysis (BSA) using the MASSarray system developed by Iowa State University (Liu et al., 2010). This approached mapped the *NDL1* locus to chromosome 8.04. To fine map the mutation, mutant plants from the original background of the mutagenesis, were crossed to B73 and selfed. The subsequent F2 population was screened and mutant plants were genotyped using the PCR-based molecular markers listed in Table 1. After narrowing down the genomic region surrounding *NDL1* to a window of 1.2 Mb, we undertook a Bulked Segregant RNA-seq approach (Liu et al., 2012). 0.5 cm to 1 cm wild type and *ndl1* tassels from the F2 mapping populations, as well as from OH43, were used for RNA extraction with the RNeasy Plant Mini Kit (Qiagen). Extracted total RNA samples were sent to the DNA Core Illumina Sequencing Services of the University of Missouri for analysis. The RNAseq reads generated by Illumina HiSeq 2000 were mapped to the maize B73 v2 genome using TopHat v2.08b with the following parameters: tophat -p 1 --bowtie1 -G ZmB73_5a.59_WGS_exons.gtf. Mapped reads were visualized using the Integrative Genomics Viewer (IGV; http://www.broadinstitute.org/igv/).

Reads within the 1.2Mb *ndl1* mapping window were manually inspected for SNPs relative to the B73 reference genome and OH43 and wild type sibling samples.

Expression analysis

For *in situ* hybridizations, 0.2-0.4 cm wild type and *ndl1* inflorescences were dissected and fixed using paraformaldehyde acetic acid (PFA). Samples were dehydrated and embedded in paraplast. Hybridizations were performed at 56°C, overnight. After several washes, samples were treated with anti-digoxygenin (DIG) antibody (Roche) and signals were detected using NBT/BCIP (Promega). The *BA1*, *SPI1*, and *ZYB15* probes were previously described (Gallavotti et al., 2008a; Gallavotti et al., 2011; Gallavotti et al., 2004). The NDL1 antisense probe was synthesized using T7 RNA polymerase (Promega) of NDL1 cDNA cloned to pENTR223.1-Sfi with primer *NDL1-F2/NDL1-R2* (Table 1) and digested with EcoR1. Images were taken using a Leica DM5500B microscope equipped with a DFC450 C digital camera.

For quantitative real-time PCR (qRT-PCR), RNA was extracted from wild type and *ndl1* 3-5 mm immature tassels using the RNeasy Plant Mini Kit (Qiagen) using three separate biological replicates. Retrotrascription was performed using the qScript cDNA Synthesis kit. cDNA was amplified with PerfeCTa® SYBR® Green FastMix® (Quanta Biosciences) on an Illumina Eco Real-Time PCR System. Relative expression levels were calculated using $2^{-\Delta\Delta Ct}$ method with *UBIQUITIN* as control. The primers used for qRT-PCR are listed in Table 2.

For confocal microscopy, the *ZmPIN1a-YFP* and *DII-VENUS* (Gallavotti et al., 2008b; Mir et al., 2017) maize maker lines were crossed with BC7(B73) *ndl1*

mutants. The resulting F1 were backcrossed with BC8(B73) *ndl1* mutants. Images were obtained using dissected 3-5 mm tassels on a Leica SP5 confocal microscope using 514 excitation and 520–575 emission.

For imaging immature ears of transgenic *pNDL::NDL-3xHA-YFP* plants, propidium idodide counterstaining was performed using 594 excitation and 625-655 emission settings. Images were analyzed using FIJI.

Complementation test

The B73 *NDL1* genomic DNA sequence was amplified with Phusion DNA polymerase (NEB), which included ~3.9kb and ~1kb up- and downstream of the coding sequence, respectively, and was cloned into the XbaI/EcoRI sites of the maize transformation vector pTF101 via Gibson assembly (Gibson et al., 2009). An in-frame 3xHA-YFP cassette was inserted downstream of the final exon using Gibson assembly. Primers used are listed in Table 2.

CRISPR/Cas9 mutagenesis

Equal volumes of 100 μM NDL1-gRNA-F and NDL1-gRNA-R were mixed and incubated at 65°C for 5 minutes. After cooled down to room temperature, the fragments were inserted into the *Bsa*I site of the pBUE411 vector (AddGene). The construct was transformed into immature embryos of maize HiII lines via *Agrobacterium*-mediated infiltration at the Plant Transformation Core Facility of the University of Missouri, Columbia. The genomic DNA was extracted from the resistant calli, and the target region was amplified with NDL1-cripsr check-F/ NDL1-cripsr check-R primers (Table 2). The genome targeting efficiency was

determined using the T7 Endonuclease I (NEB) following manufacturer's instructions. Only calli showing CRISPR/Cas9 activity were used to regenerate plants.

To genotype positive plants, the target region was amplified with NDL1-cripsr check-F/ NDL1-cripsr check-R primers (Table 2). The PCR products were purified and cloned into pGEM-T Easy Vector (Promega) for sequencing.

ROS staining

4-6 mm immature tassels were dissected using a light microscope. The staining was performed using 1mg/ml DAB in MES (10 mM, PH 6.5) solutions and incubated in the dark at room temperature for 8-12 hours. Following a 30 minute boiling (80℃) in 95% ethanol, the tissue was kept in 70% ethanol. Images were taken using a Leica DM5500B microscope equipped with a DFC450 C digital camera.

Phylogenetic analysis

FTSH protein sequences were retrieved from the National Center for Biotechnology Information (NCBI) and Phytozome v.12.1. The amino acid sequences of maize, Arabidopsis and yeast were aligned with Clustal Omega. The evolutionary tree was inferred in MEGA5 using the Neighbor-Joining method.

ATPase assay

The (Δtm) *NDL1* sequence (deletion of the first 300 amino acids) was amplified with primers NDL1-F3/NDL1-R3 (Table 1) using cDNA of wild type and *ndl1*

tassels and cloned into the SfiI sites of pENTR223-Sfi (Consortium, 2011). Subsequently, the pENTR-NDL1 clones were transferred into the expression vector pET-55-DEST (NovoPro) using LR clonase II (Life Technologies). Protein expression in Rosetta (DE3) cells (Novagen) was induced with 0.4 mM IPTG (isopropyl β-D-1-thiogalactopyranoside) at 16°C overnight. The supernatant was purified by Ni-NTA.

ATPase activities were measured using the EnzChek Phosphate Assay Kit (Invitrogen) according to the method described previously (Webb, 1992). 3 nmol purified proteins were added to the reaction mixture including 50μl 20x reaction buffer, 200μl 2-amino-6-mercapto-7-methylpurine riboside substrate solution (MESG) and 10μl purine nucleoside phosphorylase. After a 10 minute incubation at room temperature, 1mM ATP was added as substrate and the absorbance at 360 nm was recorded from 0 min to 100 min. ATPase activity was calculated according to manufacturer's instructions.

Figures

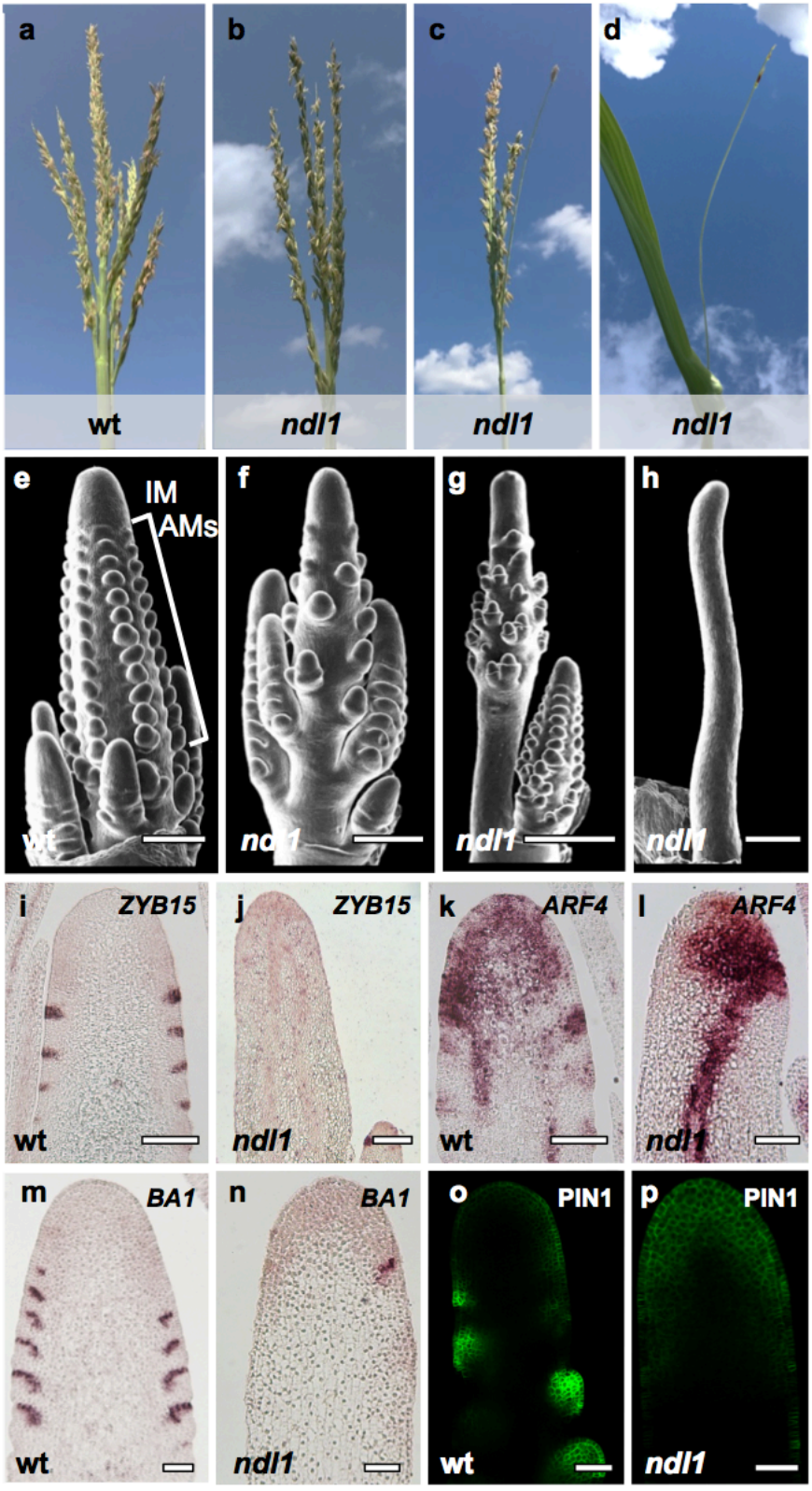
a
wt
b
ndl1
c
ndl1
d
ndl1
e
IM
AMs
wt
f
ndl1
g
ndl1
h
ndl1
i
ZYB15
wt
j
ZYB15
ndl1
k
ARF4
wt
l
ARF4
ndl1
m
BA1
wt
n
BA1
ndl1
o
PIN1
wt
p
PIN1
ndl1

Figure 1. *ndl1* is defective in reproductive organogenesis. (a-d) Mature tassel phenotype. (e-h) SEMs of immature tassels in normal and mutant plants. IM, inflorescence meristem. AMs, axillary meristems. (Scale bars, 500 μm.) (i-n) mRNA in situ hybridizations of immature tassels with *ZYB15*, *ARF4* and *BA1* antisense probes (scale bars, 250μm). (o and p) Confocal images of normal and *ndl1* immature tassels expressing ZmPIN1a-YFP fusion protein. (Scale bars, 250μm.)

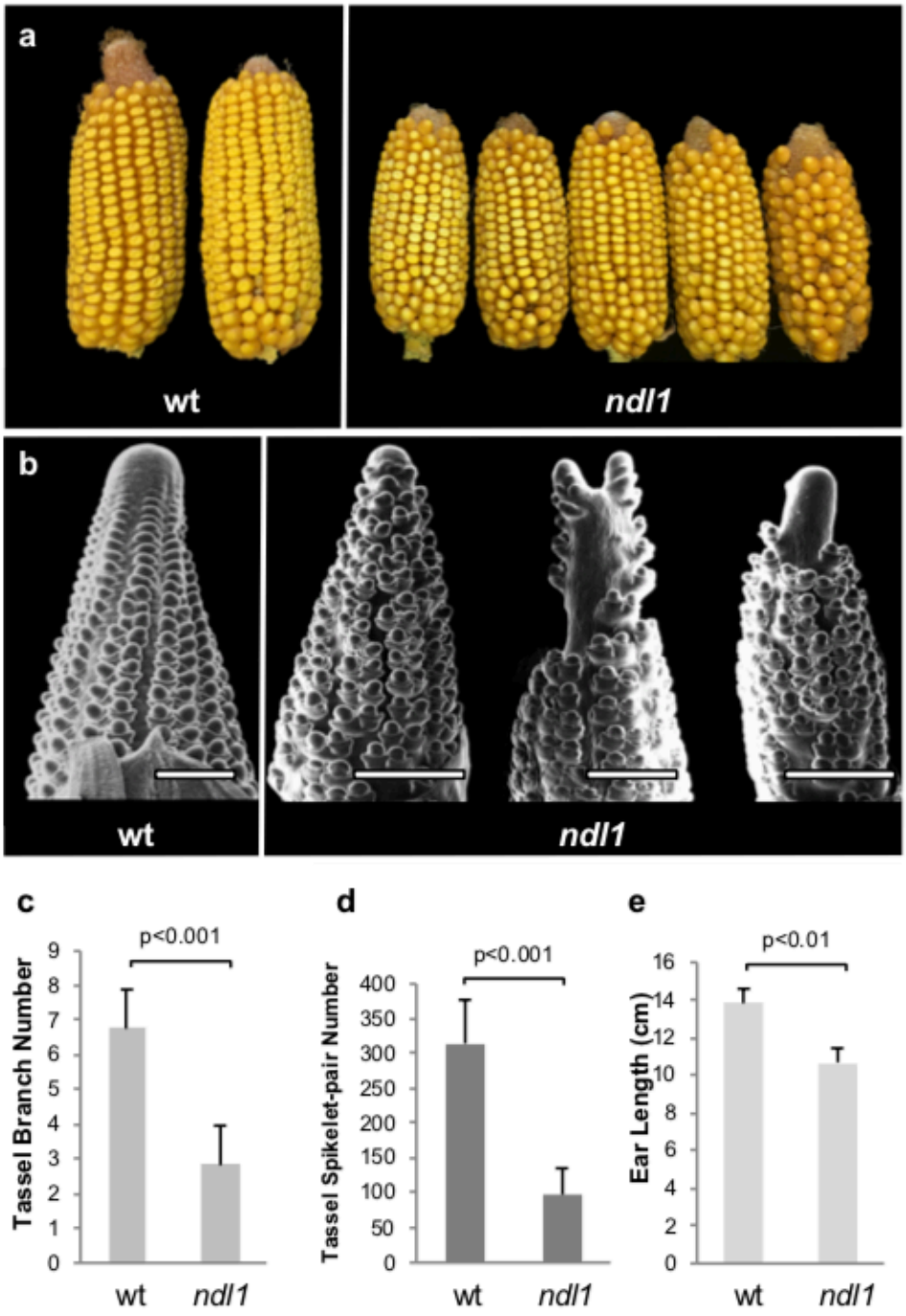

Figure 2. *ndl1* is defective in reproductive organogenesis. (a) Mature ear phenotype. (b) SEMs of immature ear of normal and mutant plants (scale bars, 500μm.) (c-e) Quantification of the reproductive defects of *ndl1* mutant inflorescences (n≥30). Error bars show SD.

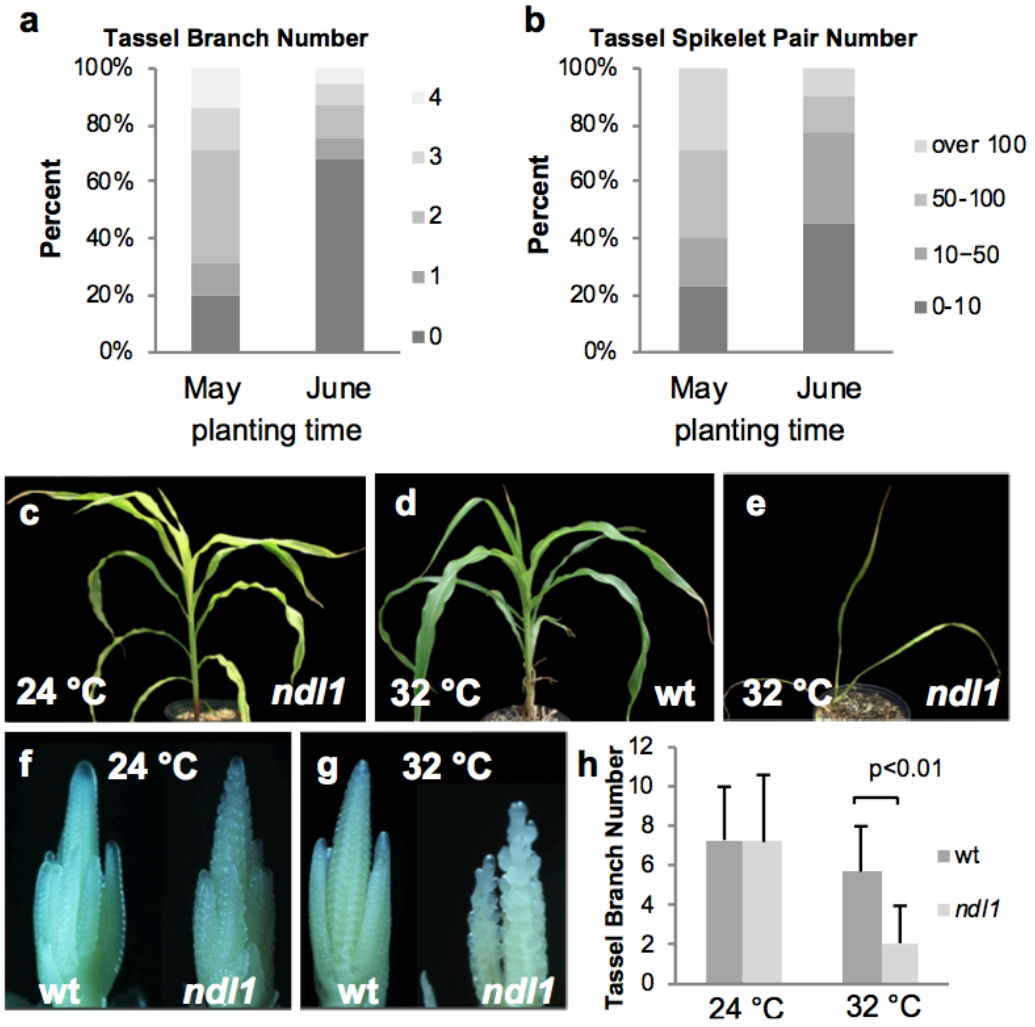

Figure 3. *ndl1* shows temperature sensitive phenotype. (a and b) Quantification of the branch number and spikelet number of *ndl1* mutants planted in May and June from two separate years (n≥35). Error bars show SD. (c-e) The whole plant phenotype of wild-type and *ndl1* mutants grown in mild (24°C day-20°C night) and high temperature (32°C day-28°C night). (f and g) The tassel phenotype of wild-type and *ndl1* mutants grown in mild and high temperature. (h) Quantification of the branch number of wild-type and *ndl1* mutants grown in mild and high temperature (wt n≥10; *ndl1* n≥20).

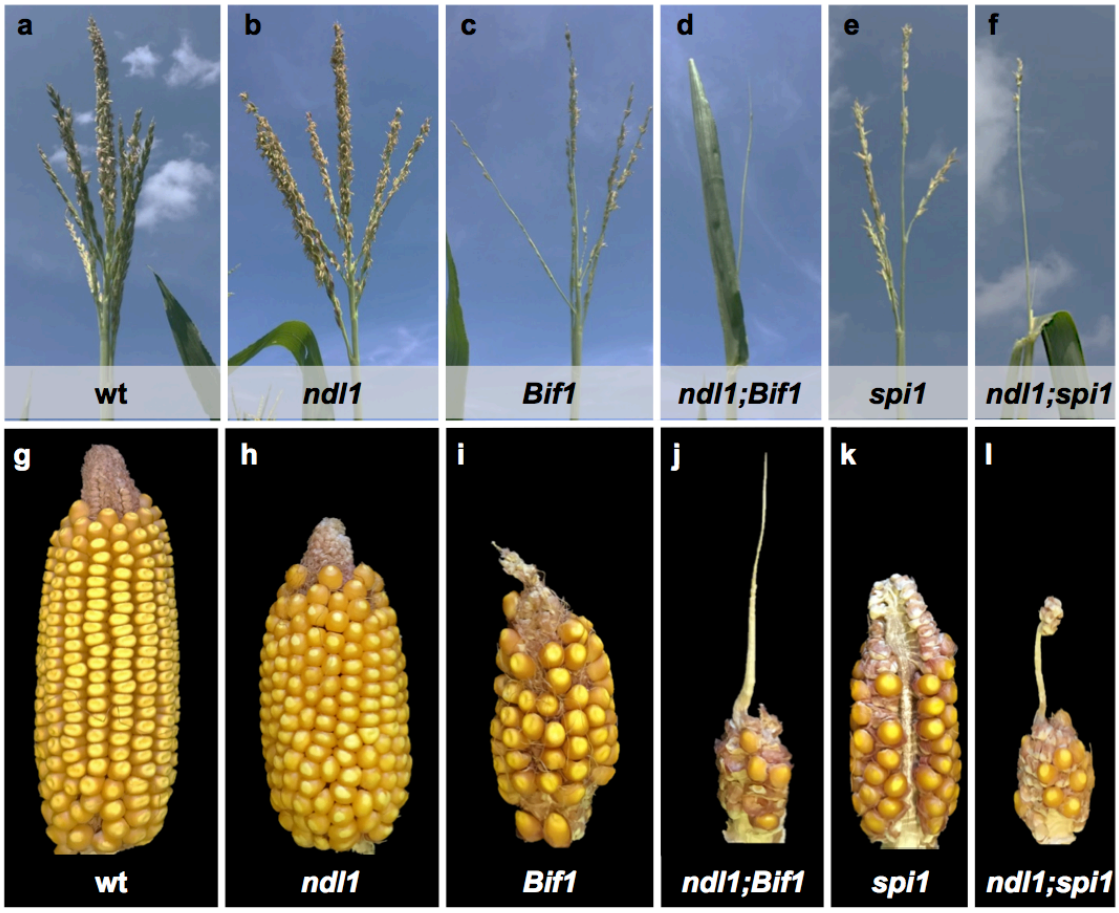

Figure 4. *ndl1* mutants enhance the inflorescence phenotype of auxin-related mutants. (a-l) Double-mutant analysis of *ndl1/ndl1* with *Bif1/+* and *spi1/spi1* in B73 background. (a-f) Mature tassel phenotype. (g-l) Mature ear phenotype.

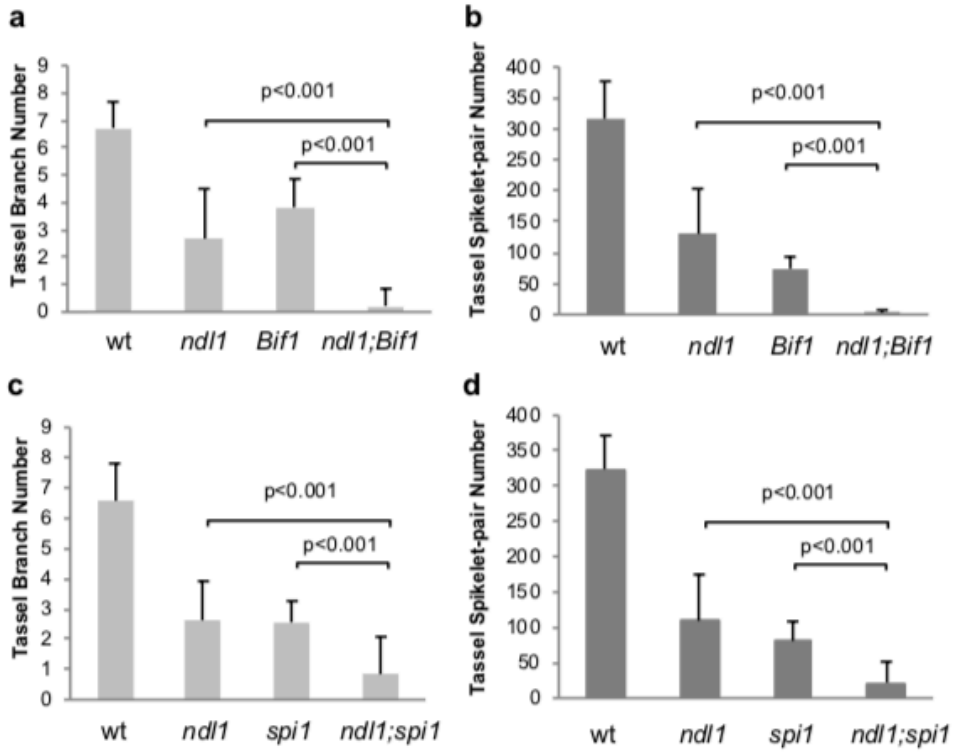

Figure 5. Genetic analysis of *ndl1* mutants. (a-d) Quantification of tassel branch number and tassel spikelet-pair number in wild-type, *ndl1/ndl1*, *Bif1/+*, *ndl1/ndl1;Bif1/+, spi1/spi1,* and *ndl1/ndl1;spi1/spi1* plants (wild-type n≥10, mutants n≥17). Error bars show SD.

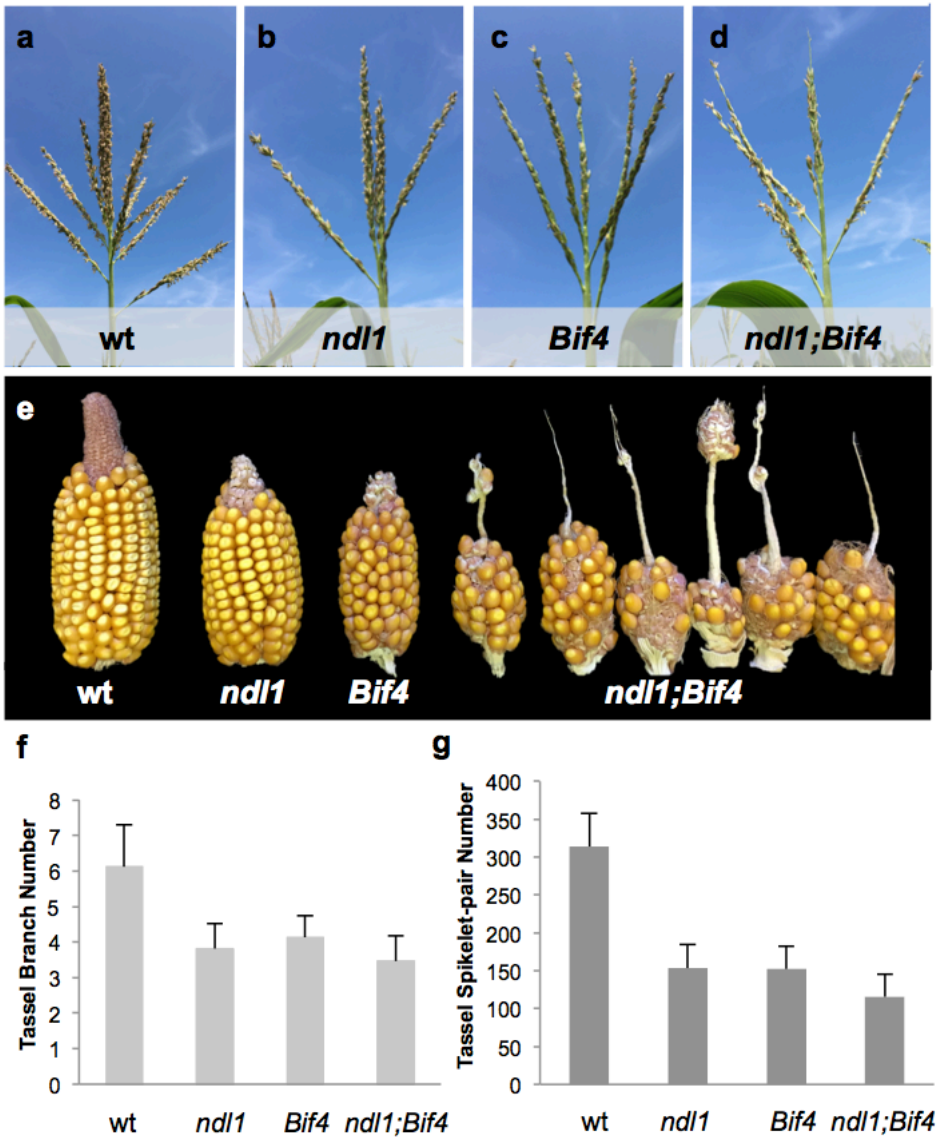

Figure 6. *ndl1* mutants enhance the ear phenotype of *Bif4* mutants. (a-d) Mature tassel phenotype. (e) Mature ear phenotype. (f and g) Quantification of tassel branch number and tassel spikelet-pair number in wild-type, *ndl1/ndl1*, *Bif4*/+ and *ndl1/ndl1;Bif4*/+ double mutants, with no significant difference (n≥17). Error bars show SD.

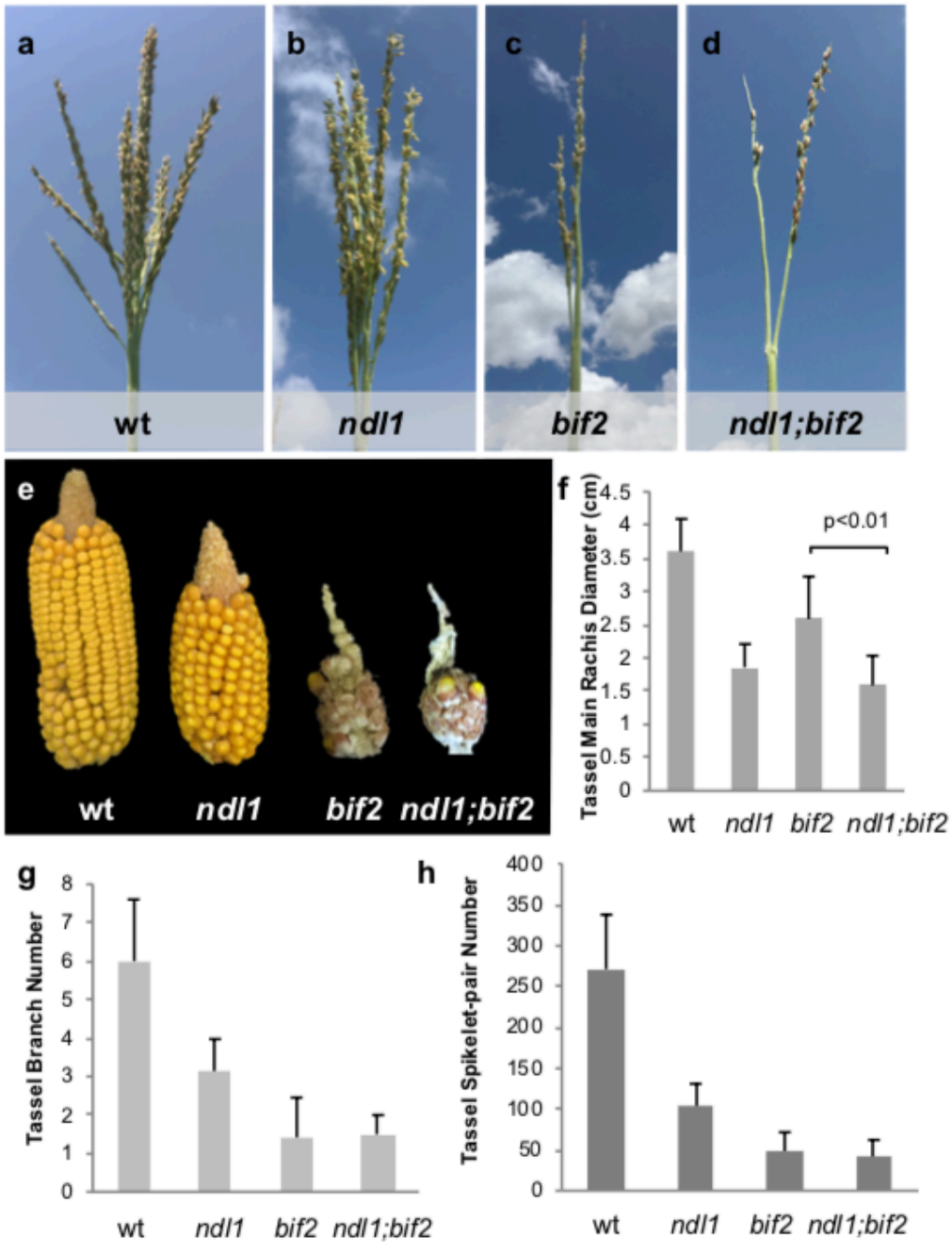
a
b
c
d
wt
ndl1
bif2
ndl1;bif2
e
wt
ndl1
bif2
ndl1;bif2
f
Tassel Main Rachis Diameter (cm)
p<0.01
wt
ndl1
bif2
ndl1;bif2
g
Tassel Branch Number
wt
ndl1
bif2
ndl1;bif2
h
Tassel Spikelet-pair Number
wt
ndl1
bif2
ndl1;bif2

Figure 7. Double mutant analysis of *ndl1* and *bif2*. (a-d) Mature tassel phenotype. (e) Mature ear phenotype. (f) Quantification of tassel main rachis diameter in in wild-type, *ndl1/ndl1*, *bif2/bif2* and *ndl1/ndl1;bif2/bif2* double mutants (n≥6). Error bars show SD. (g and h) Quantification of tassel branch number and tassel spikelet-pair number in wild-type, *ndl1/ndl1*, *bif2/bif2* and *ndl1/ndl1;bif2/bif2* double mutants, with no significant difference (n≥6). Error bars show SD.

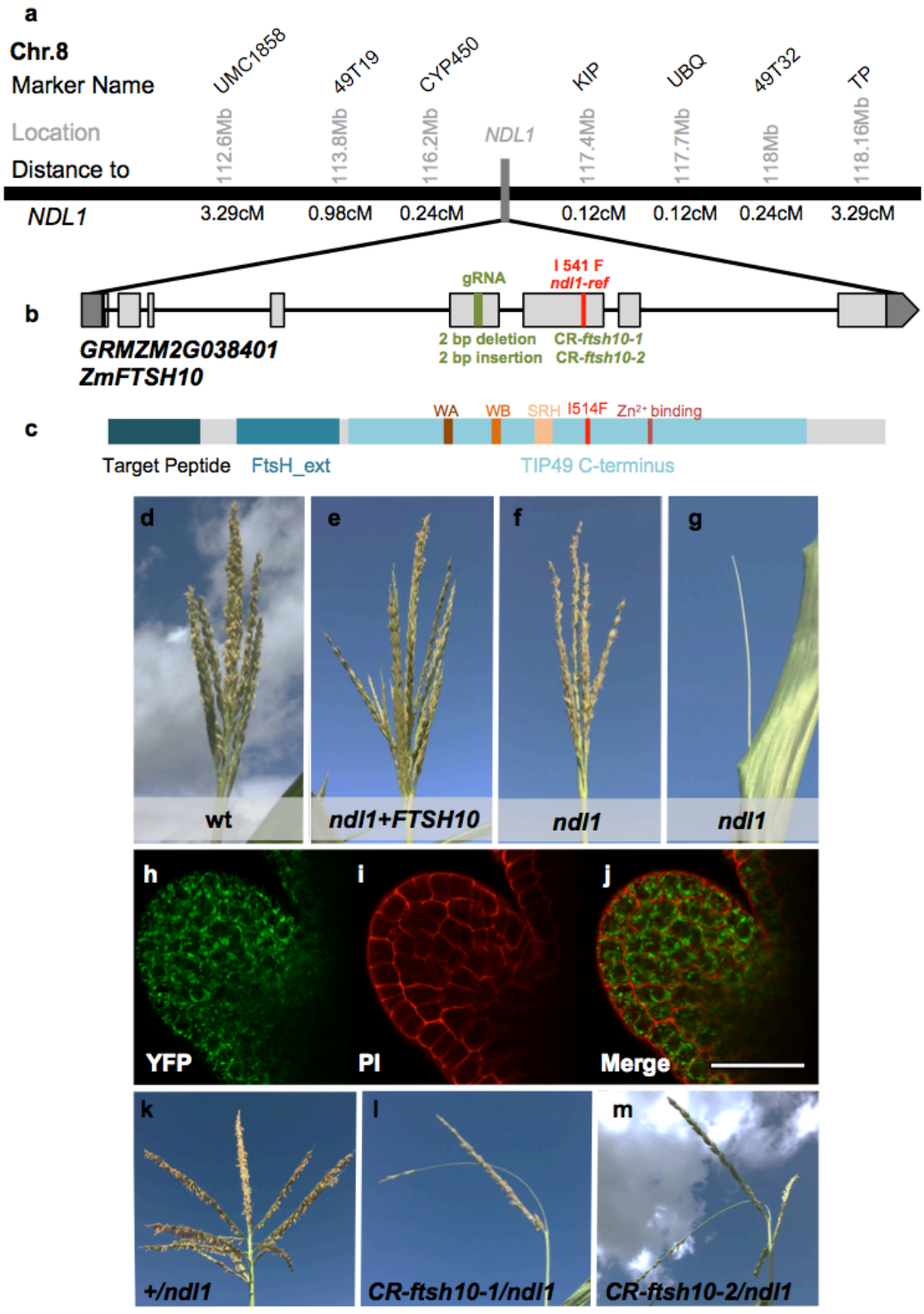
a
Chr.8
Marker Name
Location
Distance to
NDL1
UMC1858
49T19
CYP450
KIP
UBQ
49T32
TP
112.6Mb
113.8Mb
116.2Mb
NDL1
117.4Mb
117.7Mb
118Mb
118.16Mb
3.29cM
0.98cM
0.24cM
0.12cM
0.12cM
0.24cM
3.29cM
b
gRNA
I 541 F
ndl1-ref
GRMZM2G038401
ZmFTSH10
2 bp deletion
2 bp insertion
CR-ftsh10-1
CR-ftsh10-2
c
WA
WB
SRH
I514F
Zn2+ binding
Target Peptide
FtsH_ext
TIP49 C-terminus
d
e
f
g
wt
ndl1+FTSH10
ndl1
ndl1
h
i
j
YFP
PI
Merge
k
l
m
+/ndl1
CR-ftsh10-1/ndl1
CR-ftsh10-2/ndl1

Figure 8. *NDL1* encodes ZmFTSH10. (a) Positional cloning of *NDL1*. (b) Schematic representation of the *ZmFTSH10* gene and the position of mutant alleles. Exons and UTRs are depicted as gray and dark gray rectangles, respectively. The green bar indicates the guide RNA targeting site. The red bar points out the position of the missense mutation (c) Schematic representation of the ZmFTSH10 protein. FtsH_ext, FtsH-extracellular domain. WA, Walker A motif. WB, Walker B motif. SHR, Second Region of Homology motif. (d-g) The tassel phenotype of *ndl1* is rescued by the *pFTSH10::FTSH10-3xHA-YFP* construct. (h-j) Confocal images of immature ear expressing *pFTSH10::FTSH10-3xHA-YFP.* PI, Propidium Iodide. (Scale bars, 50μm.) (k-m) The tassel phenotype of wild-type and *ndl1* mutants generated by CRISPR/Cas9.

a

ZmFTSH10	R	L	A	A	L	T	P	G	F	A	G	A	D	I	A	N	V	C	N
EcFTSH	I	I	A	R	G	T	P	G	F	S	G	A	D	L	A	N	L	V	N
HsFTSH	I	I	A	R	G	T	V	G	F	S	G	A	E	L	E	N	L	V	N
AtFTSH10	R	L	A	A	L	T	P	G	F	A	G	A	D	I	A	N	V	C	N

b

Inbred lines	Codon	Inbred lines	Codon
B73	ATT	W22	ATT
A619	ATT	Mo17	ATT
CML247	ATT	CML228	ATT
KY21	ATT	CML52	ATT
CML69	ATT	Ki3	ATT
M162W	ATT	Tx303	ATT
M37W	ATT	Tzi8	ATT
CML103	ATT	Mo18w	ATT
B97	ATT	CML277	ATT
P39	ATT	LI14H	ATT
MS71	ATT	Nc350	ATT
CML333	ATT	HP301	ATT
Oh7B	ATT	Oh43	ATT
Nc358	ATT	teosinte	ATT
Ki11	ATT	*ndl1*	TTT
CML322	ATT		

c

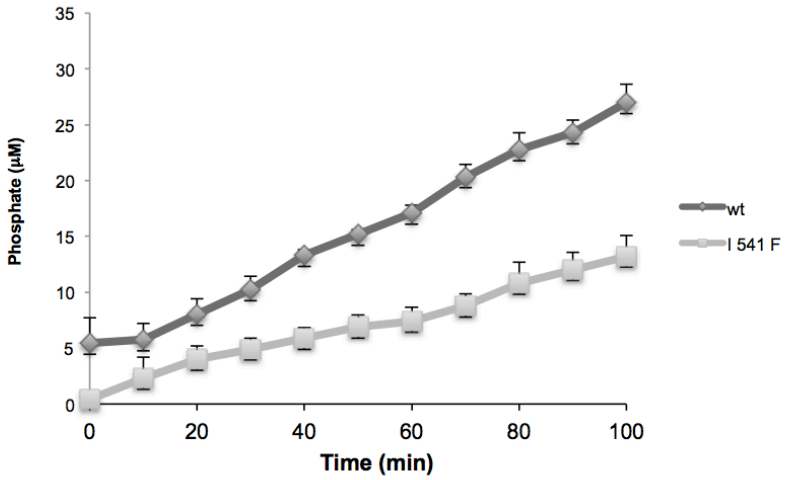

Figure 9. The I 541 F substitution affects NDL1 activity. (a) Multiple sequence alignment. *Zm, Zea mays*. *Ec, E.coli*. *Hs, Homo sapiens*. *At, Arabidopsis thaliana*. In red, the I 541 F substitution. (b) Codon containing the *ndl1-ref* mutation in different inbred backgrounds. The A to T SNP is only found in *ndl1* mutants. (c) ATPase activities of wild-type (Δtm) FTSH (the first 300 amino acids deletion) and (Δtm) I 541 F. Error bars show SD.

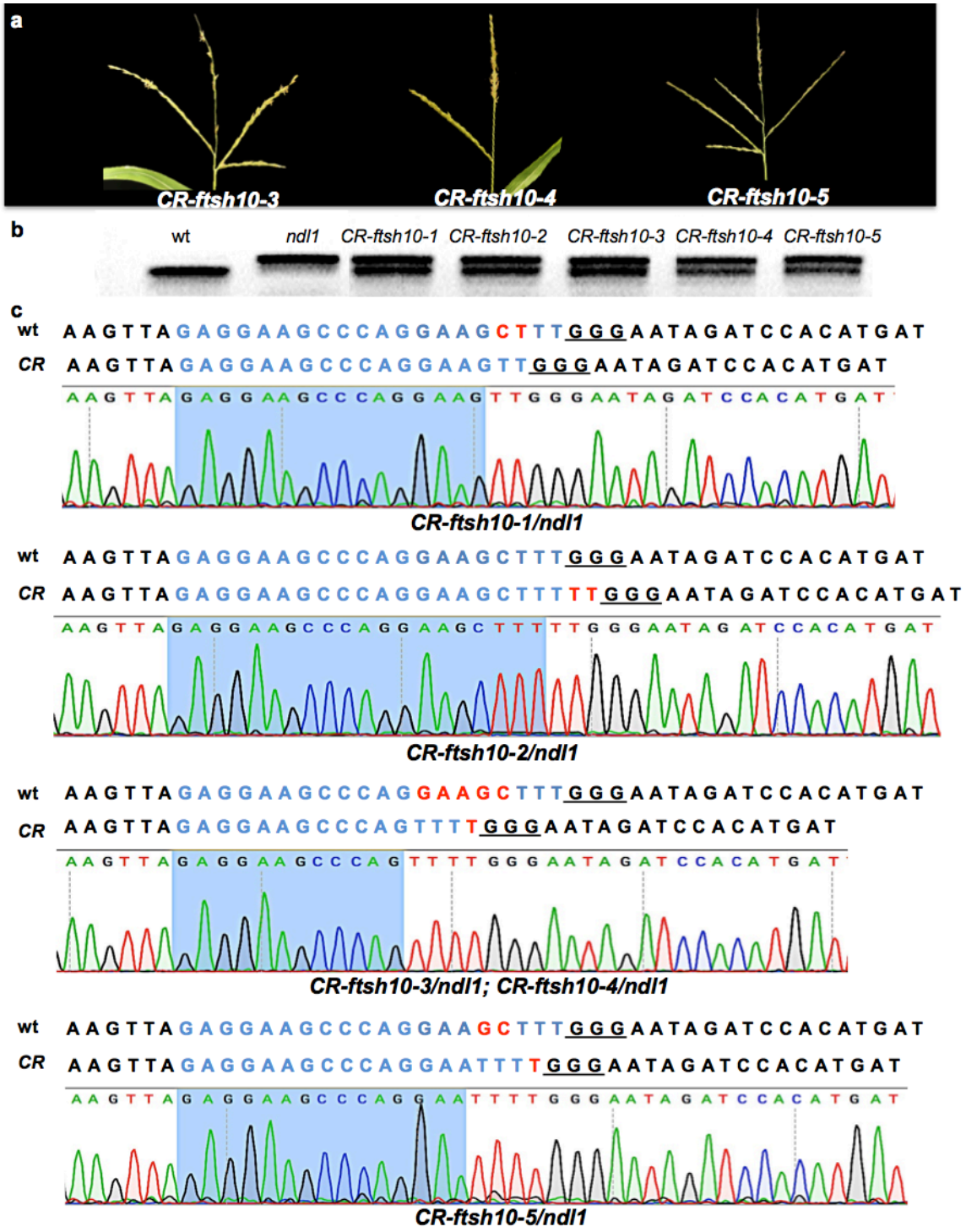
a
CR-ftsh10-3
CR-ftsh10-4
CR-ftsh10-5
b
wt
ndl1
CR-ftsh10-1
CR-ftsh10-2
CR-ftsh10-3
CR-ftsh10-4
CR-ftsh10-5
c
wt AAGTTAGAGGAAGCCCAGGAAGCTTTGGGAATAGATCCACATGAT
CR AAGTTAGAGGAAGCCCAGGAAGTTGGGAATAGATCCACATGAT
CR-ftsh10-1/ndl1
wt AAGTTAGAGGAAGCCCAGGAAGCTTTGGGAATAGATCCACATGAT
CR AAGTTAGAGGAAGCCCAGGAAGCTTTTTGGGAATAGATCCACATGAT
CR-ftsh10-2/ndl1
wt AAGTTAGAGGAAGCCCAGGAAGCTTTGGGAATAGATCCACATGAT
CR AAGTTAGAGGAAGCCCAGTTTTTGGGAATAGATCCACATGAT
CR-ftsh10-3/ndl1; CR-ftsh10-4/ndl1
wt AAGTTAGAGGAAGCCCAGGAAGCTTTGGGAATAGATCCACATGAT
CR AAGTTAGAGGAAGCCCAGGAATTTTGGGAATAGATCCACATGAT
CR-ftsh10-5/ndl1

Figure 10. CRISPR/Cas9-engineered mutations in *NDL1* result in a barren phenotype. (a-c) Mature tassel phenotype of *CR-ftsh10* plants generated by CRISPR-Cas9. (b) PCR genotyping of *CR-ftsh10* plants show that all *CR-ftsh10* alleles carry heterozygous *ndl1-ref* mutation. (c) Sequencing results of *CR-ftsh10* alleles are aligned to the reference genome sequence. Indels are shown in red letters. The gRNA targeting site is shown in blue letters. The PAM site is underlined.

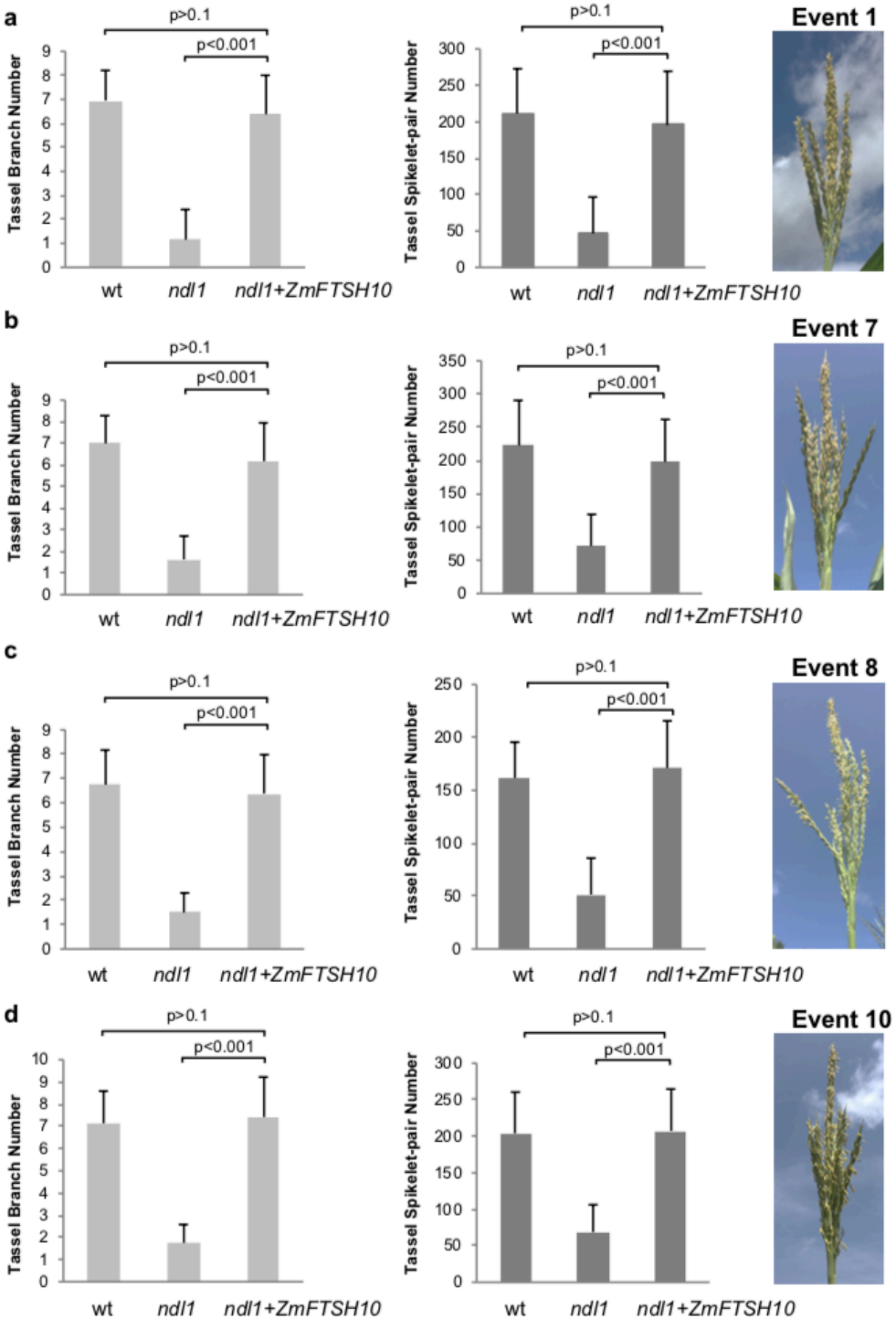

Figure 11. *ZmFTSH10* is able to rescue the *ndl1* tassel phenotype. (a-d) 4 different transgenic events expressing *pFTSH10::FTSH10-3xHA-YFP* in the *ndl1-ref* background show wild-type-like tassels (event 1 and event7, n≥20; event 8 and event 10, n≥10). Error bars show SD.

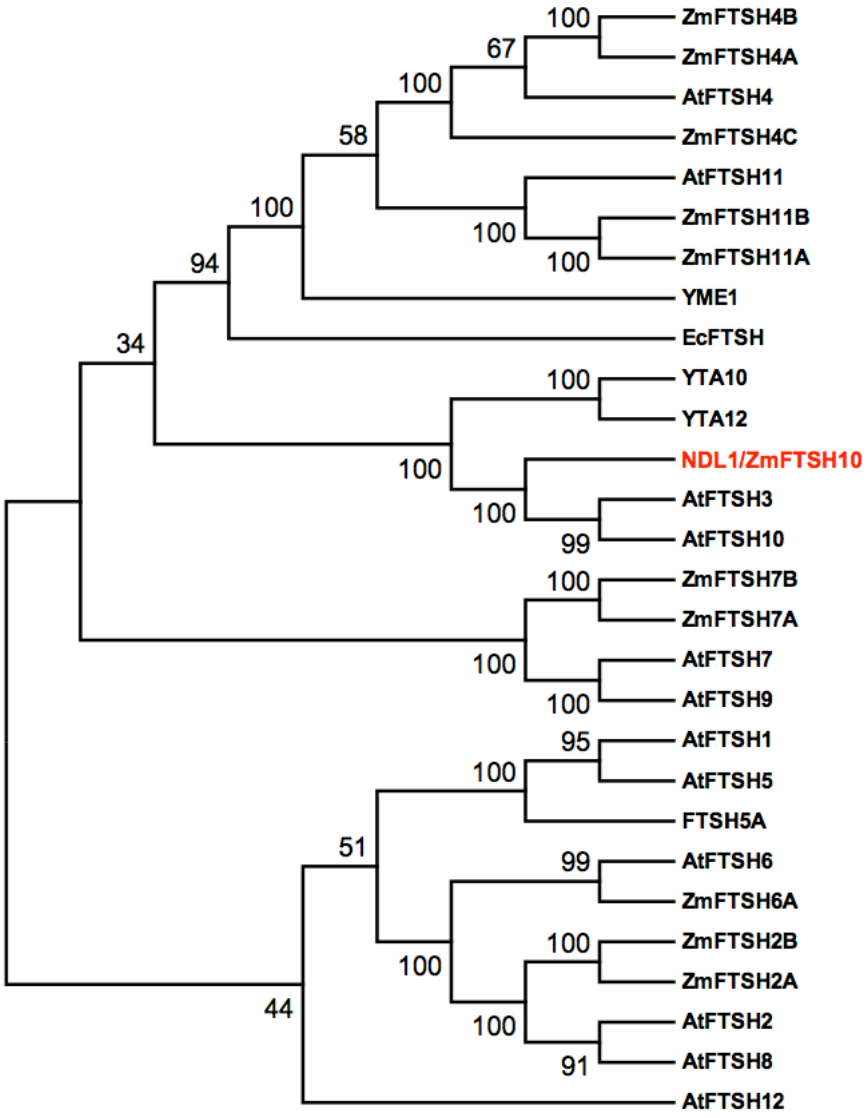

Figure 12. Neighbour-Joining tree of the FTSH protease family.

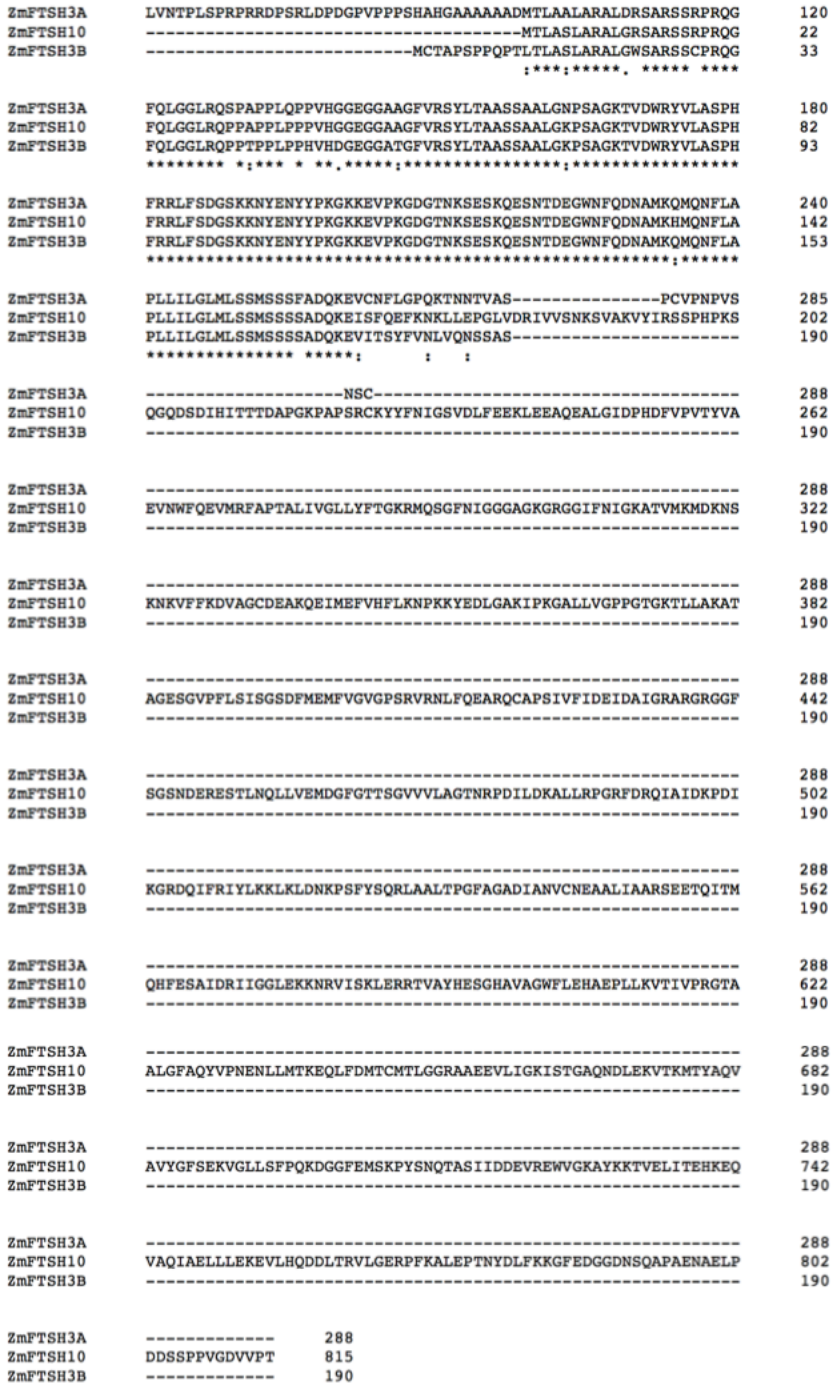

Figure 13. Multiple sequence alignment of ZmFTSH10, ZmFTSH3A and ZmFTSH3B amino acid sequences.

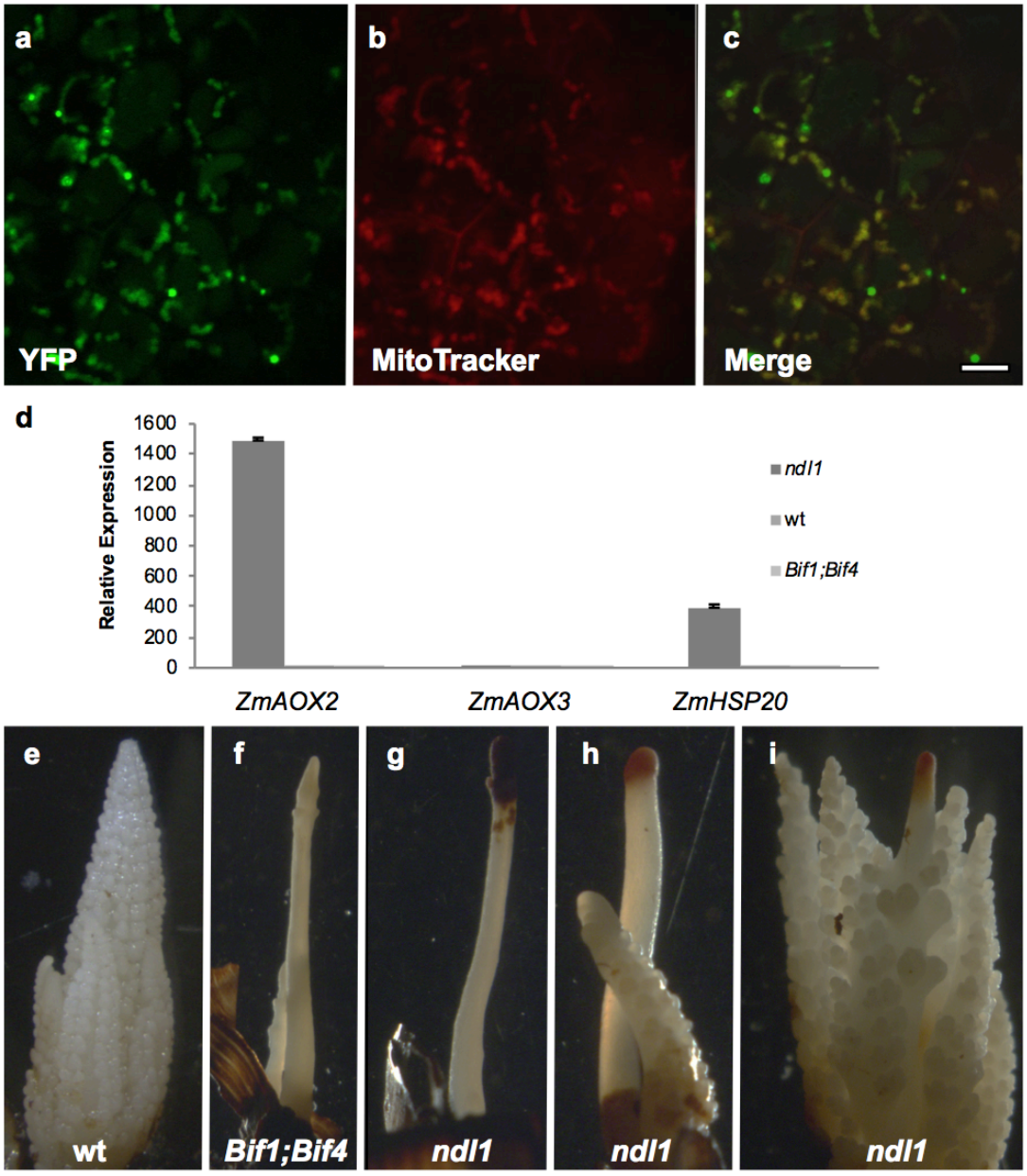

Figure 14. *ndl1* is defective in OXPHOS complexes. (a-c) Confocal images of immature ear expressing *pFTSH10::FTSH10-3xHA-YFP* stained with MitoTracker Red CMXRos (scale bars, 10μm.) (d) Quantitative RT-PCR of *ZmAOX2*, *ZmAOX3* and *ZmHSP20* in wild-type, *ndl1/ndl1* and *Bif1/+;Bif4/+* immature tassels. Error bars show SD. (e-l) Abnormal H_2O_2 accumulates at the barren tip of *ndl1* mutants only.

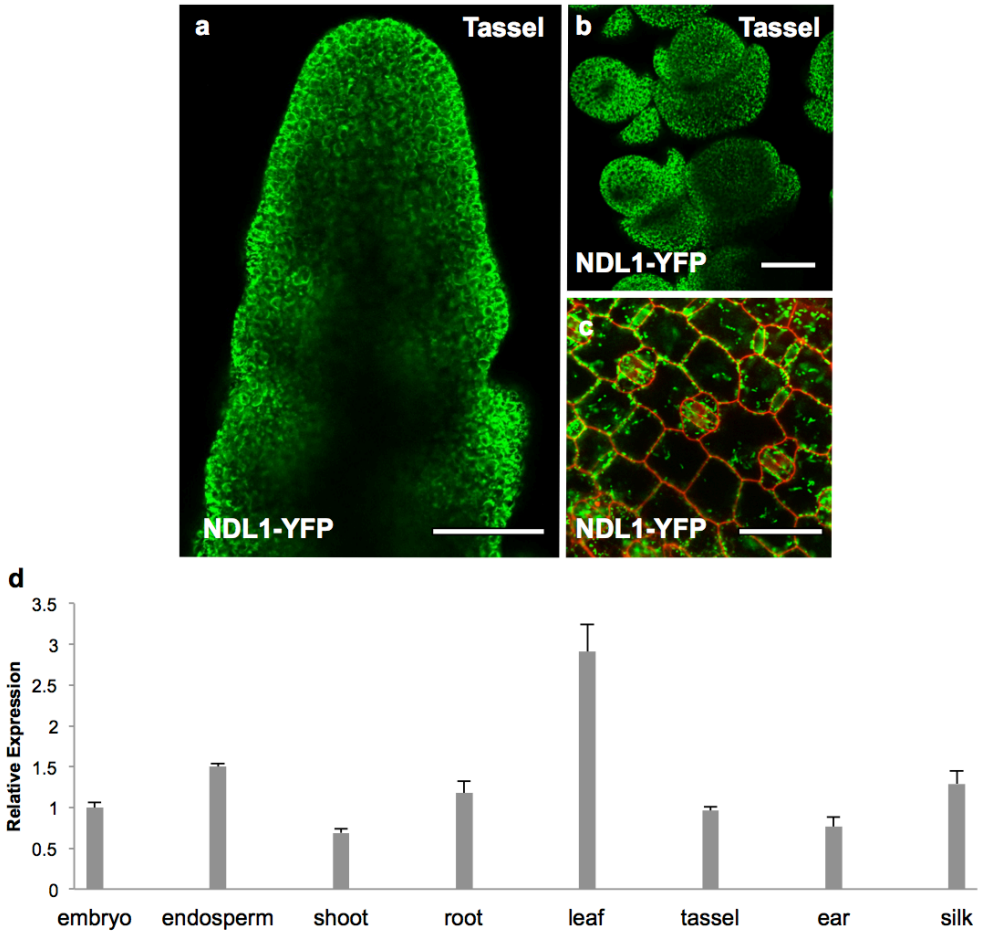

Figure 15. Expression analysis of *NDL1.* (a and b) Confocal images of NDL1-YFP in immature tassels (scale bars, 100μm.) (c) Confocal images of NDL1-YFP in leaf with PI staining (scale bar, 50μm.). (d) Quantitative RT-PCR of *NDL1* in different maize tissues. The y axis shows the fold change relative to embryo expression levels. Error bars show SD.

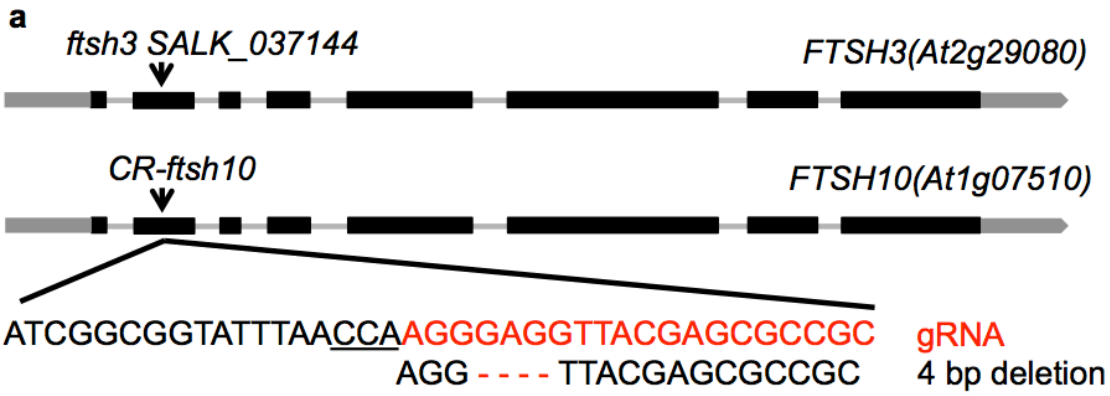
a
ftsh3 SALK_037144
FTSH3(At2g29080)
CR-ftsh10
FTSH10(At1g07510)
ATCGGCGGTATTTAACCAAGGGAGGTTACGAGCGCCGC
gRNA
AGG - - - - TTACGAGCGCCGC
4 bp deletion

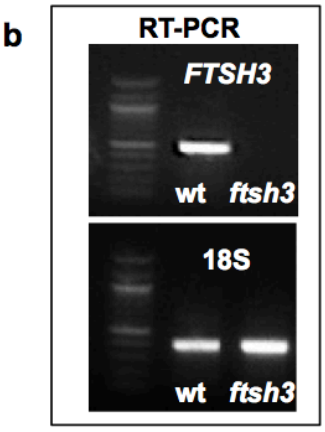
b
RT-PCR
FTSH3
wt ftsh3
18S
wt ftsh3

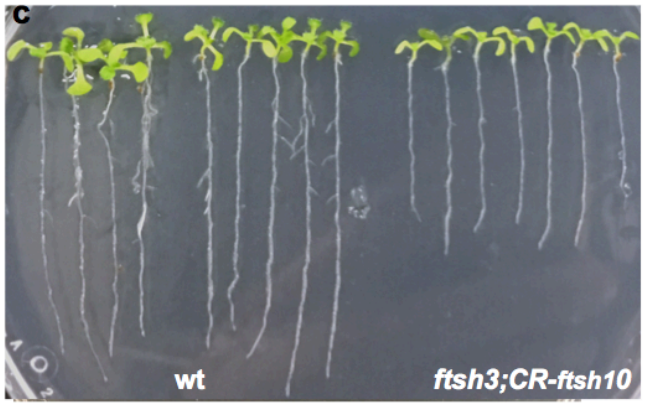
c
wt
ftsh3;CR-ftsh10


d
wt
ndl1

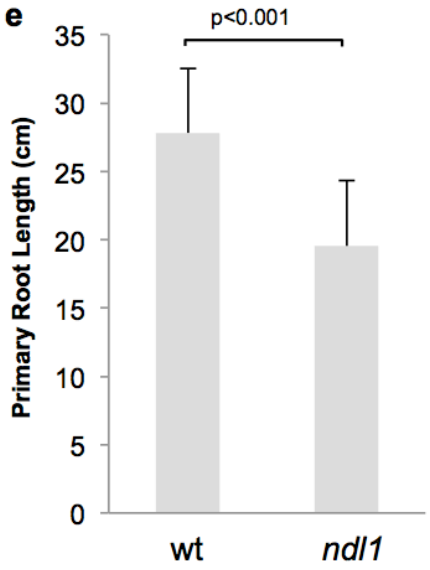
e
p<0.001
Primary Root Length (cm)
35
30
25
20
15
10
5
0
wt
ndl1

Figure 16. *ndl1* mutants show shorter primary roots, consistent with the Arabidopsis *ftsh3;ftsh10* double mutant phenotype. (a) Schematic representations of *AtFTSH3* and *AtFTSH10* genes and the location of mutant alleles used. Indels are shown in dashes. The gRNA targeting site is shown in red letters. The PAM is underlined. (b) RT-PCR of *AtFTSH3* in wild-type Arabidopsis (Columbia) and *ftsh3* mutants with 18S as an internal control. (c) The root phenotype of wild-type Arabidopsis and *ftsh3;CR-ftsh10* double mutants grown in half-strength MS plates at 22°C with 16hr/8hr light/dark cycles for 14 days. (d) The root phenotype of wild-type maize (B73) and *ndl1* mutants grown in 30°C for 7 days. (e) Quantification of the primary root length (n≥30). Error bars show SD.

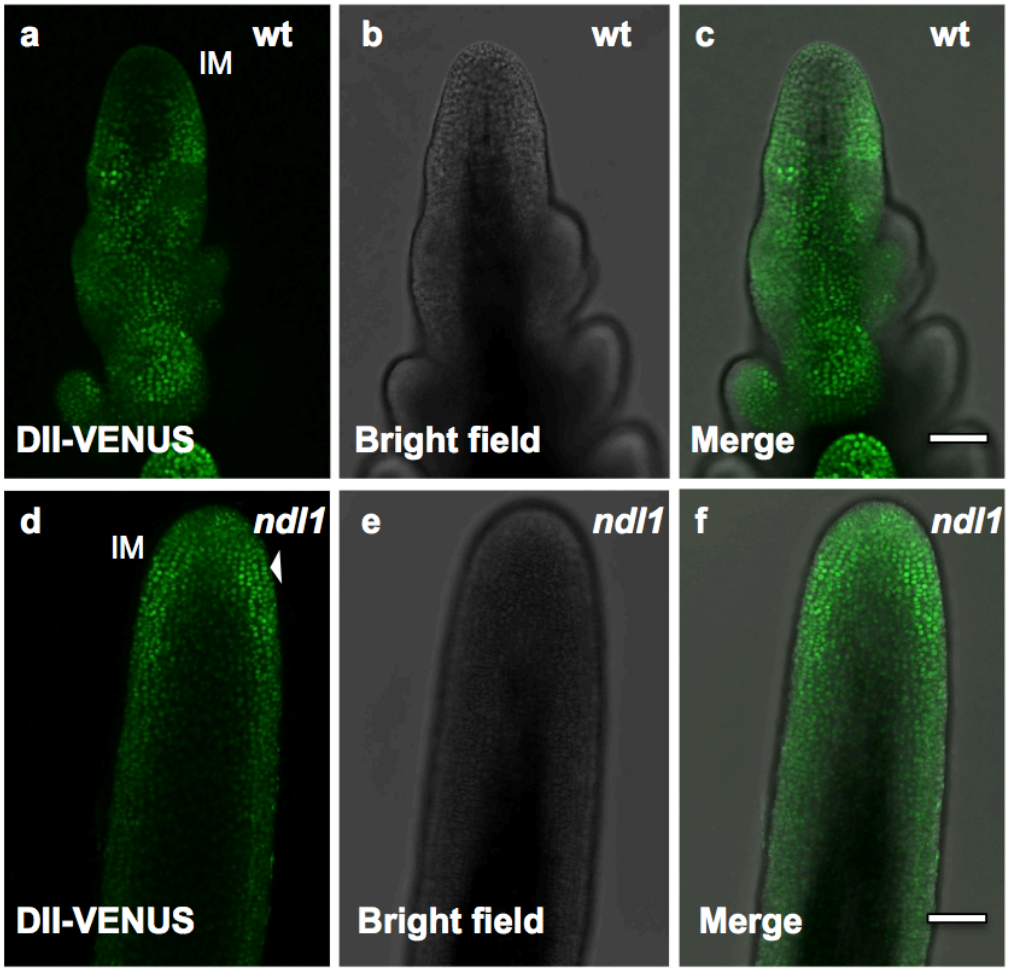

Figure 17. Confocal microscopy analysis of DII-VENUS signal in immature tassels. Maximum projection of Z-stacks of DII-VENUS signals in wild-type (a-c) and *ndl1* mutants (d-f) immature tassels. IM, Inflorescence Meristem. Arrowhead indicates high DII-VENUS signals at the tip of the IM (scale bars, 100μm.)

Tables

Location	Marker	Primer name	Primer sequence (5'-> 3')
112.6	SSR	umc1858	Forward: GTTGTTCTCCTTGCTGACCAGTTT Reverse: ATCAGCAAATTAAAGCAAAGGCAG
113.2	dCAPs	49T12-PstI	Forward: TCTTCTACGCCCAGAGACTG Reverse: GATTAGCAAACAGTGATTGCTG
113.8	Indel	49T19	Forward: GTCGCAGCCATGGAATGCTGGAT Reverse: GATTAGCAAACAGTGATTGCTG
114.4	CAPs	CDC28-SacI	Forward: GGGAATAACAAGATTCCTGATCT Reverse: CGTCCACTTTATCTGTCCTG
115.2	CAPS	MSP-MaeII	Forward: TCTTCCATTGGCATCACGTG Reverse: AGCGCTTGCATAGTAACTAC
116.05	Indel	49T25	Forward: TGCAGGTCACTGAGTCCTCG Reverse: TCACATGTAACCGCACAGGC
116.2	Indel	CYP450	Forward: AGAGCAAGGATTTGCTTGGCTTGC Reverse: GATCCTTGACGGTGCAATCAAATC
116.6	dCAPS	49T38-MluI	Forward: TGATTGGTAGGAGGTTCTCGGACGC Reverse: GTGACCACGGCATTCTTGATGGTG
116.7	dCAPS	UCE-MboI	Forward: CTAGGTGACACCATACCTGAAAAC Reverse: CAACACCACTATACGAGTGAGA
117.4	dCAPS	KIP-NalII	Forward:GATAGTGAGGGGTTTTCTAAGGCCAT Reverse: CTCAGTCTGTAATGCCAGGATCTG
117.7	CAPs	UBQ-Taq^{a}I	Forward: GTGCCACTTGTTAGCACACTTG Reverse: GGTCAGCAAATCGTTAGAGC
118	Indel	49T32	Forward: CGCAGTTCATGTTCTTCGAC Reverse: CAGGGGTAAGGTAACAAATCAAGG
118.16	Indel	TP	Forward: TGCTTCCAGACGATCACCTGCTAC Reverse: CGTCGTCCAGGTTGTTGATGATGG
119.2	Indel	49T11	Forward: GTGCTTTCTGCTGCTTATGG Reverse: CTGCAGCAGCTTCAACTTGG

Table 1. List of markers used for positional cloning.

Primer name	Sequence 5'-3'	Use
NDL1-F1	CTGGGACAAATAGACCTGACATCCTG	genotyping
NDL1-R1	CGCAGCAATTAAAGCAGCTTCATTACAAACCATGGCAA	genotyping
NDL1-Rescue-F	GTTTATTTCACAGTATTCTCACCAGAAATTGGTTTAA	genotyping
NDL1-Rescue-R	ATGTACAGCTCTGACGTTGAGGAG	genotyping
NDL1-F2	GAATTCGGCCGTCAAGGCCAATGACGCTCGCCTCCCTCGCCCG	in situ
NDL1-R2	AGTCGACGGCCCATGAGGCCCTACGTGGGTACAACGTCACCAA	in situ
HSP20-F	GACCTCTCCATCCCCAAGATCTTC	qRT-PCR
HSP20-R	CATCGGCACCTTCAGTTGCAC	qRT-PCR
AOX2-F	CCAAGACGCTGATGGATAAGGT	qRT-PCR
AOX2-R	CCACGGTTTCCAGCATCATC	qRT-PCR
AOX3-F	CGGCACCGAGAAGCATGA	qRT-PCR
AOX3-R	CTGGTCCACTTCCACTCCGT	qRT-PCR
NDL1-cripsr-F	CATCTGCAGATAAGCTTCCAAGAGTTC	genotyping
NDL1-cripsr-R	CATCAGAGGTCAAGAATTAGCCTGTGC	genotyping
NDL1-gRNA-F	TTTTGAGGAAGCCCAGGAAGCTTT	gRNA
NDL1-gRNA-R	AAACAAAGCTTCCTGGGCTTCCTC	gRNA
NDL1-F3	GAATTCGGCCGTCAAGGCCAATGGGCAAAGGAAGAGGAGGTATTTTC	cloning
NDL1-R3	AGTCGACGGCCCATGAGGCCCGTGGGTACAACGTCACCAAC	cloning

Table 2. List of primers used in this study.

REFERENCES FOR CHAPTER THREE

Barnabas, B., Jager, K., and Feher, A. (2008). The effect of drought and heat stress on reproductive processes in cereals. Plant Cell Environ *31*, 11-38.

Bashandy, T., Guilleminot, J., Vernoux, T., Caparros-Ruiz, D., Ljung, K., Meyer, Y., and Reichheld, J.P. (2010). Interplay between the NADP-linked thioredoxin and glutathione systems in Arabidopsis auxin signaling. Plant Cell *22*, 376-391.

Begg, K., Tomoyasu, T., Donachie, W., Khattar, M., Niki, H., Yamanaka, K., Hiraga, S., and Ogura, T. (1992). Escherichia coli mutant Y16 is a double mutant carrying thermosensitive ftsH and ftsI mutations. Journal of bacteriology *174*, 2416-2417.

Benková, E., Michniewicz, M., Sauer, M., Teichmann, T., Seifertová, D., Jürgens, G., and Friml, J. (2003). Local, efflux-dependent auxin gradients as a common module for plant organ formation. Cell *115*, 591-602.

Bennett, S.R., Alvarez, J., Bossinger, G., and Smyth, D.R. (1995). Morphogenesis in pinoid mutants of Arabidopsis thaliana. The Plant Journal *8*, 505-520.

Bieniossek, C., Schalch, T., Bumann, M., Meister, M., Meier, R., and Baumann, U. (2006). The molecular architecture of the metalloprotease FtsH. Proc Natl Acad Sci U S A *103*, 3066-3071.

Bommert, P., Nagasawa, N.S., and Jackson, D. (2013). Quantitative variation in maize kernel row number is controlled by the FASCIATED EAR2 locus. Nature genetics *45*, 334.

Brunoud, G., Wells, D.M., Oliva, M., Larrieu, A., Mirabet, V., Burrow, A.H., Beeckman, T., Kepinski, S., Traas, J., Bennett, M.J.*, et al.* (2012). A novel sensor to map auxin response and distribution at high spatio-temporal resolution. Nature *482*, 103-106.

Cheng, Y., Dai, X., and Zhao, Y. (2006). Auxin biosynthesis by the YUCCA flavin monooxygenases controls the formation of floral organs and vascular tissues in Arabidopsis. Genes Dev *20*, 1790-1799.

Clough, S.J., and Bent, A.F. (1998). Floral dip: a simplified method for Agrobacterium‐mediated transformation of Arabidopsis thaliana. The plant journal *16*, 735-743.

Consortium, A.I.M. (2011). Evidence for network evolution in an Arabidopsis interactome map. Science *333*, 601-607.

De Clercq, I., Vermeirssen, V., Van Aken, O., Vandepoele, K., Murcha, M.W., Law, S.R., Inze, A., Ng, S., Ivanova, A., Rombaut, D.*, et al.* (2013). The

membrane-bound NAC transcription factor ANAC013 functions in mitochondrial retrograde regulation of the oxidative stress response in Arabidopsis. Plant Cell *25*, 3472-3490.

de Jong, M., and Leyser, O. (2012). Developmental plasticity in plants. Cold Spring Harb Symp Quant Biol *77*, 63-73.

Gallavotti, A., and Whipple, C.J. (2015). Positional Cloning in Maize (Zea Mays Subsp Mays, Poaceae). Appl Plant Sci *3*.

Gallavotti, A., Barazesh, S., Malcomber, S., Hall, D., Jackson, D., Schmidt, R.J., and McSteen, P. (2008a). sparse inflorescence1 encodes a monocot-specific YUCCA-like gene required for vegetative and reproductive development in maize. P Natl Acad Sci USA *105*, 15196-15201.

Gallavotti, A., Malcomber, S., Gaines, C., Stanfield, S., Whipple, C., Kellogg, E., and Schmidt, R.J. (2011). BARREN STALK FASTIGIATE1 is an AT-hook protein required for the formation of maize ears. Plant Cell *23*, 1756-1771.

Gallavotti, A., Yang, Y., Schmidt, R.J., and Jackson, D. (2008b). The relationship between auxin transport and maize branching. Plant Physiology *147*, 1913-1923.

Gallavotti, A., Zhao, Q., Kyozuka, J., Meeley, R.B., Ritter, M., Doebley, J.F., Pe, M.E., and Schmidt, R.J. (2004). The role of barren stalk1 in the architecture of maize. Nature *432*, 630-635.

Galli, M., Liu, Q.J., Moss, B.L., Malcomber, S., Li, W., Gaines, C., Federici, S., Roshkovan, J., Meeley, R., Nemhauser, J.L.*, et al.* (2015). Auxin signaling modules regulate maize inflorescence architecture. P Natl Acad Sci USA *112*, 13372-13377.

Gälweiler, L., Guan, C., Müller, A., Wisman, E., Mendgen, K., Yephremov, A., and Palme, K. (1998). Regulation of polar auxin transport by AtPIN1 in Arabidopsis vascular tissue. Science *282*, 2226-2230.

Gibala, M., Kicia, M., Sakamoto, W., Gola, E.M., Kubrakiewicz, J., Smakowska, E., and Janska, H. (2009). The lack of mitochondrial AtFtsH4 protease alters Arabidopsis leaf morphology at the late stage of rosette development under short-day photoperiod. Plant J *59*, 685-699.

Gibson, D.G., Young, L., Chuang, R.Y., Venter, J.C., Hutchison, C.A., 3rd, and Smith, H.O. (2009). Enzymatic assembly of DNA molecules up to several hundred kilobases. Nat Methods *6*, 343-345.

Greb, T., and Lohmann, J.U. (2016). Plant Stem Cells. Curr Biol *26*, R816-821.

Heisler, M.G., Ohno, C., Das, P., Sieber, P., Reddy, G.V., Long, J.A., and Meyerowitz, E.M. (2005). Patterns of auxin transport and gene expression during

primordium development revealed by live imaging of the Arabidopsis inflorescence meristem. Curr Biol *15*, 1899-1911.

Hofmann, N.R. (2014). The Importance of Being Absent: Auxin Minima Are Required for Axillary Meristem Formation. Plant Cell *26*, 1836.

Hong, L., Dumond, M., Tsugawa, S., Sapala, A., Routier-Kierzkowska, A.L., Zhou, Y., Chen, C., Kiss, A., Zhu, M., Hamant, O.*, et al.* (2016). Variable Cell Growth Yields Reproducible OrganDevelopment through Spatiotemporal Averaging. Dev Cell *38*, 15-32.

Karata, K., Verma, C.S., Wilkinson, A.J., and Ogura, T. (2001). Probing the mechanism of ATP hydrolysis and substrate translocation in the AAA protease FtsH by modelling and mutagenesis. Molecular microbiology *39*, 890-903.

Karpova, O.V., Kuzmin, E.V., Elthon, T.E., and Newton, K.J. (2002). Differential expression of alternative oxidase genes in maize mitochondrial mutants. The Plant Cell *14*, 3271-3284.

Kawano, T. (2003). Roles of the reactive oxygen species-generating peroxidase reactions in plant defense and growth induction. Plant Cell Rep *21*, 829-837.

Kerchev, P.I., De Clercq, I., Denecker, J., Muhlenbock, P., Kumpf, R., Nguyen, L., Audenaert, D., Dejonghe, W., and Van Breusegem, F. (2014). Mitochondrial perturbation negatively affects auxin signaling. Mol Plant *7*, 1138-1150.

Kirkinezos, I.G., and Moraes, C.T. (2001). Reactive oxygen species and mitochondrial diseases. Semin Cell Dev Biol *12*, 449-457.

Knuesting, J., Riondet, C., Maria, C., Kruse, I., Bécuwe, N., König, N., Berndt, C., Tourrette, S., Guilleminot-Montoya, J., Herrero, E.*, et al.* (2015). Arabidopsis Glutaredoxin S17 and Its Partner, the Nuclear Factor Y Subunit C11/Negative Cofactor 2α, Contribute to Maintenance of the Shoot Apical Meristem under Long-Day Photoperiod. Plant Physiology *167*, 1643-1658.

Kolodziejczak, M., Kolaczkowska, A., Szczesny, B., Urantowka, A., Knorpp, C., Kieleczawa, J., and Janska, H. (2002). A higher plant mitochondrial homologue of the yeast m-AAA protease. Molecular cloning, localization, and putative function. J Biol Chem *277*, 43792-43798.

Kolodziejczak, M., Skibior-Blaszczyk, R., and Janska, H. (2018). m-AAA Complexes Are Not Crucial for the Survival of Arabidopsis Under Optimal Growth Conditions Despite Their Importance for Mitochondrial Translation. Plant Cell Physiol *59*, 1006-1016.

Laux, T. (2003). The stem cell concept in plants: a matter of debate. Cell *113*, 281-283.

Leonhard, K., Herrmann, J., Stuart, R., Mannhaupt, G., Neupert, W., and Langer, T. (1996). AAA proteases with catalytic sites on opposite membrane surfaces comprise a proteolytic system for the ATP‐dependent degradation of inner membrane proteins in mitochondria. The EMBO journal *15*, 4218-4229.

Leonhard, K., Stiegler, A., Neupert, W., and Langer, T. (1999). Chaperone-like activity of the AAA domain of the yeast Yme1 AAA protease. Nature *398*, 348.

Liu, S., Chen, H.D., Makarevitch, I., Shirmer, R., Emrich, S.J., Dietrich, C.R., Barbazuk, W.B., Springer, N.M., and Schnable, P.S. (2010). High-throughput genetic mapping of mutants via quantitative single nucleotide polymorphism typing. Genetics *184*, 19-26.

Liu, S., Yeh, C.-T., Tang, H.M., Nettleton, D., and Schnable, P.S. (2012). Gene mapping via bulked segregant RNA-Seq (BSR-Seq). PloS one *7*, e36406.

Marta, K., Marta, G., Adam, U., and Hanna, J. (2007). The significance of Arabidopsis AAA proteases for activity and assembly/stability of mitochondrial OXPHOS complexes. Physiologia plantarum *129*, 135-142.

McSteen, P., Malcomber, S., Skirpan, A., Lunde, C., Wu, X., Kellogg, E., and Hake, S. (2007). barren inflorescence2 Encodes a co-ortholog of the PINOID serine/threonine kinase and is required for organogenesis during inflorescence and vegetative development in maize. Plant Physiol *144*, 1000-1011.

Millar, A.H., Whelan, J., Soole, K.L., and Day, D.A. (2011). Organization and regulation of mitochondrial respiration in plants. Annu Rev Plant Biol *62*, 79-104.

Mir, R., Aranda, L.Z., Biaocchi, T., Luo, A., Sylvester, A.W., and Rasmussen, C.G. (2017). A DII Domain-Based Auxin Reporter Uncovers Low Auxin Signaling during Telophase and Early G1. Plant Physiol *173*, 863-871.

Møller, I.M. (2001). Plant mitochondria and oxidative stress: electron transport, NADPH turnover, and metabolism of reactive oxygen species. Annual review of plant biology *52*, 561-591.

Neuwald, A.F., Aravind, L., Spouge, J.L., and Koonin, E.V. (1999). AAA+: A class of chaperone-like ATPases associated with the assembly, operation, and disassembly of protein complexes. Genome research *9*, 27-43.

Ogura, T., Tomoyasu, T., Yuki, T., Morimura, S., Begg, K., Donachie, W., Mori, H., Niki, H., and Hiraga, S. (1991). Structure and function of the ftsH gene in Escherichia coli. Research in microbiology *142*, 279-282.

Ogura, T., and Wilkinson, A.J. (2001). AAA+ superfamily ATPases: common structure–diverse function. Genes to Cells *6*, 575-597.

Pfeiffer, A., Wenzl, C., and Lohmann, J.U. (2017). Beyond flexibility: controlling

stem cells in an ever changing environment. Curr Opin Plant Biol *35*, 117-123.

Phillips, K.A., Skirpan, A.L., Liu, X., Christensen, A., Slewinski, T.L., Hudson, C., Barazesh, S., Cohen, J.D., Malcomber, S., and McSteen, P. (2011). vanishing tassel2 encodes a grass-specific tryptophan aminotransferase required for vegetative and reproductive development in maize. Plant Cell *23*, 550-566.

Przemeck, G.K., Mattsson, J., Hardtke, C.S., Sung, Z.R., and Berleth, T. (1996). Studies on the role of the Arabidopsis gene MONOPTEROS in vascular development and plant cell axialization. Planta *200*, 229-237.

Qi, J., Wang, Y., Yu, T., Cunha, A., Wu, B., Vernoux, T., Meyerowitz, E., and Jiao, Y. (2014). Auxin depletion from leaf primordia contributes to organ patterning. Proceedings of the National Academy of Sciences *111*, 18769-18774.

Rhoads, D.M., and Subbaiah, C.C. (2007). Mitochondrial retrograde regulation in plants. Mitochondrion *7*, 177-194.

Rhoads, D.M., White, S.J., Zhou, Y., Muralidharan, M., and Elthon, T.E. (2005). Altered gene expression in plants with constitutive expression of a mitochondrial small heat shock protein suggests the involvement of retrograde regulation in the heat stress response. Physiologia Plantarum *123*, 435-444.

Sakamoto, W., Zaltsman, A., Adam, Z., and Takahashi, Y. (2003). Coordinated regulation and complex formation of yellow variegated1 and yellow variegated2, chloroplastic FtsH metalloproteases involved in the repair cycle of photosystem II in Arabidopsis thylakoid membranes. The Plant Cell *15*, 2843-2855.

Santos, D., and De Almeida, D.F. (1975). Isolation and characterization of a new temperature-sensitive cell division mutant of Escherichia coli K-12. Journal of bacteriology *124*, 1502-1507.

Schieber, M., and Chandel, N.S. (2014). ROS function in redox signaling and oxidative stress. Curr Biol *24*, R453-462.

Schippers, J.H., Foyer, C.H., and van Dongen, J.T. (2016). Redox regulation in shoot growth, SAM maintenance and flowering. Current opinion in plant biology *29*, 121-128.

Skirpan, A., Culler, A.H., Gallavotti, A., Jackson, D., Cohen, J.D., and McSteen, P. (2009). BARREN INFLORESCENCE2 Interaction with ZmPIN1a Suggests a Role in Auxin Transport During Maize Inflorescence Development. Plant and Cell Physiology *50*, 652-657.

Smakowska, E., Skibior-Blaszczyk, R., Czarna, M., Kolodziejczak, M., Kwasniak-Owczarek, M., Parys, K., Funk, C., and Janska, H. (2016). Lack of FTSH4 Protease Affects Protein Carbonylation, Mitochondrial Morphology, and Phospholipid Content in Mitochondria of Arabidopsis: New Insights into a

Complex Interplay. Plant Physiol *171*, 2516-2535.

Sokolenko, A., Pojidaeva, E., Zinchenko, V., Panichkin, V., Glaser, V.M., Herrmann, R.G., and Shestakov, S.V. (2002). The gene complement for proteolysis in the cyanobacterium Synechocystis sp. PCC 6803 and Arabidopsis thaliana chloroplasts. Current genetics *41*, 291-310.

Stepanova, A.N., Robertson-Hoyt, J., Yun, J., Benavente, L.M., Xie, D.Y., Dolezal, K., Schlereth, A., Jurgens, G., and Alonso, J.M. (2008). TAA1-mediated auxin biosynthesis is essential for hormone crosstalk and plant development. Cell *133*, 177-191.

Tauer, R., Mannhaupt, G., Schnall, R., Pajic, A., Langer, T., and Feldmann, H. (1994). Yta10p, a member of a novel ATPase family in yeast, is essential for mitochondrial function. FEBS letters *353*, 197-200.

Tognetti, V.B., MÜHlenbock, P.E.R., and Van Breusegem, F. (2012). Stress homeostasis - the redox and auxin perspective. Plant, Cell & Environment *35*, 321-333.

Urantowka, A., Knorpp, C., Olczak, T., Kolodziejczak, M., and Janska, H. (2005). Plant mitochondria contain at least two i-AAA-like complexes. Plant Mol Biol *59*, 239-252.

Van Aken, O., Pecenkova, T., van de Cotte, B., De Rycke, R., Eeckhout, D., Fromm, H., De Jaeger, G., Witters, E., Beemster, G.T., Inze, D.*, et al.* (2007). Mitochondrial type-I prohibitins of Arabidopsis thaliana are required for supporting proficient meristem development. Plant J *52*, 850-864.

Van Aken, O., Zhang, B., Carrie, C., Uggalla, V., Paynter, E., Giraud, E., and Whelan, J. (2009). Defining the mitochondrial stress response in Arabidopsis thaliana. Mol Plant *2*, 1310-1324.

Vatulescu, A.D., Fortunato, A.S., Sa, M.C., Amancio, S., Ricardo, C.P., and Jackson, P.A. (2004). Cloning and characterisation of a basic IAA oxidase associated with root induction in Vitis vinifera. Plant Physiol Biochem *42*, 609-615.

Webb, M.R. (1992). A continuous spectrophotometric assay for inorganic phosphate and for measuring phosphate release kinetics in biological systems. Proceedings of the National Academy of Sciences *89*, 4884-4887.

Woodson, J.D., and Chory, J. (2008). Coordination of gene expression between organellar and nuclear genomes. Nature Reviews Genetics *9*, 383.

Yang, F., Bui, H.T., Pautler, M., Llaca, V., Johnston, R., Lee, B.H., Kolbe, A., Sakai, H., and Jackson, D. (2015). A maize glutaredoxin gene, abphyl2, regulates shoot meristem size and phyllotaxy. Plant Cell *27*, 121-131.

Zhang, S., Wu, J., Yuan, D., Zhang, D., Huang, Z., Xiao, L., and Yang, C. (2014). Perturbation of auxin homeostasis caused by mitochondrial FtSH4 gene-mediated peroxidase accumulation regulates arabidopsis architecture. Mol Plant *7*, 856-873.

Zhao, Y., Christensen, S.K., Fankhauser, C., Cashman, J.R., Cohen, J.D., Weigel, D., and Chory, J. (2001). A role for flavin monooxygenase-like enzymes in auxin biosynthesis. Science *291*, 306-309.